UNCLASSIFIED

THIS PAGE IS UNCLASSIFIED

AFFDL-TR-71-12
Part I

AD885275

MULTIWHEEL LANDING GEAR - SOILS INTERACTION AND FLOTATION CRITERIA - PHASE III

PART I

DAVID C. KRAFT

HENRY LUMING

J. RICHARD HOPPENJANS

UNIVERSITY OF DAYTON

RESEARCH INSTITUTE

DAYTON, OHIO

AD No.___
DDC FILE COPY

TECHNICAL REPORT AFFDL-TR-71-12, PART I

MAY 1971

Best Available Copy 200

DOCUMENT CONTROL DATA - R & D

(Security classification of title, body of abstract and indexing annotation must be entered when the overall report is classified)

1. ORIGINATING ACTIVITY (Corporate author)	2a. REPORT SECURITY CLASSIFICATION
University of Dayton Research Institute	Unclassified
300 College Park Avenue	2b. GROUP
Dayton, Ohio 45409	

3. REPORT TITLE

Multiwheel Landing Gear-Soils Interaction and Flotation Criteria, Phase III - Part I

4. DESCRIPTIVE NOTES (Type of report and inclusive dates)

Technical Report

5. AUTHOR(S) (First name, middle initial, last name)

David C. Kraft
Henry Luming
J. Richard Hoppenjans

6. REPORT DATE	7a. TOTAL NO. OF PAGES	7b. NO OF REFS
May 1971	182	29

8a. CONTRACT OR GRANT NO.	9a. ORIGINATOR'S REPORT NUMBER(S)
F33615-70-C-1170	
b. PROJECT NO.	N/A
1369	
c. Task No. 136908	9b. OTHER REPORT NO(S) (Any other numbers that may be assigned this report)
d.	AFFDL-TR-71-12, Part I

10. DISTRIBUTION STATEMENT This document is subject to special export controls and each transmittal to foreign governments or foreign nationals may be made only with prior approval of the Air Force Flight Dynamics Laboratory (AFFDL/FEM), Wright-Patterson AFB, Ohio 45433.

11. SUPPLEMENTARY NOTES	12. SPONSORING MILITARY ACTIVITY
	Vehicle Equipment Division
	AF Flight Dynamics Laboratory
	Wright-Patterson AFB, Ohio 45433

13. ABSTRACT

The operational use of military aircraft in forward area situations has necessitated a comprehensive look at the critical factors which define the aircraft flotation performance and operations capability on semi- and unprepared soil runways. This investigation, which is a part of a continuing program, was directed primarily at defining the drag-sinkage response of multiple wheel landing gear on soil and the development of multiwheel flotation criteria to permit comparative evaluation of the relative merits of various landing gear configurations.

The total multiwheel/soil interaction study consisted of four parts. Part 1 was an evaluation of existing full scale field test data from aircraft or test carts operating with multiple tire configurations (twin and tandem). The second part was a Twin Plate Vertical Load (dynamic) Test Program which yielded sinkage interaction effects from single and twin plate load tests in sand and clay. An analytical study was made in Part 3 using a lumped parameter iteration technique together with an elastic-plastic soil model for investigating adjacent load (twin) interaction effects. Part 4 was the Rolling Multiple Wheel Verification Test Program. The results of the study show that certain multiwheel configurations and spacing are beneficial in terms of sinkage-drag performance. The results of the multiwheel/soil interaction study were used to develop multiwheel flotation criteria (guidelines for evaluation performance).

The flotation variable of braking was also studied on a preliminary basis. Braked tire/soil interaction equations suitable for defining the braking coefficient on soil were developed, and the results of a comparative study using these braked tire equations were favorable.

DD FORM 1473
1 NOV 65

14 KEY WORDS	LINK A		LINK B		LINK C	
	ROLE	WT	ROLE	WT	ROLE	WT
Aircraft Flotation; Aircraft Ground Surface Drag; Aircraft Tire Sinkage; Aircraft Tire; Soil Mechanics; Dynamic Loading of Soil; Relative Merit Index of Aircraft Tire Flotation Capability (R.M.I.); Finite Element Method; Lumped Parameter Iteration Method; Computer Program; Aircraft Flotation Tests; Multiple Wheel Tire Performance; Braked Wheel Tire Performance.						

AFFDL-TR-71-12
Part I

MULTIWHEEL LANDING GEAR - SOILS INTERACTION AND FLOTATION CRITERIA - PHASE III

PART I

DAVID C. KRAFT

HENRY LUMING

J. RICHARD HOPPENJANS

UNIVERSITY OF DAYTON

RESEARCH INSTITUTE

DAYTON, OHIO

FOREWORD

This report was prepared by the Aerospace Mechanics Group of the University of Dayton Research Institute under USAF Contract F33615-70-C-1170. The contract was initiated under Project No. 1369, "Launching and Alighting Systems for Military Aircraft," Task No. 136908, "Aircraft Surface Operation on Soil." This work was conducted under the direction of the Vehicle Equipment Division, Air Force Flight Dynamics Laboratory, Wright-Patterson Air Force Base, Ohio, Mr. George Sperry (AFFDL/FEM) Project Engineer.

This report covers work conducted from 17 November 1969 to 17 December 1970.

The authors wish to thank Mr. Sperry for his considerable efforts in coordinating and integrating the research program to meet Air Force objectives. This report was submitted by the authors in January 1871.

Publication of this technical report does not constitute Air Force approval of the reported findings or conclusions. It is published only for the exchange and stimulation of ideas.

KENNERLY H. DIGGES
Chief, Mechanical Branch
Vehicle Equipment Division
Air Force Flight Dynamics Laboratory

ABSTRACT

The operational use of military aircraft in forward area situations
has necessitated a comprehensive look at the critical factors which define
the aircraft flotation performance and operations capability on semi- and
unprepared soil runways. This investigation, which is a part of a con-
tinuing program, was directed primarily at defining the drag-sinkage
response of multiple wheel landing gear on soil and the development of
multiwheel flotation criteria to permit comparative evaluation of the
relative merits of various landing gear configurations.

The total multiwheel/soil interaction study consisted of four parts.
Part 1 was an evaluation of existing full scale field test data from air-
craft or test carts operating with multiple tire configurations (twin and
tandem). The second part was a Twin Plate Vertical Load (dynamic)
Test Program which yielded sinkage interaction effects from single and
twin plate load tests in sand and clay. An analytical study was made in
Part 3 using a lumped parameter iteration technique together with an
elastic-plastic soil model for investigating adjacent load (twin) interaction
effects. Part 4 was the Rolling Multiple Wheel Verification Test Program.
The results of the study show that certain multiwheel configurations and
spacing are beneficial in terms of sinkage-drag performance. The results
of the multiwheel/soil interaction study were used to develop multiwheel
flotation criteria (guidelines for evaluating performance).

The flotation variable of braking was also studied on a preliminary
basis. Braked tire/soil interaction equations suitable for defining the
braking coefficient on soil were developed, and the results of a compara-
tive study using these braked tire equations were favorable.

TABLE OF CONTENTS

ILLUSTRATIONS

ILLUSTRATIONS (Continued)

ILLUSTRATIONS (Continued)

LIST OF TABLES

LIST OF TABLES (Continued)

LIST OF SYMBOLS

A, A_1, A_2	Tire contact area (rigid surface)
A_c	Cone base area
A_Z	Area of equivalent plane of contact at sinkage Z
a	Width of applied pressure
B	A variable related to the stress invariants
B'	Braking torque
b	Tire section width
CBR	California bearing ratio
CI_{avg}	Average cone index of soil over 0" to 6" depth
CMN	Clay mobility number
CPR	Cone penetration resistence
CPR_{avg}	Average cone penetration resistence
CPR_F	Average cone penetration resistence subsequent to full insertion of the cone tip
CPR_N	Average cone penetration resistence - twin plate tests
CPR_{unif}	Uniform cone penetration resistance
c	Cohesion of soil
c_1	Dilatational wave propagation velocity
c_1, c_2, c_3, c_4	Finite element equation constants
D	Tire outside diameter
DI	Drag index
D_c	Cone diameter
D_p	Plate diameter
d	Tire deflection in inches
d_1, d_2, d_3, d_4	Finite element equation constants
E	Young's modulus
F	Redefined yield function for stress correction
F_{avg}	Average penetration resistence per plate
$(FI)_S$	Flotation index for single wheels
$(FI)_M$	Flotation index for multiple wheel configurations

LIST OF SYMBOLS (Continued)

fps	Feet per second
G	Modulus of rigidity
G_b	Slope of the cone index vs. depth profile in sand
g	Acceleration due to gravity
h	Space mesh size
I	First invariant of the stress tensor
i	Location identifier (column)
J	Second invariant of the deviatoric stress tensor
j	Location identifier (row)
K_m	Drag modifier for tandem wheel tracking situations
K_n	Drag modifier for twin wheel situations
K_r	Drag modifier for tandem wheel nontracking situations
$[K]$	Stiffness matrix
ℓ	Tire footprint length (rigid surface)
ℓ_Z	Equivalent plane of contact
M_M	Multiple wheel drag modifier
m	Fraction of tire diameter
N	Number of tires per landing gear
$\overline{N}$	Unit normal vector to the function F
N_m	Number of wheels in a tandem-tracking situation
N_n	Number of wheels in a twin situation
N_r	Number of wheels in a tandem-nontracking situation
n'	Spacing ratio (ratio of G_L spacing between contact areas to diameter of contact areas)
n	Fraction of tire width and exponent of sinkage
OI	Operations index
P	Vertical load
P_s	Vertical soil reaction
P_c	Cone vertical load
PR	Ply rating
$\{P\}$	Vector of imposed nodal displacement

LIST OF SYMBOLS (Continued)

$P(\Omega)$	Power spectral density of the surface profile height
p	Tire contact stress or prescribed surface pressure
P_{max}	Peak surface pressure
P_n	Uniform vertical pressure
P_o	Circular uniform pressure distribution
P_s	Uniform shear distribution
pcf	Pounds per cubic foot
psi	Pounds per square inch
psf	Pounds per square foot
P_1, P_2	Loaded areas
Q	Constant for incremental stress-strain relation use
R	Rolling drag resistence to forward motion
R_B	Braked tire drag force
R_{Dual}	Drag for dual wheel tracking situations
R_R	Horizontal soil resistence to forward motion exclusive of shear resistence during braking
R_{single}	Drag for single wheel situation
R_T	Horizontal component of net shear force resistence
$(R/P)_S$	Single wheel drag ratio
$(R/P)_M$	Multiple wheel drag ratio
r	Radial coordinate
r'	Fraction of tandem-nontracking tire spacing
ΔR	Incremental change in rolling drag resistence
ΔR_R	Incremental change in resistence to forward motion exclusive of clear resistence
S	Percent tire slip
S_m	Tire spacing, C_L to C_L of wheel centers in tandem arrangements
S_n	Tire spacing, C_L to C_L of twin tires
T	Net tangential shear force at interface
t	Elasped time
t_d	Time duration of load pulse

LIST OF SYMBOLS (Continued)

t_r	Rise time
Δt	Time increment
$U, \dot{U}, \ddot{U},$	Displacement, velocity, acceleration in η direction
$u, \dot{u}, \ddot{u},$	Displacement, velocity, acceleration in the x-direction
ΔU	Incremental radial displacement
$V, \dot{V}, \ddot{V}$	Aircraft horizontal ground velocity; also displacement, velocity, acceleration in the ζ-direction
V_a	Horizontal velocity of the axle
V_W	Peripheral speed of wheel
$v, \dot{v}, \ddot{v}$	Displacement, velocity, acceleration in y-direction
ΔV	Incremental velocity
W	Moisture content
ΔW	Incremental work done on the soil medium
$w, \dot{w}, \ddot{w}$	Displacement, velocity, and acceleration in the z-direction
w_s	Surface deflection of a mass point
Δw	Incremental vertical displacement
x	x-coordinate
Z	Instantaneous soil sinkage
Z_{single}	Sinkage for single wheel situations
Z_{twin}	Sinkage for twin wheel configuration
Z_c	Vertical penetration of cone
Z_e	Elastic sinkage
Z_R	Rut depth
z	Downward space coordinate
(Z/D)	Sinkage ratio
σ	Ratio of vertical load to tire contact area
σ_1	Soil parameter related to the friction angle
β	Constant used to define loading and unloading
γ	Unit density of soil
$\{\Delta\}$	Vector of independent nodal variables
$\Delta v_{\eta\zeta}$	Shear strain increment in the η-ζ direction
ϵ	Vector of stress and displacement values

LIST OF SYMBOLS (Continued)

$\Delta\epsilon_\eta, \Delta\epsilon_\zeta, \Delta_\xi$	Normal strain increment in the η, ζ, and ξ directions
ζ	Coordinate system axis label
η	Coordinate system axis label
η_c	Stress correction equation parameter
λ	Lame's constant
$\mu(S)$	Nonlinear function which varies with slip
ν	Poisson's ratio
ξ	Coordinate system axis label
π_R	Total Reissner energy
π_r	Reissner energy of a finite element
ρ	Mass density of soil
γ_d	Dry soil density
$\bar{\sigma}$	Effective normal stress
$\sigma_x, \sigma_y, \sigma_z, \sigma_\eta, \sigma_\zeta$	Normal stresses in the x, y, z, η, and ζ directions
τ	Shear stresses at the braked tire interface
$\tau_{xz}, \tau_{xy}, \tau_{\eta\zeta}$	Shear stresses in the x-z, x-y, and η-ζ directions
ρ	Angle defining equivalent plane of contact
ϕ	Friction angle of soil

SECTION I

INTRODUCTION AND SUMMARY

Comprehensive efforts at studying the problems associated with the operation of aircraft on forward area soil runways have been conducted over the past several years[1,2,3,4,5]. Those factors which influence the flotation/operation performance of aircraft on soil runways are aircraft landing gear configuration, tire inflation pressure, aircraft surface speed, soil strength and texture, surface roughness, turning effects, landing impact, braking action, multipass operations of the aircraft. The results of past research[1] have identified what have been termed the primary and secondary variables as related to aircraft flotation/operation performance. The primary variables are drag, sinkage, multiple wheel effects, and braking effects. Secondary variables include roughness, speed, multipass, landing impact, and turning.

In order to develop the necessary criteria to permit the efficient and effective utilization of soil runways while including adequate safety provisions, it is necessary to define the interaction effects between the tire and soil during rolling, turning, and braking modes. The current research effort described in this report is a part of a comprehensive aircraft flotation research program. The objective of the program is to analytically define landing gear-soil interaction and to develop a system for rating the relative flotation capacity of landing gear contact elements and landing gear systems during aircraft operation on semi- and unprepared soil runways. Flotation in this context is defined as the tire-soil interaction and the ability of the soil to support the tire load system.

Phase I[5] of this program included a survey of the flotation problem, establishment of the critical flotation parameters, and an investigation of available flotation data leading to the development of a flotation analysis equation. Phase II[1] included the development of an empirical sinkage prediction equation, development of a lumped parameter simulation sinkage

1

prediction technique for moving tires, conducting the Rolling Single Wheel Verification Tests, and the development of the single wheel Relative Merit Index (RMI) system for defining comparative flotation capacity. Phase III of the research program consists of two segments. The first segment, which is detailed in this report includes:

- Multiwheel sinkage-drag analysis equations
- Twin Plate Vertical Load Test Program
- Lumped parameter multiwheel simulation computer program for twin and tandem configurations
- Rolling Multiwheel Verification Tests
- Preliminary studies of braking effects.

The second segment of Phase III will concentrate on more detailed studies of braking as well as preliminary evaluations of the effects of speed, turning, multipass, and roughness on flotation performance.

The results of the current research program, as well as the results of mobility and flotation studies conducted by others, were used in developing the Quick Reference - Tires On Soil Flotation Guide shown in Table 1. Reference to Figure 1 indicates considerable progress has been made in recent years in defining tire/soil flotation performance.

TABLE 1

Quick Reference-Tires on Soil Flotation Guide

FLOTATION VARIABLE	SINKAGE AND DRAG	VELOCITY

Single Wheel	- Drag Ratio (R/P) correlates with sinkage ratio (Z/D)
	  $R/P = 0.018 + 3.23$ (Z/D), all soils, Region II velocity range
	- Sinkage prediction techniques available for sand and clay, Region II
	  UDRI
	  WES
	- High speed (Region III) sinkage/drag relationship not adequately defined
	- Low speed (Region I) sinkage/drag relationship not important
	- Flotation performance improves with:
	  increasing tire diameter increasing soil strength
	  increasing tire deflection decreasing tire load
	- Flotation criteria developed (Flotation Index, FI_S)
		3 Regions of sinkage/drag variance (see Figure 1)
		
		Approximate
		
		$0 \leq$ Region I < 5 knots
		5 knots $<$ Region II < 40 knots
		40 knots $<$ Region III

Multiple Wheel Twin Tandem-Tracking Tandem-Nontracking	Optimum spacing based on drag minimization (Region II velocity range) - 1.5b to 2.5b, sand; 2.5b to 3.5b, clay - ≤ 1.5D or < 3D, sand; 1.5D to 2D, clay - Results similar to twin operations - Flotation criteria proposed (Flotation Index, FI_M)	Velocity influence on optimum multiple wheel spacing is not known. Very likely optimum spacing not influenced by Region I and III velocities.

Braked Wheel	- Braking drag ratio (R_B/P) analysis equations available partially verified
	- Braking drag ratio (R_B/P) independent of initial sand soil strength
	- Sinkages increase markedly for braking in sand
	- Sinkages increase slightly for braking in clay
	- Braking drag ratio increases with:
	  increasing sinkage, sand and clay
	  increasing slip, sand and clay
	  increasing tire diameter, sand and clay
	  increasing soil strength, clay
	- Flotation criteria proposed (Drag Index, DI)
		Velocity influence known on a preliminary basis.

R = Rolling Drag Z = Instantaneous Soil Sinkage R_B = Braked Drag

P = Vertical Load   D = Tire Outside Diameter   b = Tire Section Width
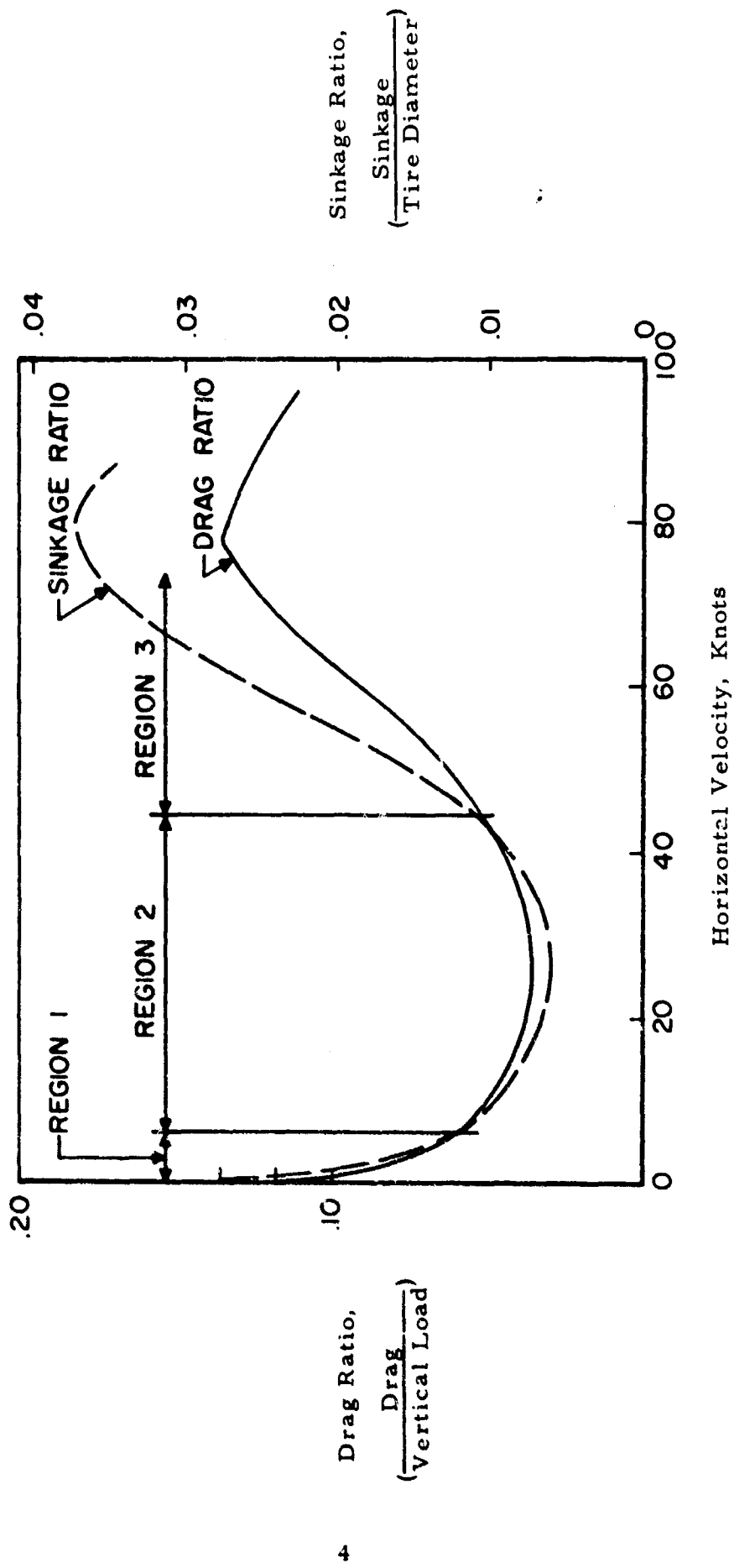
Figure 1. Typical Drag Ratio, Sinkage Ratio vs. Horizontal Velocity in Soil

4

SECTION II

MULTIWHEEL SINKAGE AND DRAG ANALYSIS

1.   General Considerations in Multiwheel Performance

The growth in size and weight of military aircraft with designed operational capability on soil runways has led to an increasing use of multiple wheel landing gear configurations. Possible multiple tire configurations include twin (dual), tandem-tracking and tandem-nontracking as shown in Figure 2. Previous studies[1, 6] had shown that adjacent loaded areas influence the performance of aircraft tires operating on soil runways. The nature and magnitude of this influence, however, had not been established in these studies.

A comprehensive four-part program was undertaken to study the tire-soil sinkage and drag interaction effects for multiple tire landing gears. Part 1 consisted of an evaluation of existing full scale field test data from aircraft, or test carts operating with multiple tire configurations. The second part was a Twin Plate Vertical Load Test Program in which both single and twin plates were dynamically penetrated into cohesive (clay) and cohesionless (sand) type soils. An analytical study was made in Part 3 using a lumped parameter iteration technique together with an elastic-plastic soil model (soil simulation) for studying adjacent load interaction effects. Part 4 was the full scale Rolling Multiwheel Verification Tests.

2.   PART 1 - Review of Existing Multiwheel Test Data

Availability of existing multiple tire test data[4, 6, 7, 8, 9] was restricted to cohesive soils. A summary of available data for the drag performance of twin tires on clay at various tire spacings is shown in Figure 3. The comparison is made between the drag ratio, R/P (R = total rolling drag for both tires, P = total vertical load on both tires), for the
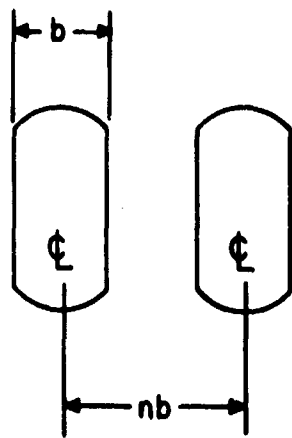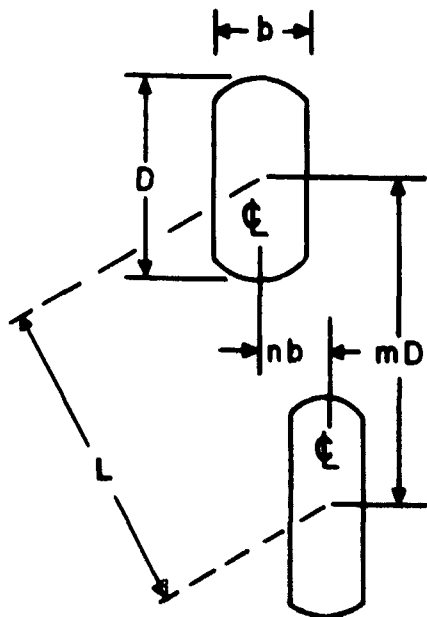
Twin Wheel Configuration

b = Tire Section Width

D = Tire Outside Diameter

m = Fraction of Tire Outside Diameter

n = Fraction of Tire Section Width

r' = Fraction of Tandem-Nontracking
     Tire Spacing

$$r' = \frac{L}{\sqrt{b^2 + D^2}} \quad \text{where} \quad L = \sqrt{(nb)^2 + (mD)^2}$$

Tandem Wheel Configuration

Figure 2. Multiple Tire Configurations

6

$$\frac{\frac{R}{P} \text{ per Tire Dual}}{\frac{R}{P} \text{ Single Tire}}$$

Ratio of Dual Wheel Spacing to Tire Width, n

Data Band

- ⊙ 56X16 TIRES, BUCKSHOT CLAY
- ▫ 25.00-28 TIRES, BUCKSHOT CLAY
- △ 33.75X9.75 TIRES, LONDON CLAY
- ⊙ 40X14 TIRES, HARPERS LAKE CLAY
- ● 40X14 TIRES, SILTY CLAY
- R = ROLLING DRAG
- P = VERTICAL LOAD
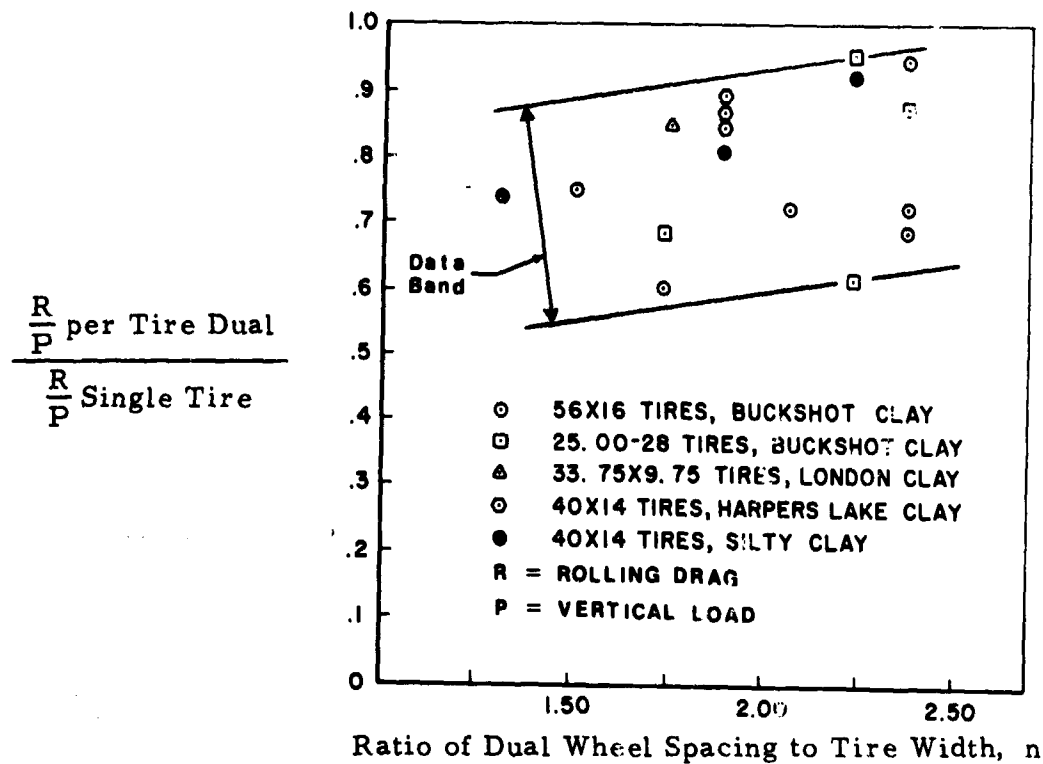
Figure 3.   Twin Tire Performance on Clay

$$\frac{\frac{R}{P} \text{ per Tire Tandem}}{\frac{R}{P} \text{ Single Tire}}$$

Ratio of Tandem-Tracking Spacing to Tire Diameters, m

- ⊙ 56X16 TIRES, BUCKSHOT CLAY
- ▲ 20.00-20 TIRES, BUCKSHOT CLAY
- ▫ 10.00-20 TIRES, CLAY
- ▼ 33.75X9.75 TIRES, LONDON CLAY
- ● 40X14 TIRES, HARPERS LAKE CLAY
- R = ROLLING DRAG
- P = VERTICAL LOAD
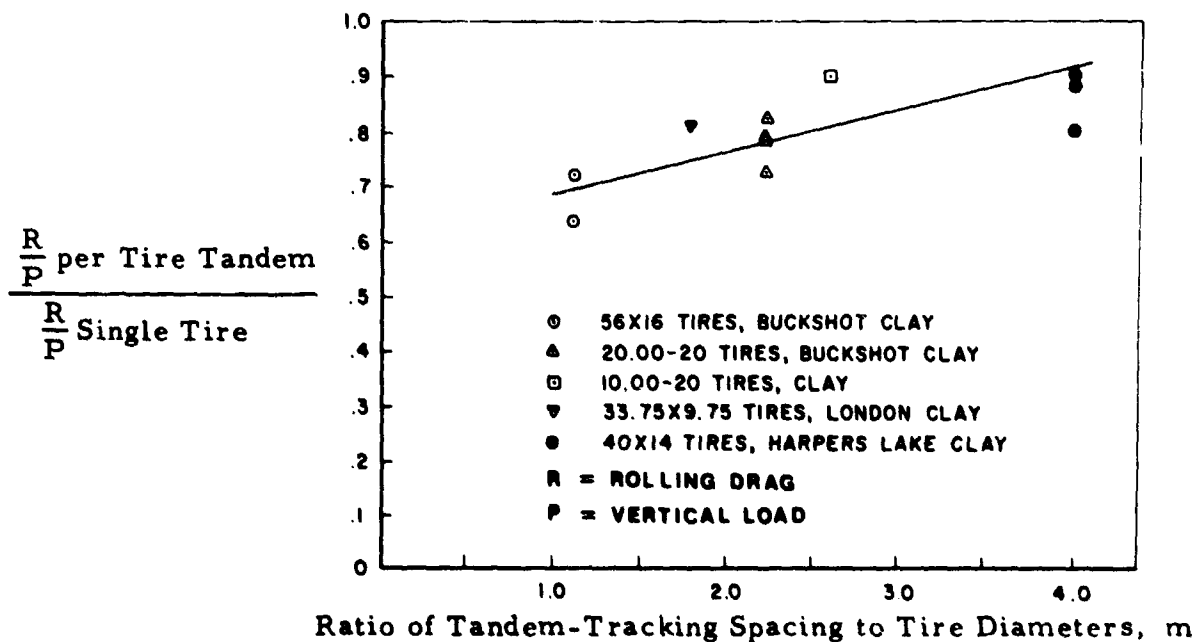
Figure 4.   Tandem-Tracking Performance on Clay

7

twin tire case, and the drag ratio for the single (isolated) tire case. The test data shown in Figure 3 was primarily for low sinkages (<3/4"). A similar drag ratio comparison was made using available tandem-tracking test data as shown in Figure 4. Again the test data was primarily for low sinkages.

Reference to Figures 3 and 4 shows considerable scatter in the test data but generally indicates that within certain spacing limitations, some reduction in rolling drag can be expected for twin and/or tandem-tracking tire configurations over that for single tires when operated on cohesive soils at low sinkages. Since drag has been shown to be directly related to sinkage through the relationship

$$\frac{R}{P} = 0.018 + 3.23 \left(\frac{Z}{D}\right) \tag{1}$$

where

    Z = instantaneous sinkage

    D = tire diameter,

corresponding reductions in sinkage can be inferred from the use of Equation (1). No usable test data was found for multiple tires operated on cohesionless soils.

3.   PART 2 - Twin Plate-Vertical Load Test Program

Objective

The purpose of the dual vertical plate tests was to obtain initial information and data concerning the sinkage interaction effects produced by adjacent dynamic plate loads as compared to a single isolated plate load under similar test conditions. Plate spacing was also varied to permit a detailed look at the influence of this variable. While dynamic vertical plate load tests do not simulate the action of a rolling tire, such tests can be used to study the influence of sinkage interaction. As indicated by Equation (1), since sinkage is directly related to drag for rolling

8

tires, the sinkage results of the plate tests can be used to interpret drag effects by inference.

Test Program

To accomplish the objectives, a series of single and twin vertical load plate tests were conducted in two different soils: buckshot clay and a mixture of mortar sand and Yuma sand. Dynamic loads were applied through the plates at a constant rate of penetration. Sufficient cone penetrometer tests were made to fully define the soil properties of each test specimen. A summary of the test program is given in Table 2. The full details of the soil properties, soil preparation, test procedure, and uniformity of placement are given in Appendix I.

Test Setup

A. Instrumentation

Dynamic vertical loads were applied to the test specimens by an MTS 5000 pound dynamic load system containing two service modules and a load frame. The soil was contained in a test box of the dimensions 16 inches by 13 inches by 9 inches deep. The complete test system, including the soil test box, is shown in Figure 5. Loads were monitored by a SR-4 Baldwin-Lima-Hamilton 0.5KIP load cell attached to the loading head. Both loads and sinkages were recorded on a Honeywell Visicorder.

All plate tests in sand were conducted at a rate of 12.5 inches per second, all plate tests in clay at a 4.2 inches per second velocity, and cone penetrometer tests were run at a rate of 1.25 inches per second.

B. Test Plates

The application of the load to the soil was accomplished through the use of circular plates, 1-1/2 inches in diameter and 5/16 inch thick. The twin plate tests used two such plates mounted in an aluminum block with a shaft which permitted varying the plate spacing. Figure 6 shows the single and dual plate test equipment.

9

TABLE 2
DUAL VERTICAL PLATE TEST PROGRAM (DESIGN)

Test No.	Soil Type	Soil Stiffness CI_{avg} (1b)	Plate Spacing, nD_p	Plate Repeat Tests
1S	Sand*	9.0	Cone Only	
2S	"	9.0	Single	
3S	"	9.0	Single	
4S	"	9.0	Cone Only	
5S	"	9.0	Single	
6S	"	9.0	Cone Only	
7S	"	9.0	1-1/2 D	
8S	"	9.0	1-1/2 D	Repeat
9S	"	9.0	Cone Only	
10S	"	9.0	2-1/2 D	Repeat
11S	"	9.0	2-1/2 D	Repeat
12S	"	9.0	4 D	
1C	Buckshot Clay	30-35	Single	
2C	"	20-25	1-1/2 D	Repeat
3C	"	30-35	2-1/2D	Repeat
4C	"	20-25	Single	
5C	"	30-35	4 D	Repeat
6C	"	30-35	2-1/2 D	Repeat
7C	"	30-35	Single	
8C	"	20-25	1-1/2 D	Repeat
9C	"	20-25	4 D	Repeat

* Mixture of Mortar Sand and Yuma Sand

n = Plate Spacing / Plate Diameter

D_p = Plate Diameter = 1.50"

CI_{avg} = Average Cone Index

10
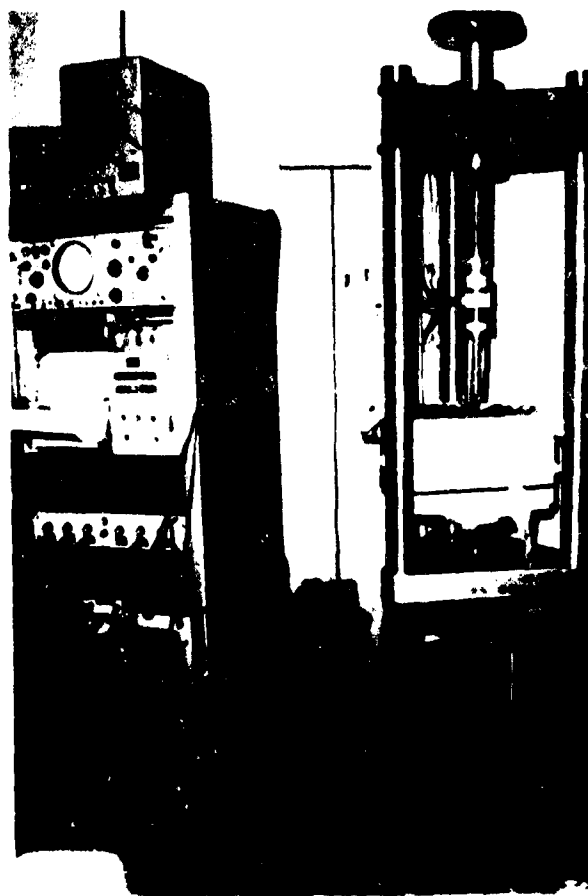
Figure 5.   Plate Test System

NOT REPRODUCIBLE
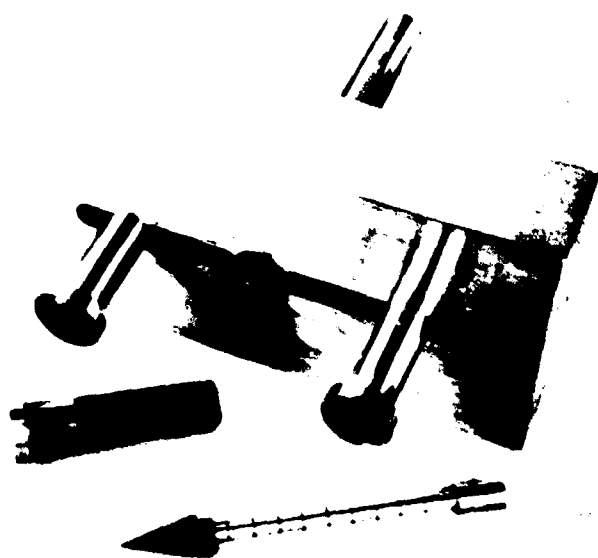
Figure 6.   Plate Test Fixture and Cone Penetrometer

11

C. Test Penetrometer

A cone penetrometer was used to measure the soil strength and uniformity after placement. The cone was made of stainless steel, ground to a smooth finish, and was of the same dimensions as the Army cone penetrometer used in mobility studies. The cone penetrometer is shown in Figure 6.

Sand Tests

A typical cone and single plate penetration resistance recording is shown in Figures 7 and 8. The results of the cone penetration tests which reflect the uniformity of the sand test sections are given in Appendix I along with the formula used in calculating the average soil cone penetration resistance (CPR_{avg}) for each test section. The results of the single and twin plate tests conducted in the sand sections are given

TABLE 3

PLATE FORCE RESISTANCE DATA, SAND
(Initial Load)

Test Sequence No.	Comments	Force Resistance per Plate in lb at Penetration of			
		1/4"	1/2"	3/4"	1"
2S	1st Single Plate Test	14.3	15.5	17.6	20.7
3S	2nd Single Plate Test	16.	18.1	21.1	25.0
5S	3rd Single Plate Test	6.5	9.2	12.5	16.0
7S	1st Twin at 1-1/2 D_p	8.5	10.2	11.8	14.5
8S	2nd Twin at 1-1/2 D_p	12.6	15.6	17.6	20.2
10S	1st Twin at 2-1/2 D_p	6.9	9.2	11.9	15.1
11S	2nd Twin at 2-1/2 D_p	10.0	12.7	14.8	17.0
12S	1st Twin at 4 D_p	8.9	10.9	13.1	15.8

in Table 3. Figure 9 shows this same data presented as the average penetration resistance (CPR_{avg}) versus sinkage for each plate spacing. F_{avg} was determined by the results of three tests (2S, 3S, and 5S) for the single plate, and two tests for the twin plate tests, at spacings of

12
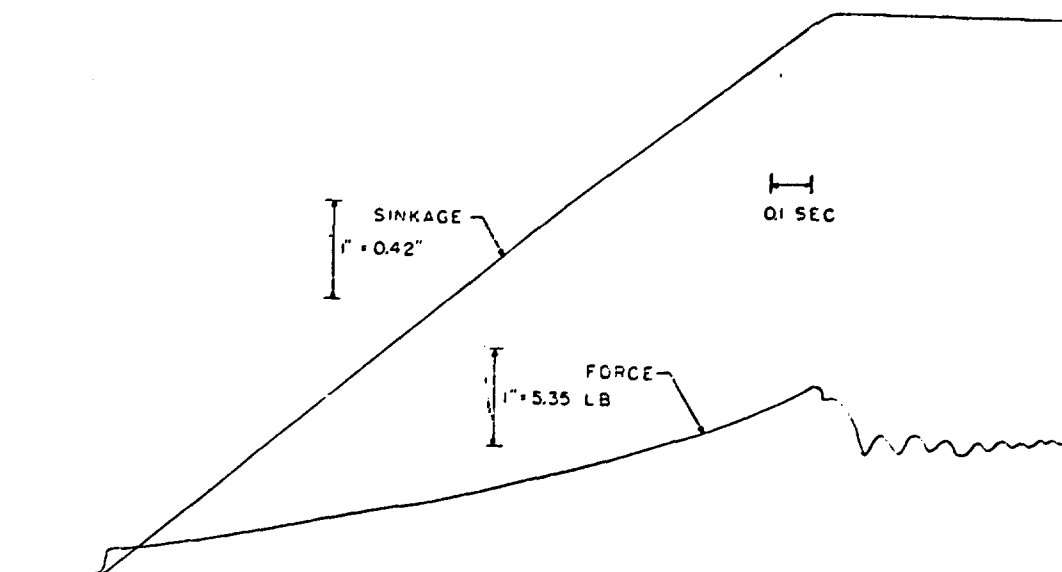
Figure 7. Typical Cone Penetration Test Result, Sand
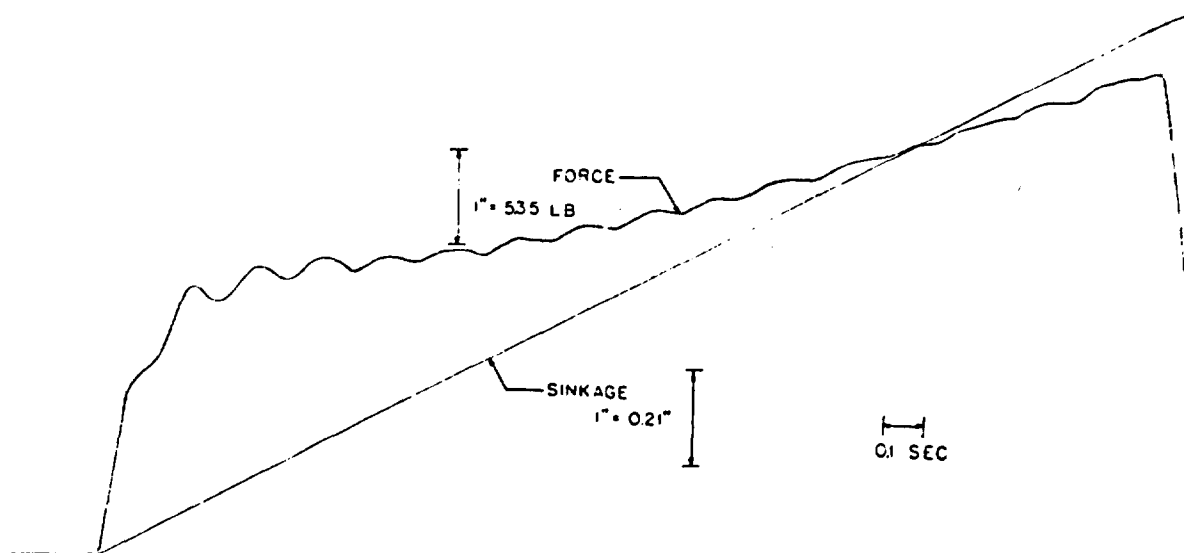
Figure 8. Typical Single Plate Test Result, Sand

13
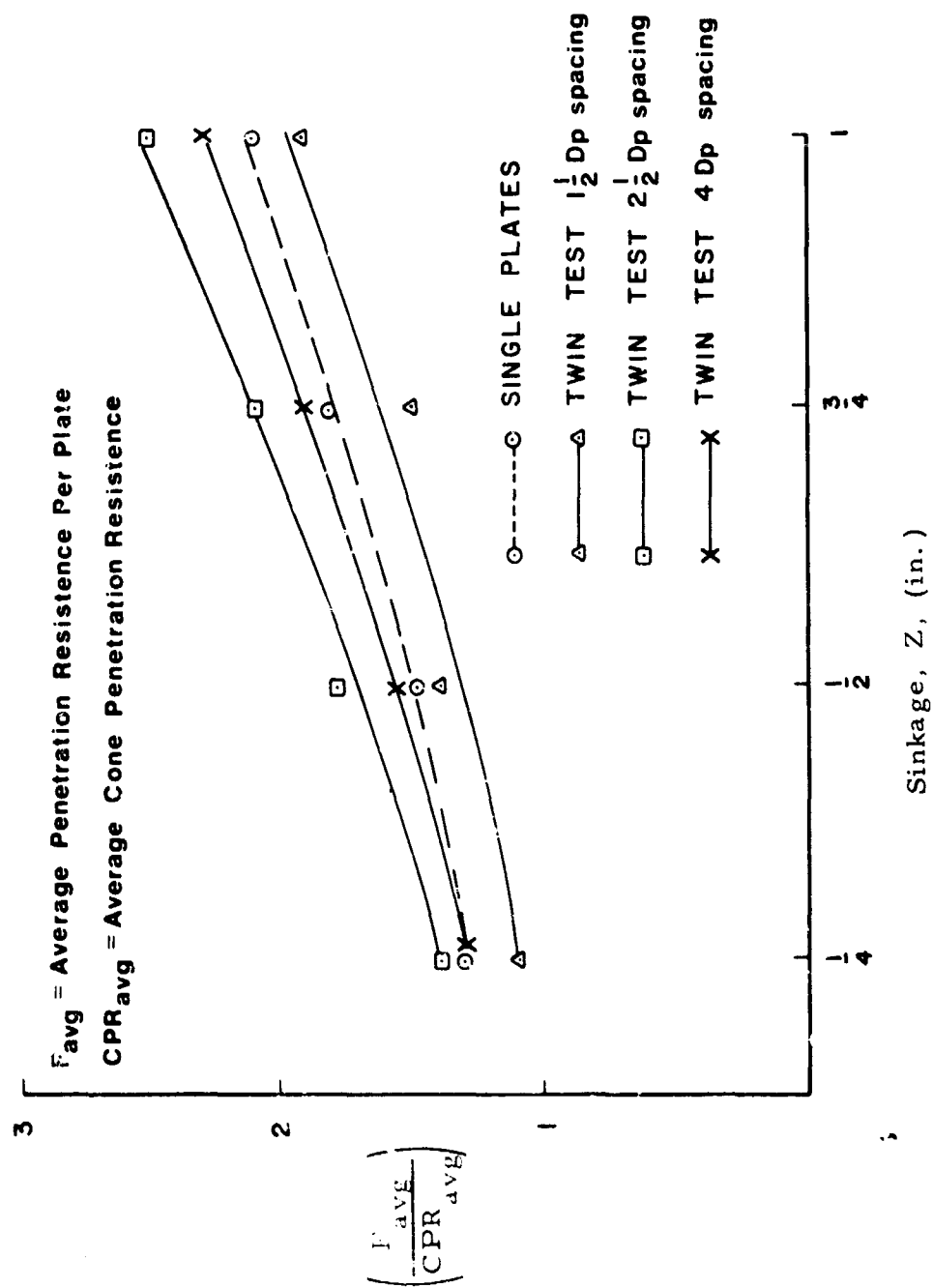
Figure 9. F_{avg}/CPR_{avg} vs. Sinkage, Sand Tests

1-1/2 D_p and 2-1/2 D_p. Only one twin plate test was conducted at a spacing of 4 D_p. Analysis of Figure 9 shows that more force (per plate) is required in a twin plate situation for a given sinkage than for a corresponding single plate penetrated to the same sinkage, with the exception of the closest plate spacing, 1-1/2 D_p.

Clay Tests

Figures 10 and 11 show the typical recordings for a cone penetration test and a twin plate test, respectively, in clay. The results of the cone penetration tests which reflect the uniformity of the clay test sections are given in Appendix I along with means of determining the average cone penetration resistence (CPR_{unif}) for each test section. The results of the single and twin plate penetration tests are summarized in Table 4. These results along with

TABLE 4

PLATE FORCE RESISTANCE DATA, CLAY
(Initial Loading)

Test Sequence No.	Comments	Force Resistance per Plate in lb. at Penetration of			
		1/4"	1/2"	3/4"	1"
1C	1st Single Plate Test	84.0	95.2	97.4	101.5
2C	1st Twin at 1-1/2 D_p	55.0	61.5	63.5	64.3
3C	1st Twin at 2-1/2 D_p	74.3	80.5	82.0	81.5
4C	2nd Single Plate Test	51.9	57.8	61.5	63.6
5C	1st Twin at 4 D_p	74.8	83.0	81.6	80.6
6C	2nd Twin at 2-1/2 D_p	77.8	85.8	86.5	86.5
7C	3rd Single Plate Test	87.7	97.9	98.9	98.6
8C	2nd Twin at 1-1/2 D_p	56.5	59.5	64.0	67.0
9C	2nd Twin at 4 D_p	74.0	82.2	80.9	80.0

the soil strength data were used to analyze the results in a manner similar to that used for sand as given in Figure 12 which shows the variation of F_{avg}/CPR_{unif} for each plate spacing including the single plate condition. Each F_{Avg} represents the average of the results presented in Table 4, and CPR_{unif} is defined in Appendix I. Reference to Figure 12 for clay shows
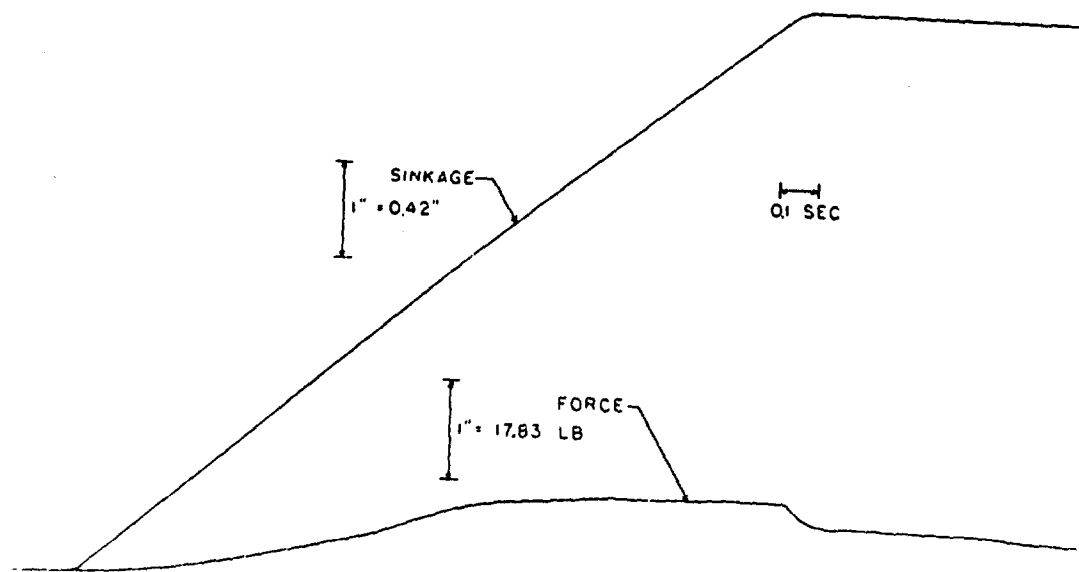
Figure 10.   Typical Cone Penetration Test Result, Clay
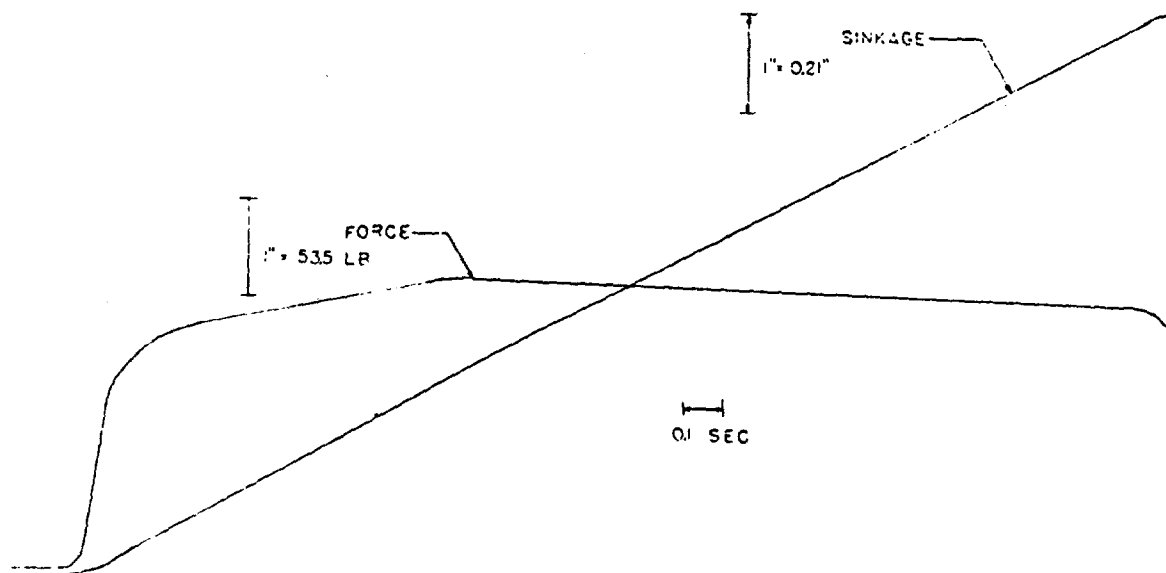
Figure 11.   Twin Plate Test Result, Spacing of 4 D, Clay

16
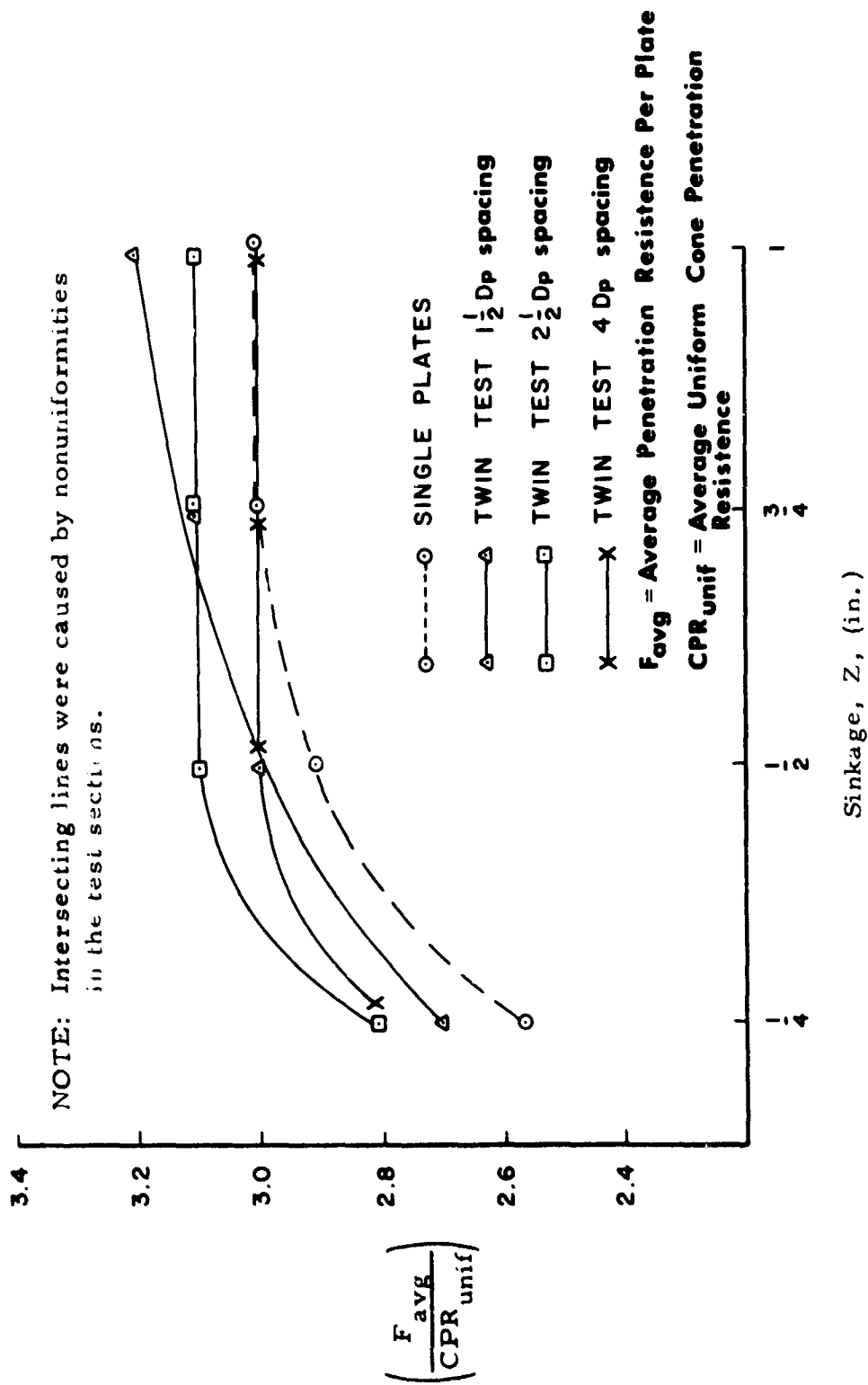
Figure 12. F_{avg}/CPR_{unif} vs. Sinkage, Clay Tests

17

a trend similar to that for sand, that is, within certain spacing limitations, more force is required per plate for dual plate configurations at a particular sinkage than is required for a single isolated plate at the same sinkage. The tendency of the plate spacing lines (see Figure 12) to intersect was caused by variations in strength with depth in the buckshot clay test specimens. Tests involving the single plate and the plates at a spacing of $1-1/2\,D_p$ had test sections exhibiting a slight increase in strength with depth, while tests involving plate spacings of $2-1/2\,D_p$ and $4\,D_p$ had test sections showing a slight decrease in strength with depth.

Analysis and Interpretation of Test Results

The results of the sand and clay tests were previously interpreted in terms of plate resistance to penetration at different sinkages. A clearer picture of sinkage interaction effects is gained by plotting sinkages at a common dimensionless plate force resistance (F_{avg}/CPR_{unif}). Figure 13, which was developed from Figures 9 and 12 for $F_{avg}/CPR_{avg} = 1.5$ for sand and $F_{avg}/CPR_{unif} = 2.9$ for clay, shows this interaction. Reference to Figure 13 and use of Equation (1) would suggest approximately a 15% to 20% reduction in rolling drag for optimum spacing of twin tires on sand while optimum spacing of twin tires in clay would lead to an approximate 20% to 25% drag reduction for relatively low sinkages (<3/4"). It should be recognized that such conclusions are only approximate since plate size (diameter) and magnitude of sinkage are very likely influencing factors.

The reduction in sinkage caused by the proximity of an adjacent loaded area is caused by an interference between the two plastic zones associated with each surface load. Figure 14a shows qualitatively the elements of a bearing capacity theory as developed by Terzaghi[12]. Reference to Figure 14a indicates a triangular wedge of soil undergoing upward displacement as indicated by the dashed line. As the second loaded area P_2 moves toward the first loaded region P_1, the plastic zones begin to overlap creating interference in the slip fields. As indicated by

18
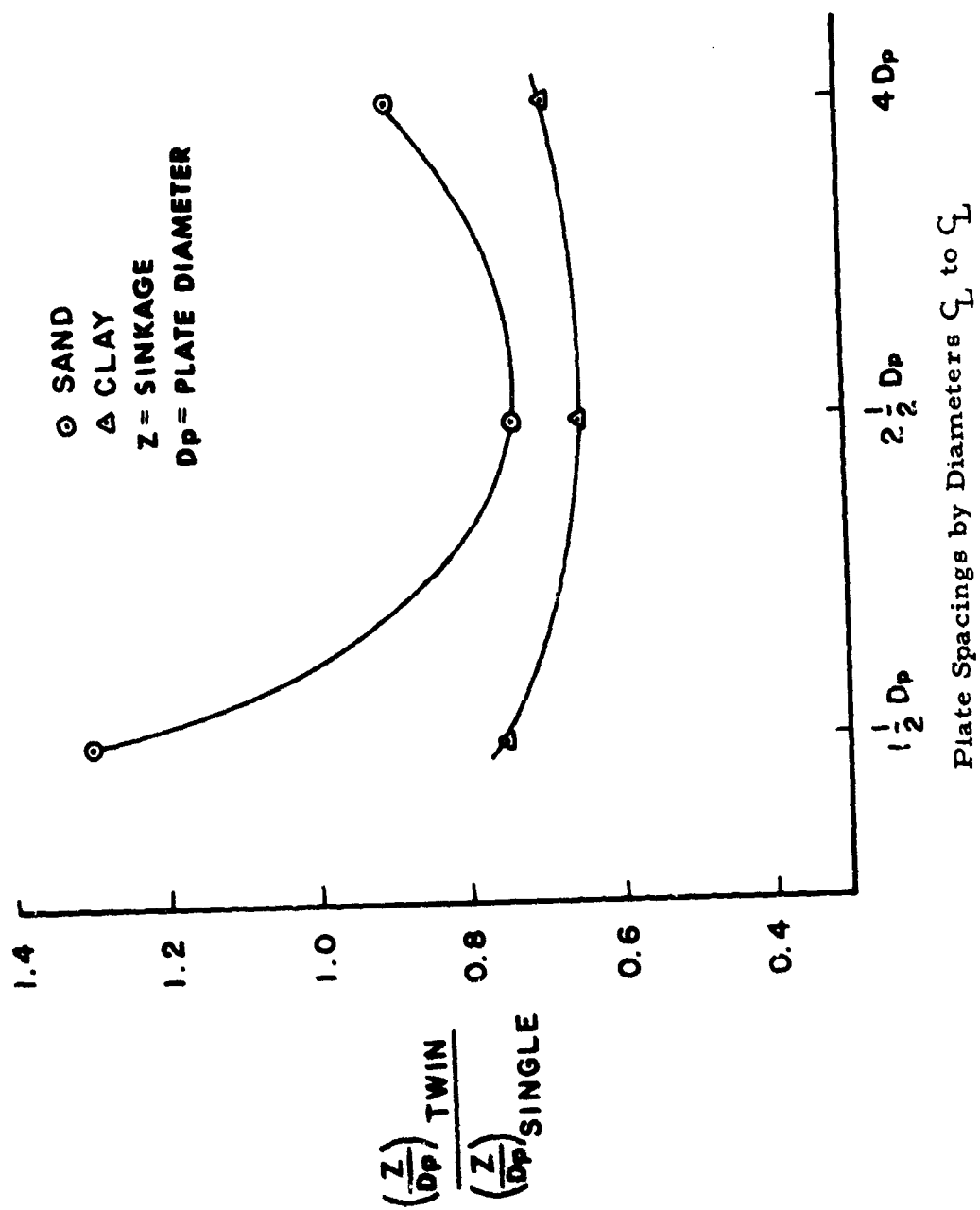
Figure 13. Influence of Sinkage Interaction, Sand and Clay
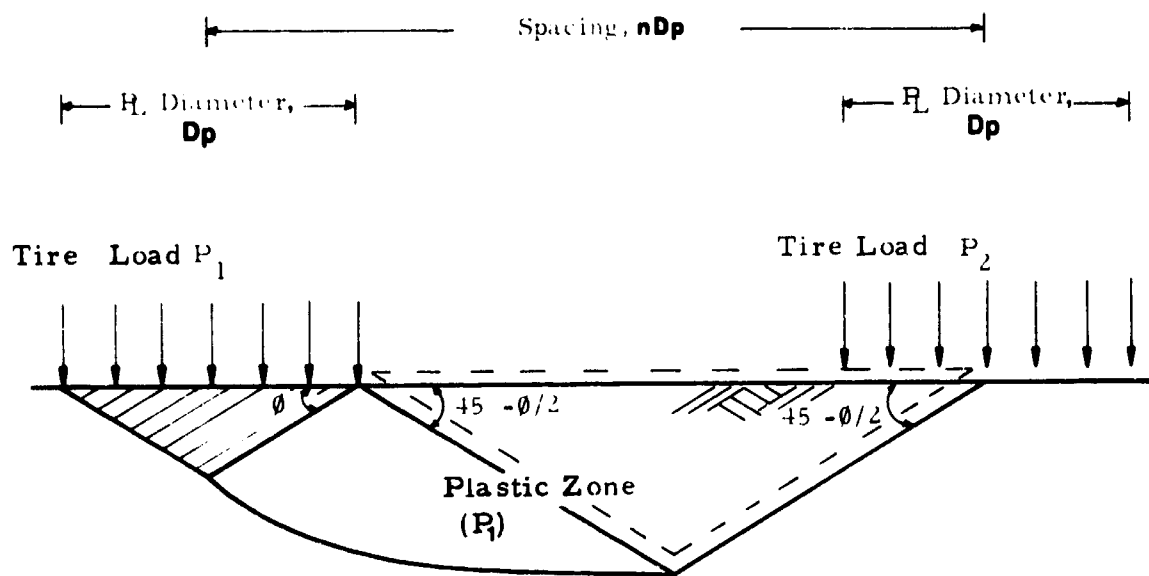
(a) Terzaghi Elements of Bearing Capacity
Depicting Development of Slip Fields
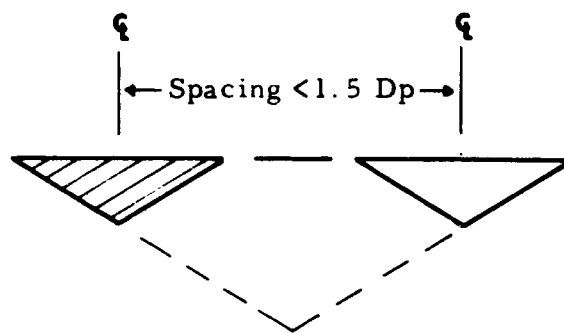
(b) Adjacent Load Areas Acting as a Single Load

Figure 14. Adjacent Loading Plastic Zone Interaction

the results of the plate tests, within certain spacing limitation this interference of slip fields is beneficial in reducing sinkage (and drag reduction if inference of rolling tire performance is valid). For spacings less than approximately 1-1/2 times the plate diameter, the adjacent load effects are detrimental since the two loaded areas tend to act as a single load as indicated in Figure 14b.

In general, then, the results of the vertical twin-plate tests conducted in sand and clay have shown:

1. Within certain spacing limitations, the presence of an adjacent loaded area will cause a reduction in sinkage (over that which occurs for a single plate) for plates under similar vertical load conditions.

2. Optimum spacing very likely exists leading to the maximum reduction in sinkage. This phenomenon is suggested by both the plate tests results and an analysis of bearing capacity theory.

If the performance of rolling twin tires can be inferred from the results of plate tests based on sinkage interaction, then reductions in rolling tire drag (for relatively low sinkages) can be expected through use of twin type tire configurations with proper spacing.

4. PART 3 - Analytical Approach

A. Twin Wheel

The analytical approach employed in studying the multiwheel effects on sinkage and drag is similar to that employed previously in the single wheel analysis[1]. Multiwheel effects on the sinkage of the tire into the soil were first studied and then related back to drag by use of previously established drag-sinkage relationships.

The sinkage of a multiwheel landing gear configuration is different from that of a single wheel primarily due to the difference

21

in stress distribution and yielding patterns within the soil medium resulting from the interactions of the other tires. For a twin wheel configuration, since both wheels are moving about the same wheel axis, the interaction effect is instantaneous. For tandem-tracking wheel configuration, since one wheel is moving in front of the other, the interaction effect is over a certain time period; the stress and yielding pattern in a region of soil rolled over by the front wheel changes over the time period it takes for the trailing wheel to arrive in the region for interaction.

As an initial approach to studying the multiwheel interaction effects, the sinkage prediction technique for the stationary vertical pulse load problem was first developed. This technique for a vertical pulse load problem is similar to the one considered for the single wheel analyzed in Phase II[1] of this research program, except that two surface contact pressure distributions instead of one are applied on the surface. Since the interaction effect is simultaneous, this problem simulates the twin wheel configuration. Tandem wheel configuration will be considered in a later section in which rolling multiwheels are studied.

In the following paragraphs, the two-dimensional plane strain approximation, the multiwheel effects evaluation, and the method of solution of the vertical pulse load problem are discussed.

Two-Dimensional Plane Strain Approximations

The vertical pulse load problem with two surface contact pressure distributions is a three-dimensional problem and its solution by the lumped parameter iteration method or the finite element method would require the use of a three-dimensional space mesh. Comparison of this problem with the three-dimensional moving single wheel problem considered in Phase III[11] indicated that the computer run time required for this analysis would be quite excessive in relation to the benefit in results that might be obtained, and the problem with computer core capacity would be difficult to overcome. Therefore, the two-dimensional plane strain approximated problem was used in the analytical development.

22

The two-dimensional problem is much less difficult in comparison to the three-dimensional problem, and yet, can give a reliable indication of the influence of the stress distribution within the soil on the sinkage. The reason is that the stress distribution in the region immediately between the tires is the major influence on the sinkage due to the twin wheel configuration, and the stress distribution in this region for the three-dimensional problem is quite similar to that for the two-dimensional problem.

The Two-Dimensional Multiwheel Vertical Pulse Load Problem

The two-dimensional problem considered is a semi-infinite half-space soil medium with two infinitely long uniformly distributed pressure strips applied on the surface. The magnitude of the uniform pressure varies with time and was taken to be equal to the average pressure experienced by a point near the surface of the soil when a rolling tire moves across the point. The pressure-time dependence has been measured experimentally for land vehicles[12,13] and has the form of a pressure pulse as shown in Figure 15. This pressure-time curve is the same as the one used in the single wheel analysis[1]. A sectional view of the soil medium with the applied pressure is shown in Figure 16. In this figure, the width of each pressure distribution, b, is equal to the tire footprint width of the twin wheel configuration. It can be seen that the x=0 plane is a plane of symmetry; therefore, it is necessary only to consider half of the soil medium and use symmetry boundary conditions at the x=0 plane.

The Elastic-Plastic Soil Medium

A review of the existing soil models indicated that the most suitable soil model for the present analysis is an elastic-perfectly plastic material with the elastic deformations governed by Hooke's law, the plastic
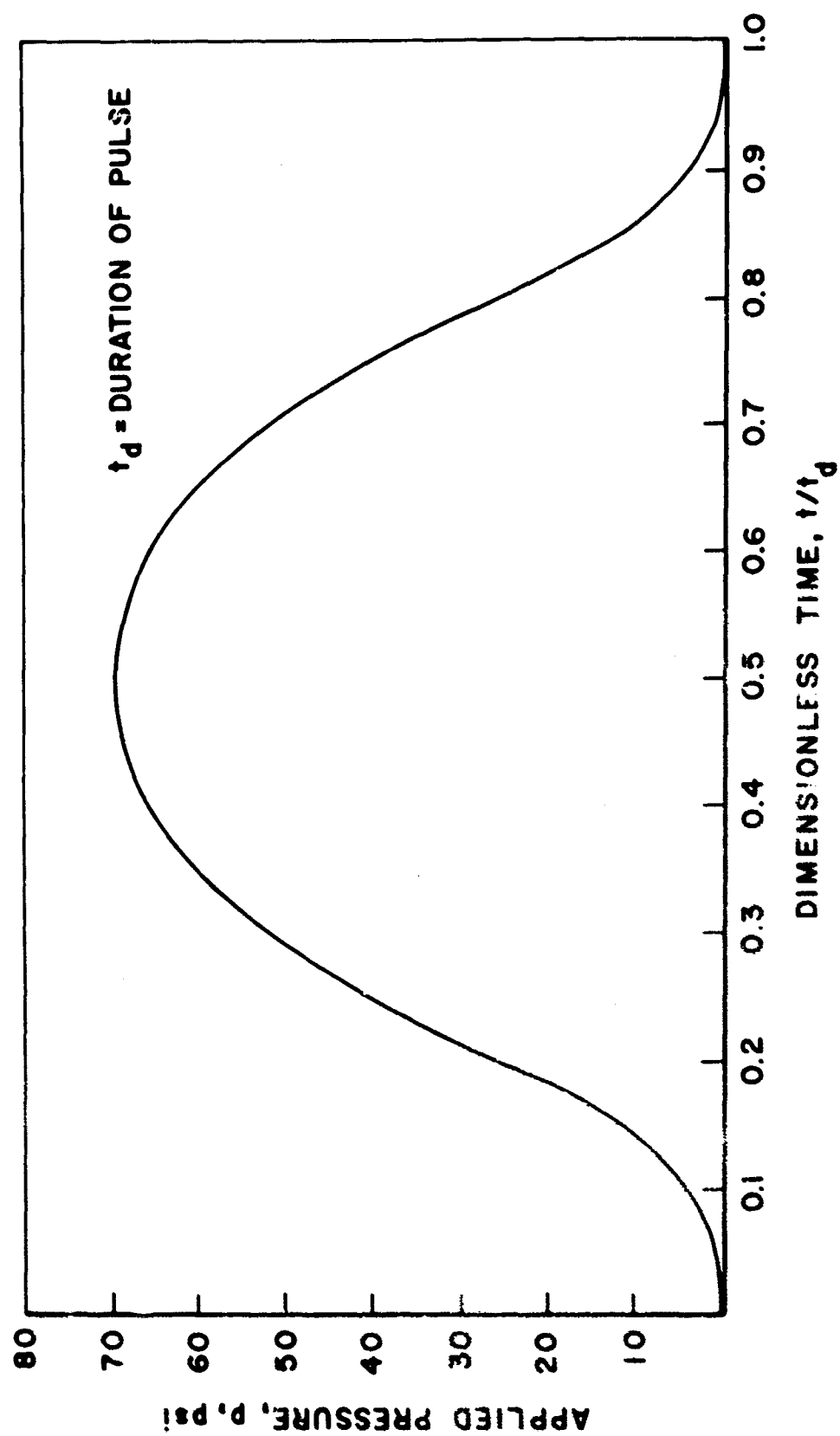
Figure 15. Typical Vertical Impulse Pressure Curve

24
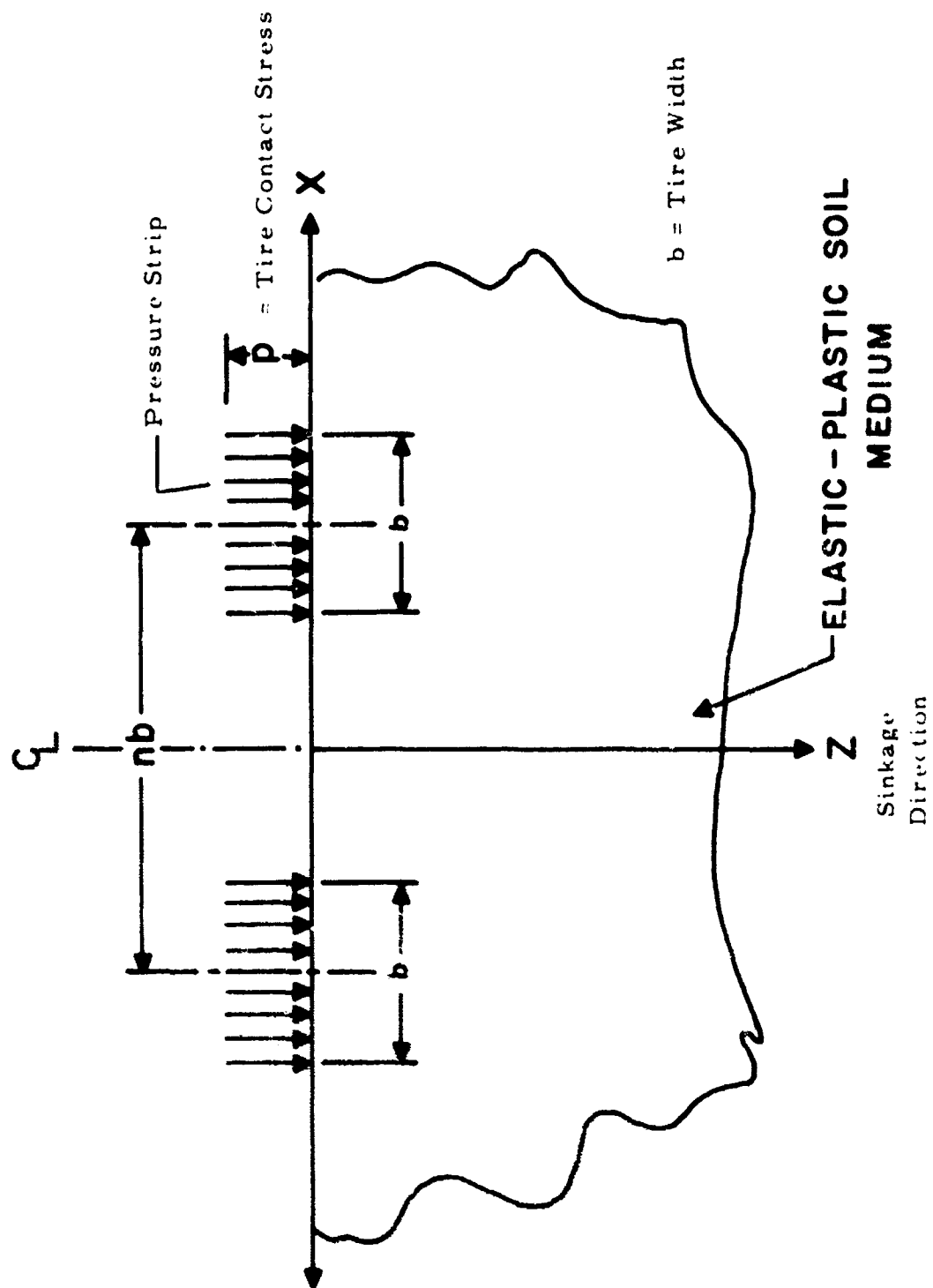
Figure 16. Soil Medium With Applied Pressure Strips for Vertical Load Problem

25

deformations governed by an incremental stress-strain relation which is based on the normality flow rule, and the plastic yielding governed by the Drucker-Prager yield criterion[14, 15]. The soil parameters of this model consist of the elastic Young's modulus, the cohesion, and the friction angle. These parameters can be determined experimentally from soil samples so that analytical results may be compared with experimental results. Strain-hardening was not incorporated in this model because no satisfactory theory with experimentally determinable parameters is currently available.

Method of Evaluation of the Multiwheel Effects

The multiwheel effects were evaluated from the results of the two-dimensional vertical pulse load problem in the following manner. First, the sinkages due to a specific vertical load for various values of tire spacing, nb (see Figure 16), were obtained. The spacing was expressed as nb, where b is the tire width and n is a numerical factor greater than or equal to one. For example, spacings for twin wheel of n = 1.6, 2.3, 3.1, 3.9, 4.7, 5.4, and infinity were analyzed, where the case for n=∞ corresponds to the single wheel problem and is the same as the case for n=0. The multiwheel effects were then evaluated by studying the ratio of the sinkages for n≠∞ (twin wheel) and that for n=∞ (single wheel).

Method of Solution - Lumped Parameter Iteration Method

In the lumped parameter iteration method, a lumped parameter model is used for developing the governing equations. The model chosen for the two-dimensional plane strain problem is quite similar to that for the axisymmetric problem used in the single wheel analysis. It also is composed of alternately interwoven mass and stress points, except that the points are oriented at a 45 degree angle from the soil surface as shown in Figure 17. A (η, ζ) coordinate system is used for designating the diagonal directions, and the ζ-coordinate is used for indicating the

26
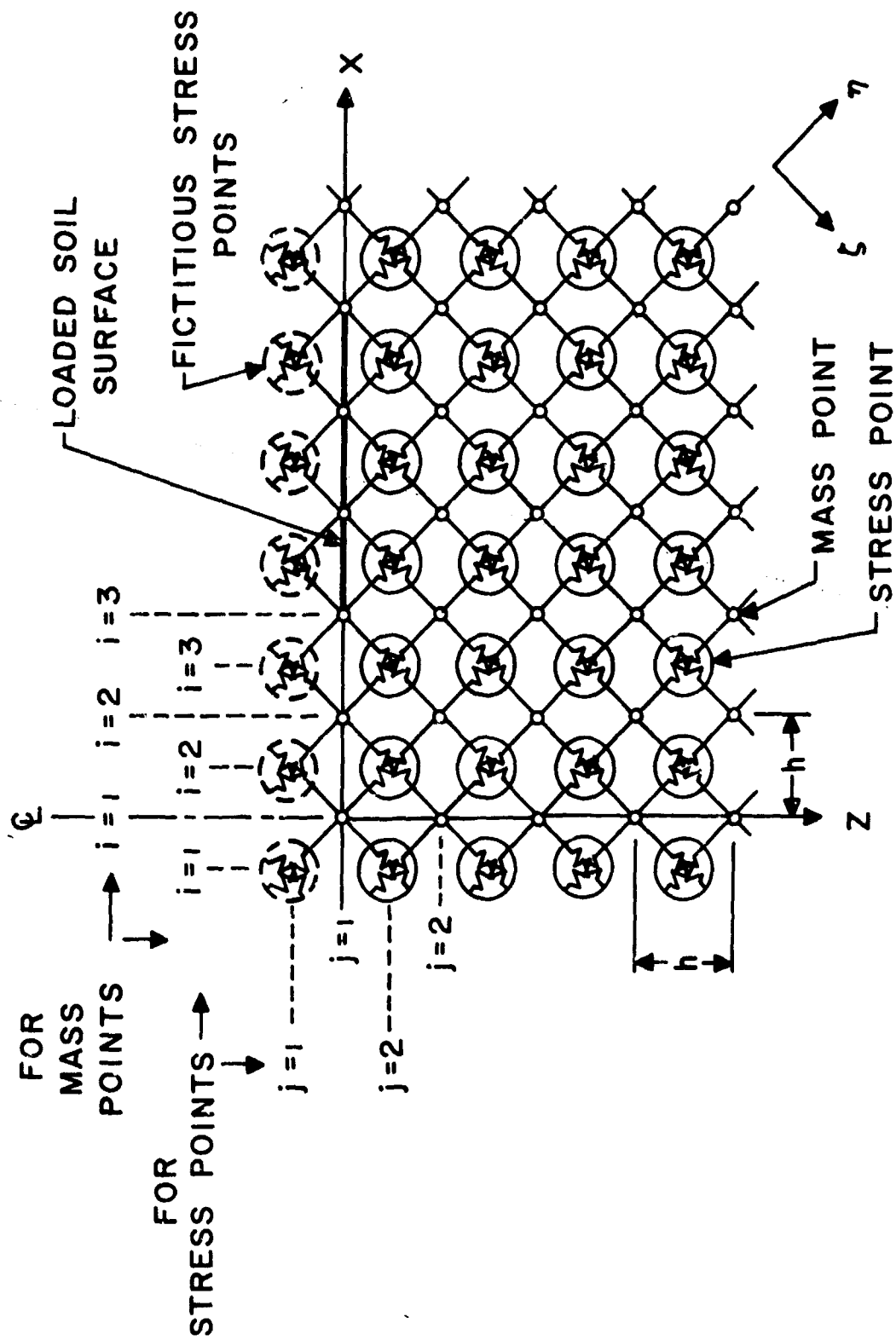
Figure 17. Lumped Parameter Model for Plane Strain

direction normal to the η and ζ coordinates (that is, normal to the plane of the paper). The displacements in the η and ζ directions are U and V, respectively. Then, the displacements, u and w, in the x and z directions are related to U and V as follows:

$$u = U \cos45° - V \sin45° = \frac{\sqrt{2}}{2}(U-V) \tag{2}$$

$$w = U \sin45° + V \cos45° = \frac{\sqrt{2}}{2}(U+V) \tag{3}$$

and the stresses σ_x, σ_z, and τ_{xz} are related to σ_η, σ_ζ, and $\tau_{\eta\zeta}$ by the transformation equations,

$$\sigma_x = \frac{\sigma_\eta + \sigma_\zeta}{2} - \tau_{\eta\zeta} \tag{4}$$

$$\sigma_z = \frac{\sigma_\eta + \sigma_\zeta}{2} + \tau_{\eta\zeta} \tag{5}$$

$$\tau_{xz} = \frac{\sigma_\eta - \sigma_\zeta}{2} \ , \tag{6}$$

and

$$\sigma_\varepsilon = \nu(\sigma_\eta + \sigma_\zeta) \quad . \tag{7}$$

The pressure boundary conditions are applied on the soil surface, z=0, through a row of fictitious stress points (Row j=1 in Figure 17). Outside the loaded surface, the normal and shear stresses of the fictitious stress points are zero. At the fictitious stress points which are above the loaded area, σ_z=-p, σ_x=0, and τ_{xz}=0, where the prescribed surface shear stress was assumed to be zero for the present problem. With the inversion of the transformation equations, Equations (4), (5), and (6), the stresses at the loaded fictitious stress points in the 45 degree directions were obtained as follows:

$$\sigma_\eta = \frac{\sigma_x + \sigma_z}{2} + \tau_{xz} = -\frac{p}{2} \tag{8}$$

28

$$\sigma_\zeta = \frac{\sigma_x + \sigma_z}{2} - \tau_{xz} = -\frac{p}{2} \qquad (9)$$

$$\tau_{\eta\zeta} = \frac{\sigma_z - \sigma_x}{2} = -\frac{p}{2} \qquad (10)$$

where p is the prescribed surface pressure according to the pressure pulse curve.

An advantage of this plane strain model over the axisymmetric model is that there are no stress points at the surface plane whose vertical stresses must be approximated.

Governing Equations, Numerical Procedures, and Computer Programs

The governing equations for this problem are the dynamic equations of motion, the quadrature equations, the yield criterion, the incremental strain-displacement relations, the incremental stress-strain relations, and the equations for stress correction. The derivations of these equations and the development of the numerical procedures for the plane strain lumped parameter model follow the same basic approach as those for the axisymmetric model used in the single wheel analysis, so they are not repeated here. The reader is referred to Reference 13 for the approach used in the derivations and the development of the numerical procedures. For convenience, the governing equations and the numerical procedures are presented without derivation in Appendix II. A computer program was written based on these governing equations and numerical procedures. A general flow chart of the computer program is shown in Figure 18. A Fortran IV source program listing of the computer program, a sample set of input data, a list of definition of symbols, and some remarks about running the computer program are given in Appendix III.

Test Cases and Results

Seven cases were run with the computer program developed for twin wheel simulation. All the cases have the same soil, load, and

29
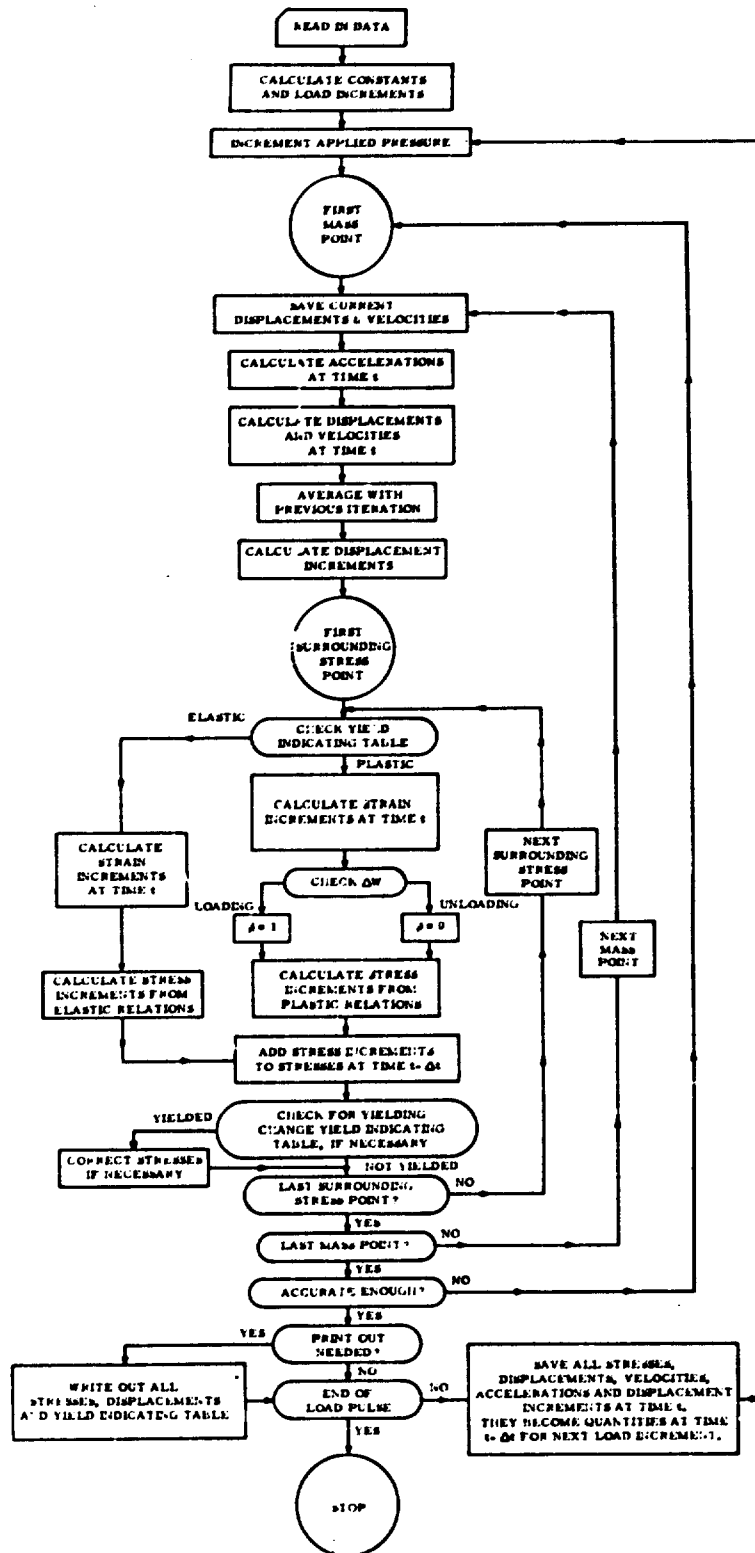
Figure 18.   Flow Chart of Computer Program

computational parameters, which are listed below. This set of parameters
is that of a typical multiwheel aircraft tire-soil interaction.

Soil Parameters:

Density	ρ = 130 lb./cu. ft.
Poisson's ratio	ν = 0.45
Young's Modulus	E = 8950 psi
Cohesion	c = 2000 psf
Friction angle	φ = 15°
Yield stress in shear	k = 2440 psf

(These soil parameters correspond approximately to a clay soil with
CBR = 8 to 10.)

Load Parameters:

Tire Footprint Width	b = 12.0 inches
Peak Surface Pressure	p_{max} = 24600 psf
Time Duration of Pulse	t_d = 0.05 sec.

Computational Parameters:

Space Mesh Size	h = 3.0 inches
Time Increments	Δt = 6.25 x 10^{-5}
Finite Boundary Size	Depth = 60"
	Width = 69" to 111" from the line of symmetry

The only difference between each of the cases is wheel
spacing. One of the cases corresponds to the single wheel case, $n'=\infty$
(or $n'=0$), and the rest of the cases correspond to twin wheel configurations
with spacing ratios of $n'=1.6$, 2, 3, 3.1, 3.9, 4.7, and 5.4. In order to
minimize the influence of the finite boundary on the sinkage when the
wheel spacings were changed, the distance between the finite boundary and
the edge of the applied pressure strip was maintained constant by changing
the distance of the finite boundary from the line of symmetry. The peak
instantaneous sinkages for each case and their comparison with that for

31

the single wheel case are shown in Table 5. Sinkage in this analysis
was taken as the average of the vertical displacements of the mass points
which are immediately under the applied surface pressure distribution.

TABLE 5

TWIN WHEEL SINKAGES FOR DIFFERENT WHEEL SPACINGS

Case	Spacing Ratio n'	Instantaneous Sinkage, Z (inches)	Z_{Twin}/Z_{Single}	Dimensionless Sinkage, Z/b
1	∞	0.48	1.000	0.0403
2	1.6	0.51	1.050	0.0423
3	2.3	0.45	0.942	0.0379
4	3.1	0.43	0.886	0.0357
5	3.9	0.42	0.871	0.0351
6	4.7	0.43	0.882	0.0355
7	5.4	0.43	0.900	0.0362

In Figure 19, the sinkage for twin wheel, normalized with
respect to the sinkage for single wheel ($n'=\infty$), is plotted against the wheel
spacing ratio, n'. This curve shows that as wheel spacing decreases
from infinity, the sinkage gradually decreases due to the interaction
between the two tires, and reaches a minimum at a particular wheel
spacing. The wheel spacing corresponding to the minimum sinkage
probably depends on many factors, for example, intensity of wheel load,
size of contact area, soil strength, etc. For the particular loads and
soil conditions of these test cases, the minimum falls between $n'=3.0$
and $n'=4.5$. Further decrease of the wheel spacing from the minimum
sinkage point leads to higher sinkage because the soil medium between
and under the twin contact area starts to interact strongly and begins to
act as a whole mass similar to that underneath a single wheel.

The trend of the curve shown in Figure 19 was also exhibited
in the experimental results obtained from the dual circular plate vertical
load test given in Section II - Part 2 and shown in Figure 13. The plate
tests showed the minimum sinkage as occurring between $n'=2$ and $n'=3$.

32
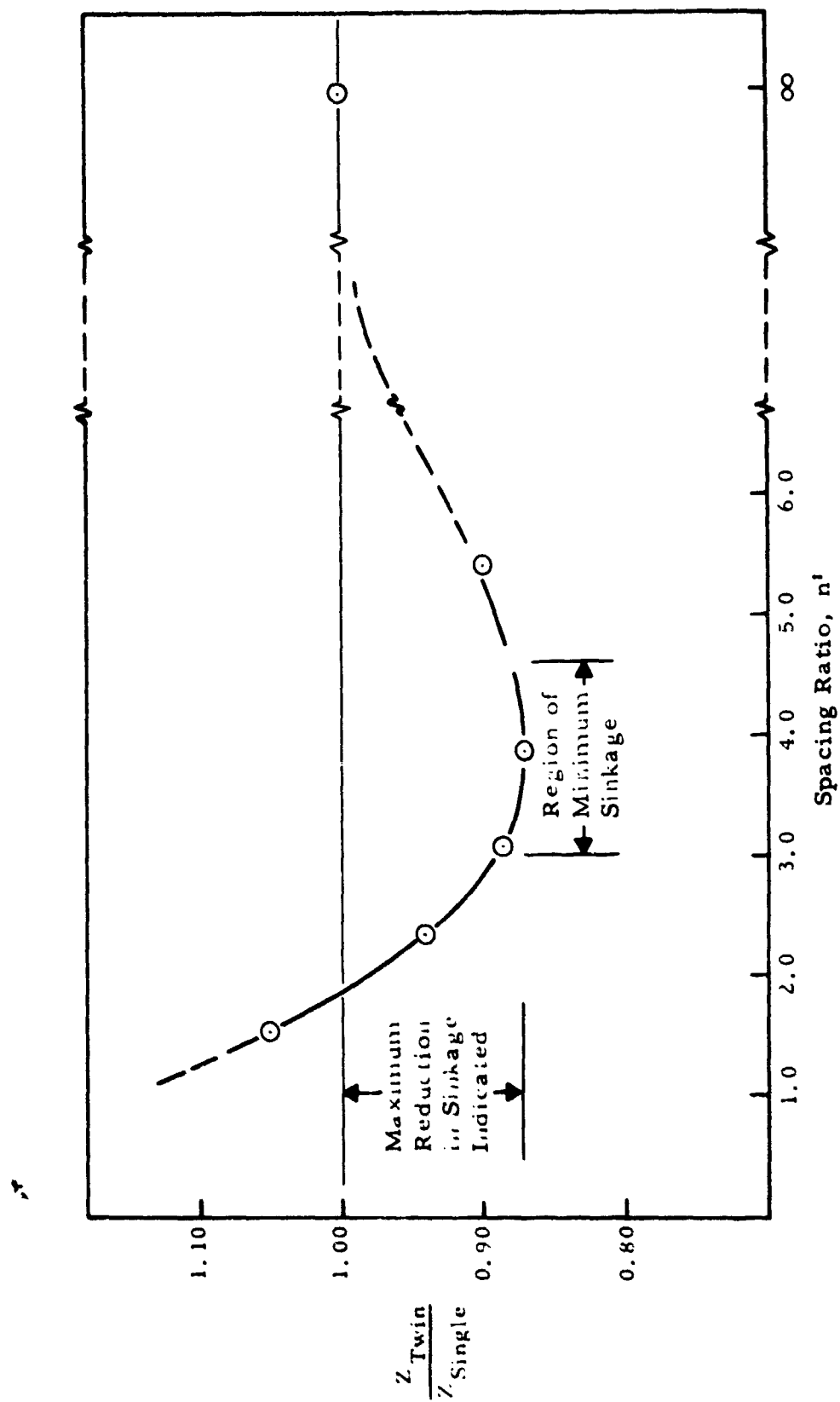
Figure 19. Z_{Twin}/Z_{Single} vs. Wheel Spacing, Clay Soil

33

Consideration of the ideal slip line field using Terzahgi bearing capacity theory[10] also indicated that the minimum sinkage probably falls between $n'=2.5$ and $n'=3.5$ for clays.

The vertical displacements of the surface mass points were plotted against the horizontal distance from the axis of symmetry for several times during the downward movement of the soil surface. These graphs are shown in Figure 20, 21, 22, and 23 for $n'=\infty$, $n'=1.6$, $n'=3.1$, and $n'=4.7$. The comparison of these graphs shows the difference of the patterns of soil surface deflection, w_s, for the various wheel spacings. In particular, the deflection pattern for $n'=1.6$ is more similar to the pattern for a single large contact area than that for $n'=3.1$. This shows the reason why the sinkages for n between 1.0 and 2.0 tend to be higher than that for $n'=3.1$.

Some preliminary test cases[16] run with a smaller finite boundary size and a smaller grid size show the same results as those reported here, but because of the limited boundary size, some influence of the finite boundary was evident.

With the present computer program, soil parameters, load parameters, and computational parameters, the length of computer run time required for each case is approximately 40 minutes. With the completion of the CDC 6600 computing facility at WPAFB, this computer run time can be reduced considerably thus permitting the evaluation of additional cases to determine the dependency of optimum spacing on the load and soil parameters.

B. Rolling-Tandem Wheels

The stationary vertical pulse load problem discussed in the preceding sections does not simulate the tandem wheel configuration because of the time-lapse effect between leading and trailing wheels.

34
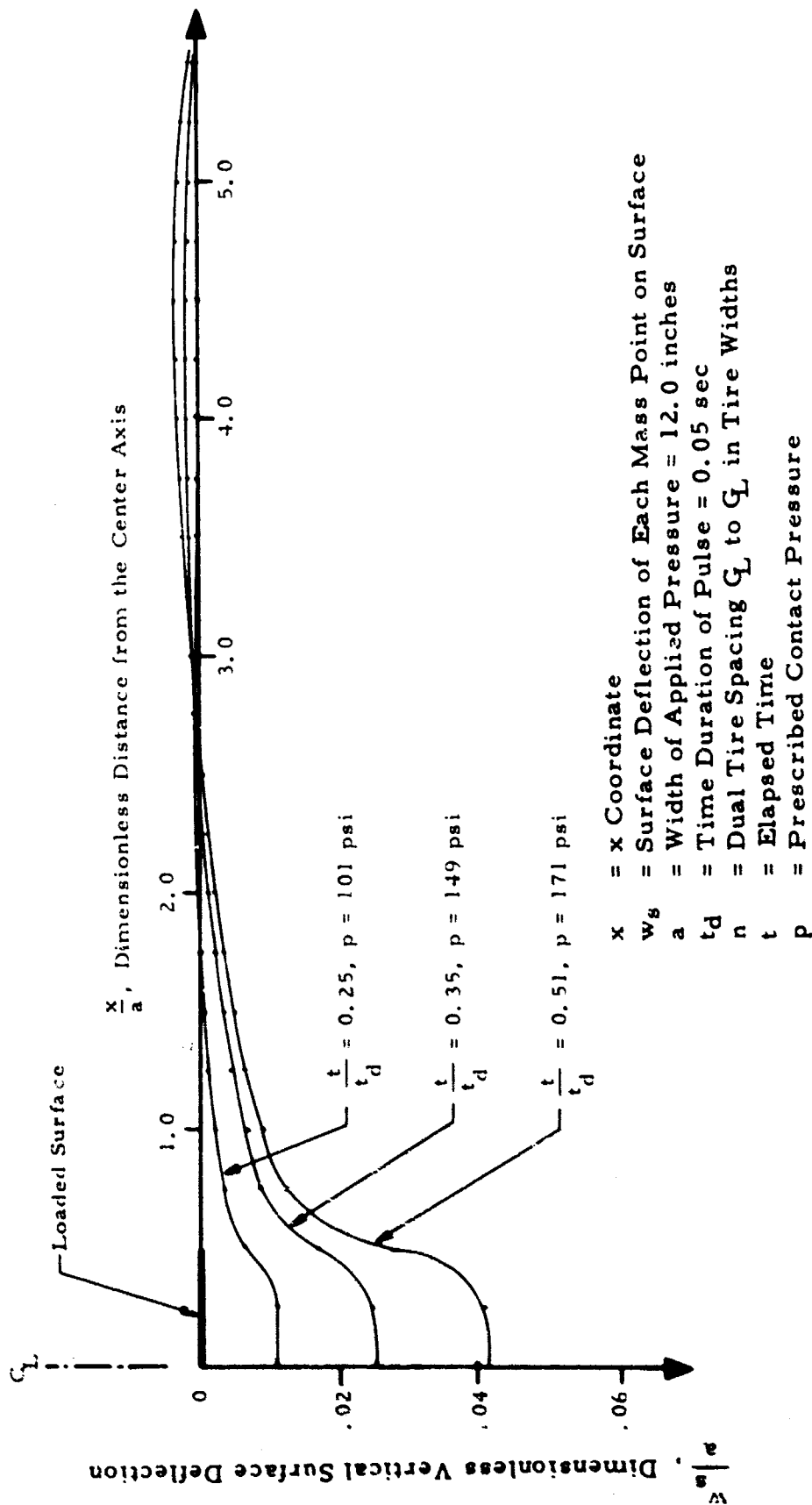
Figure 20. Vertical Deflection of Soil Surface vs. Distance from the Axis of Symmetry for Case n = ∞

x = x Coordinate
w_s = Surface Deflection of Each Mass Point on Surface
a = Width of Applied Pressure = 12.0 inches
t_d = Time Duration of Pulse = 0.05 sec
n = Dual Tire Spacing C_L to C_L in Tire Widths
t = Elapsed Time
p = Prescribed Contact Pressure

$\frac{t}{t_d}$ = 0.25, p = 101 psi

$\frac{t}{t_d}$ = 0.35, p = 149 psi

$\frac{t}{t_d}$ = 0.51, p = 171 psi

$\frac{x}{a}$, Dimensionless Distance from the Center Axis

$\frac{w_s}{a}$, Dimensionless Vertical Surface Deflection

Loaded Surface

35
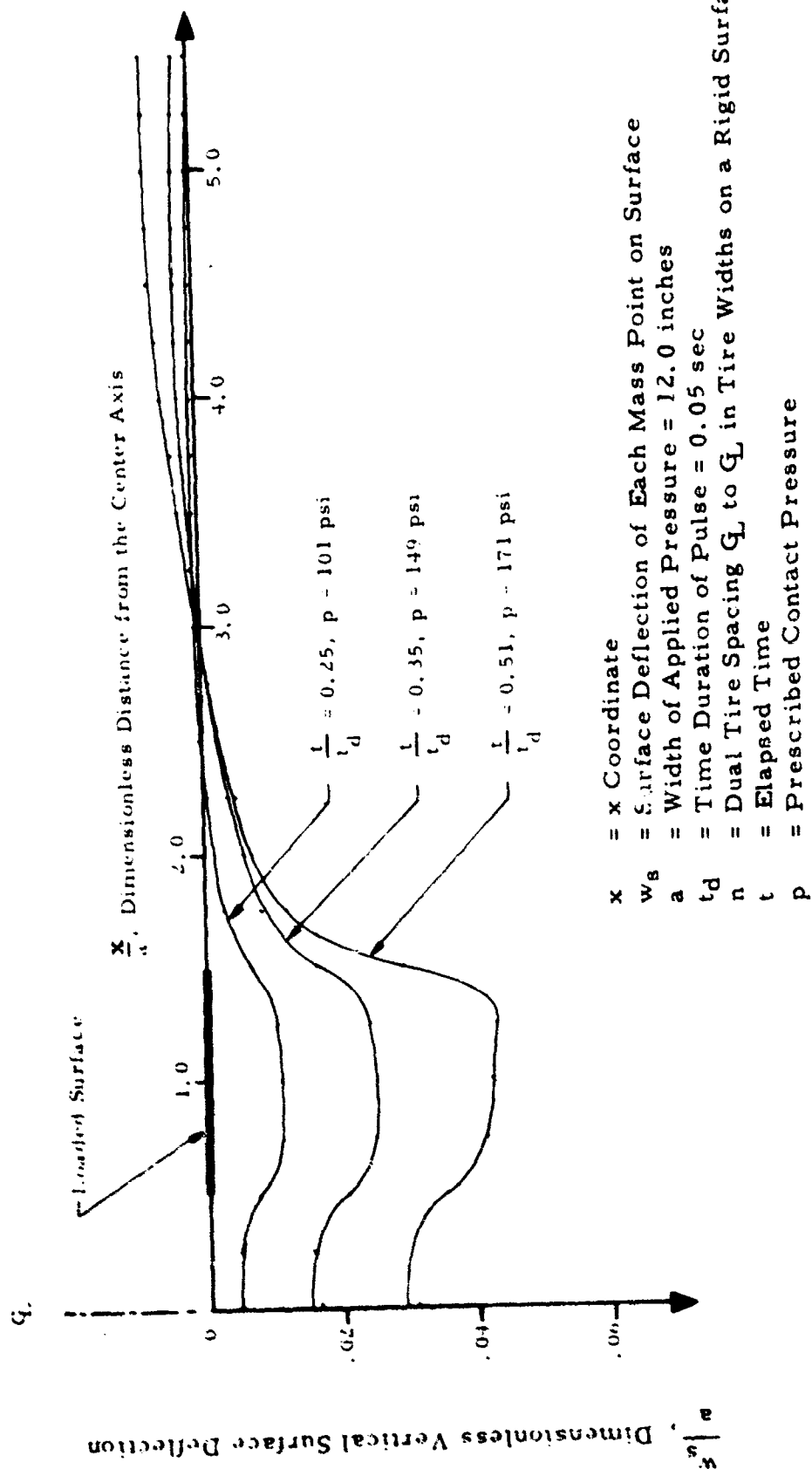
Figure 21. Vertical Deflection of Soil Surface vs. Distance from the Axis of Symmetry for Case n = 1.6
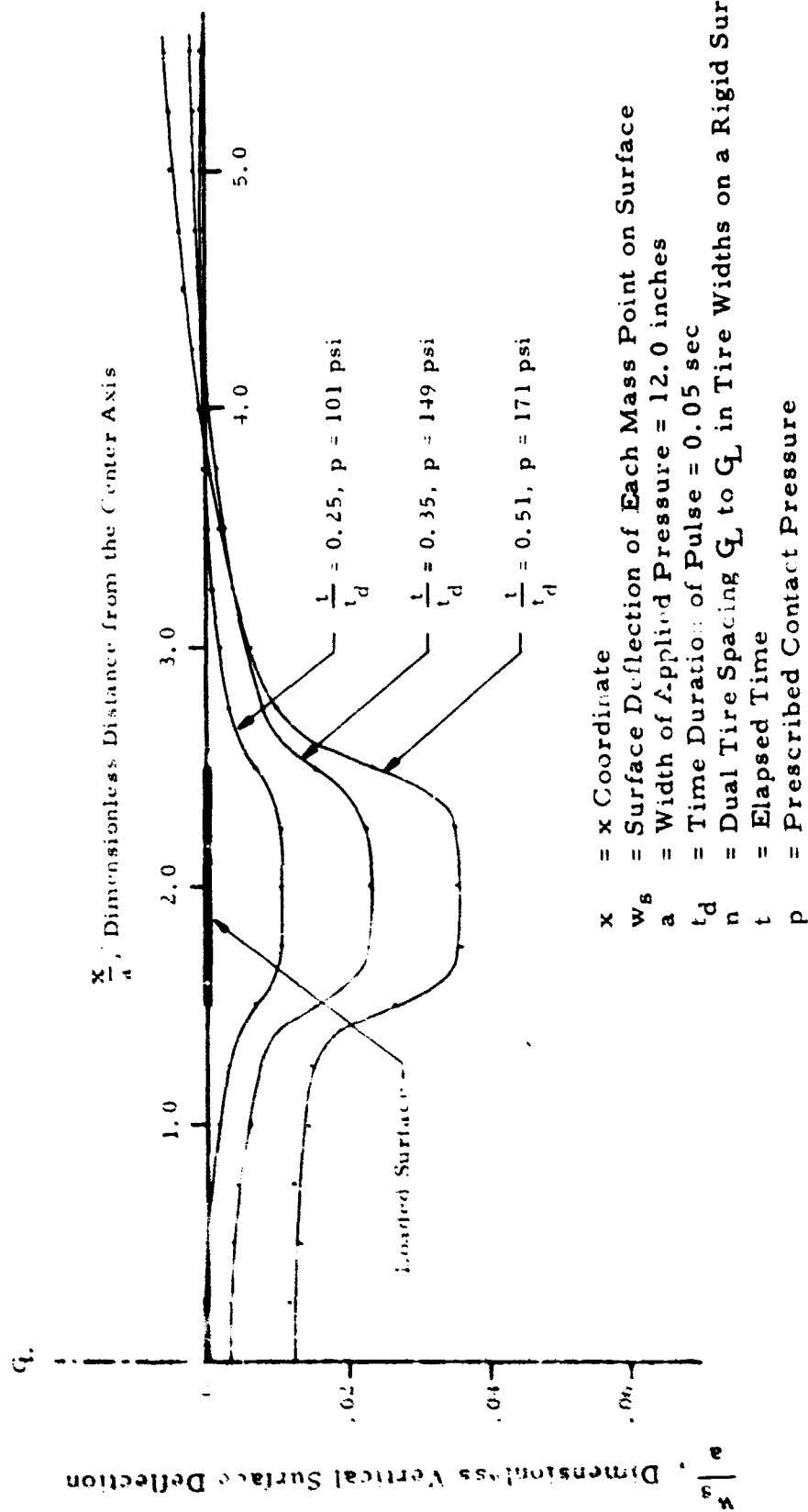
Figure 22. Vertical Deflection of Soil Surface vs. Distance from the Axis of Symmetry for Case n = 3.1

x = x Coordinate
w_s = Surface Deflection of Each Mass Point on Surface
a = Width of Applied Pressure = 12.0 inches
t_d = Time Duration of Pulse = 0.05 sec
n = Dual Tire Spacing C_L to C_L in Tire Widths on a Rigid Surface
t = Elapsed Time
p = Prescribed Contact Pressure

$\frac{t}{t_d}$ = 0.25, p = 101 psi

$\frac{t}{t_d}$ = 0.35, p = 149 psi

$\frac{t}{t_d}$ = 0.51, p = 171 psi

$\frac{x}{a}$, Dimensionless Distance from the Center Axis

$\frac{w_s}{a}$, Dimensionless Vertical Surface Deflection

47

Figure 23. Vertical Deflection of Soil Surface vs. Distance from the Axis of Symmetry for Case n = 4.7

x = x Coordinate
w_s = Surface Deflection of Each Mass Point on Surface
a = Width of Applied Pressure = 12.0 inches
t_d = Time Duration of Pulse = 0.05 sec
n = Dual Tire Spacings G_L to G_L in Terms of Rigid Surface Tire Width
t = Elapsed Time
p = Prescribed Contact Pressure

$\frac{t}{t_d}$ = 0.25, p = 101 psi

$\frac{t}{t_d}$ = 0.35, p = 149 psi

$\frac{t}{t_d}$ = 0.51, p = 171 psi

Loaded Surface

$\frac{x}{a}$, Dimensionless Distance from the Center Axis

$\frac{w_s}{a}$, Dimensionless Vertical Surface Deflection

In progress, however, is the development of a computer program to simulate multiwheel effects in rolling tandem wheel configurations. For the same reasons given in developing the twin wheel simulation format, the actual three-dimensional problem for rolling tandem wheels was approximated by the corresponding two-dimensional plane strain problem.

The Two-Dimensional Plane Strain Approximation

The two-dimensional plane strain approximation to the problem for rolling tandem wheels has the same pressure boundary condition and soil medium assumption as for the stationary vertical load pulse problem. The differences are as follows:

a) The two infinite pressure strips move in the x-direction at the aircraft ground velocity, as shown in Figure 24a.

b) The pressure-time dependence is different. As the pressure strip moves, the uniform pressure is increased gradually to a pressure equal to the landing gear vertical load divided by the total contact area, as shown in Figure 24b. The manner and rates at which the pressure is increased initially depends on the stability of the numerical calculation and the rate with which steady state is achieved.

c) There is no longer a plane of symmetry between the pressure strip, so two applied pressure strips must be considered.

d) The width of each applied pressure strip is equal to the tire footprint length, ℓ, and the wheel spacing is expressed as mD, where m is a fraction of tire outside diameter and D is the tire outside diameter see Figure 24).

Method of Solution-Lumped Parameter Iteration Method

The method of solution of the two-dimensional problem for rolling tandem wheels is similar to the method of solution for the vertical load (multiwheel) problem. The method of prescribing the boundary conditions, governing equations, and numerical procedures is the same. The governing equations, presented in Appendix II, are also applicable

mD

V

V

p

X

elastic — plastic soil medium

ℓ

ℓ

Z

V = Aircraft Horizontal Ground Velocity

ℓ = Tire Footprint Length
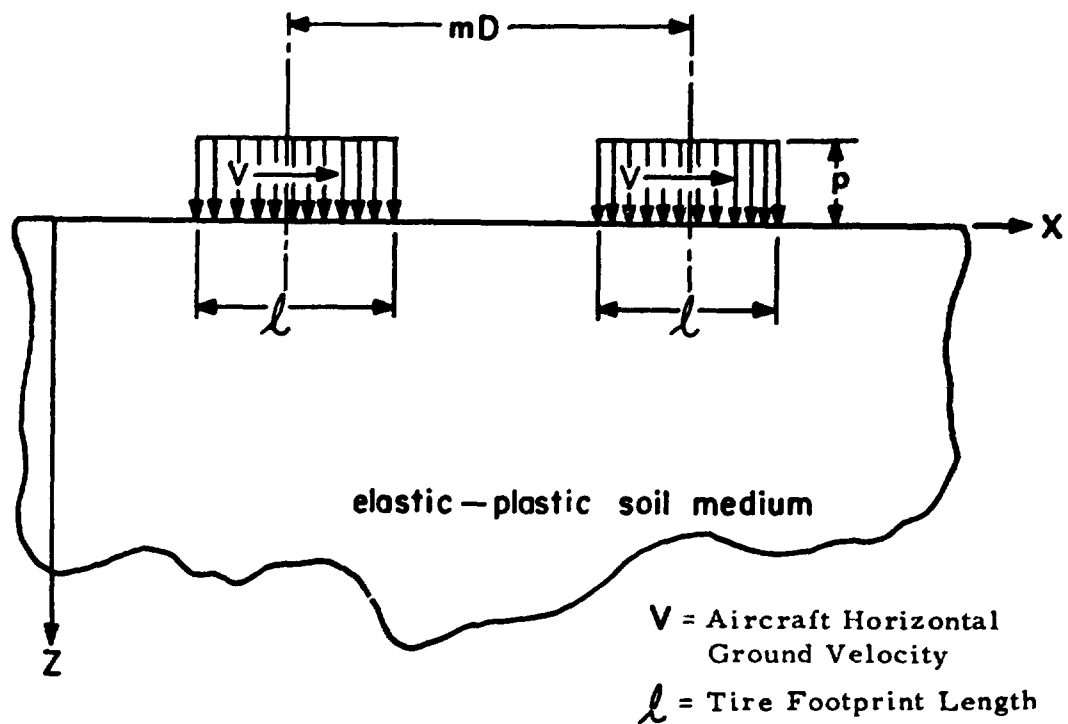
(a) Soil Medium with Moving Strip Pressure

P = Vertical Tire Load

A = Tire Contact Area

t_r = Rise Time

$\frac{P}{A}$

t_r

p

t
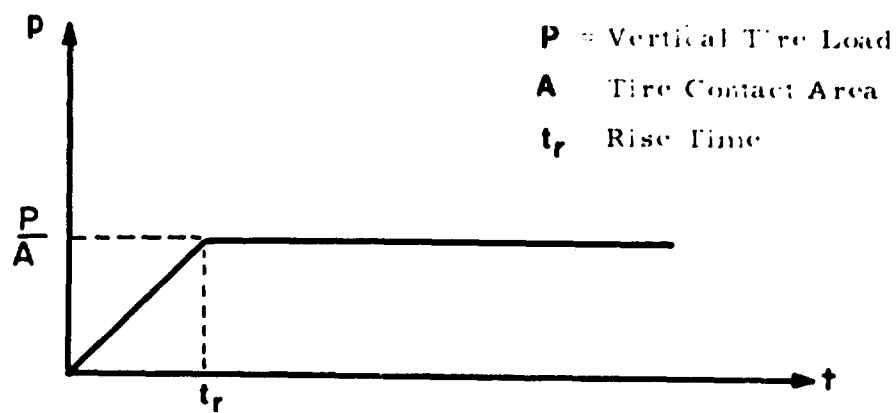
(b) Pressure-Time Curve

Figure 24. Rolling Tandem-Wheel Interface Boundary Condition

here. The main difference was the boundary condition defined by the two moving pressure strips. The pressure strip distributions were moved in the x-direction at the aircraft horizontal ground velocity, V, in the following manner. The prescribed equivalent pressure exerted on the mass point located at the extreme left of each loaded area was reduced to zero in incremental steps through the time h/V; at the same time, the equivalent pressure exerted on the mass point located at the extreme right of each loaded area was increased incrementally from zero to the prescribed value in the same manner.

Method of Evaluation of the Multiwheel Effects

The method for evaluating the multiwheel effects of the rolling tandem wheel configuration from the results of the two-dimensional moving pressure strips problem is as follows: First, the case with m=0 corresponding to the single moving wheel is run and the drag, R_{Single}, is obtained from its sinkage (see Equation 1). Then, the cases with other values of m are run and, for each case, the total drag, R_{Tandem}, is obtained from summing the drags corresponding to the sinkages of the leading and trailing pressure strips. The multiwheel effects are then evaluated by studying the ratio,

$$\frac{\left(\dfrac{R_{Tandem}}{P} \right)}{\left(\dfrac{R_{Single}}{P} \right)}$$

for various wheel spacing factor, m.

Computer Program and Test Cases

A computer program has been written based on the method of solutions just outlined. This program is now being used to evaluate the tandem-tracking cases with wheel spacing factors of m=∞, 1.05, 1.5, and 2.0. All these cases have the same soil, load, and computational parameters, and these parameters are the same as those used in the twin wheel cases conducted. The complete results of all the cases, together with the listing of the final computer program, will be presented at a later date as a Research and Development computer program interim report.

41

5.   PART 4 - Multiwheel Verification Tests

Purpose

The purpose of this test program was to study the variables that control the performance of aircraft tire flotation while operating in multiwheel configurations. The program provided data to:

1) confirm the preliminary multiwheel flotation performance criteria with tires operating in twin, tandem, and tandem-nontracking configurations;

2) use in the development of semi-empirical relationships for the extension of the single wheel prediction equations to multi-wheel data; and

3) aid in preliminary verification of the finite element based analytical rolling wheel sinkage prediction techniques (both twin and tandem) currently under development.

During the testing, the effects of twin wheel spacing, tandem wheel spacing in tracking configuration, and wheel offset combined with tandem spacing in the nontracking configuration were investigated with the objective of evaluating the drag modification effects of the various spacings.

Test Program

In order to accomplish the objectives, the following test program was designed such that the sinkages and drag loads would be in the range of application to aircraft flotation analysis. The test program, which is shown in Table 6 for clay type soil and in Table 7 for sand type soil, was designed for a Type III 7.00-6, 6 PR tire with a 35% operating deflection. Each multiple wheel configuration had two 7:00-6 tires equally loaded and all tests were run at 10 fps. The following parameters were measured for each test:

Vertical Load

Drag Load

Tire Deflection

42

TABLE 6

Multiwheel Test Program for Clay Soil

Bogie Configuration	Soil Strength CI_{avg} (psi)	Vertical Assembly Load (#) P	Lateral Spacing nb	Longitudinal Spacing mD
Twin	20-25	1200	1.5b	-
"	"	"	2.0b	-
"	"	"	3.0b	-
"	"	"	4.0b	-
Tandem-Tracking	"	1400	-	2.0D
"	"	"	-	3.0D
"	"	"	-	4.0D
Tandem-Nontracking	"	"	2.0b	2.0D
"	"	"	3.0b	2.0D
"	"	"	3.0b	3.0D
"	"	"	2.0b	2.0D
Twin	"	1000	1.5b	-
"	"	"	1.5b	-
"	"	"	2.0b	-
"	"	"	2.0b	-
"	"	"	3.0b	-
"	"	"	4.0b	-
Tandem-Tracking	"	1200	-	1.5D
"	"	"	-	2.0D
"	"	"	-	3.0D
"	"	"	-	4.0D
Twin	"	800	1.5b	-
"	"	"	1.5b	-
"	"	"	2.0b	-
Tandem-Tracking	"	1000	-	1.5D
"	"	"	-	2.0D
"	"	"	-	3.0D
"	"	"	-	4.0D

TABLE 7

Multiwheel Test Program for Sand Soil

Bogie Configuration	Soil Strength CI_{avg} (psi)	Vertical Assembly Load (#) P	Lateral Spacing nb	Longitudinal Spacing mD
Twin	40-45	1600	1.5b	-
''	''	''	1.75b	-
''	''	''	2.0b	-
''	''	''	3.0b	-
''	''	''	3.0b	-
''	''	''	4.0b	-
Tandem-Tracking	''	1400	-	1.5D
''	''	''	-	2.0D
''	''	''	-	3.0D
''	''	''	-	4.0D
Tandem-Nontracking	''	1400	2b	1.5D
''	''	''	2b	2.0D
''	''	''	2b	3.0D
''	''	''	3b	1.5D
''	''	''	3b	2.0D
''	''	''	3b	3.0D
Twin	''	800	1.5b	-
''	''	''	2.0b	-
''	''	''	3.0b	-
''	''	''	3.0b	-
''	''	''	4.0b	-
Tandem Tracking	''	600	-	1.5D
''	''	''	-	2.0D
''	''	''	-	3.0D
''	''	''	-	4.0D
''	25-30	500	-	1.5D
''	''	600	-	3.0D
Single	40-45	700	-	-
''	''	400	-	-

44

Soil Strength

Soil Sinkage

Wheel Velocity (horizontal)

The lateral and longitudinal spacings listed in Tables 6 and 7 were selected to permit a thorough evaluation of the multiwheel phenomena based on the preliminary multiwheel flotation criteria.

Test Equipment

All multiple rolling wheel tests in the program were conducted at the U.S. Army Waterways Experiment Station, Vicksburg, Mississippi, at the model wheel facility of the Mobility and Environmental Division between the dates of August 25, 1970 and November 12, 1970. WES modified their dynamometer to conduct the multiwheel tests, and provided adequate professional and technician support for conducting the tests. The modified dynamometer shown in Figure 25 used the existing single wheel dynamometer as a frame to mount a lever arm to hold the multiwheel carriage. The lever arm pivot is located at the front of the existing single wheel carriage and applies the load to the geometric center of the multiwheel carriage where the carriage pivots freely. The test data is monitored using some existing instrumentation on the single wheel dynamometer and some new instrumentation mounted on the multiwheel carriage. Figure 25 shows the carriage in a twin wheel configuration with the multiwheel carriage fastened to the lever arm so that it cannot rotate relative to the lever arm. Figure 26 shows the carriage in a tendem configuration with the carriage free to rotate so as to distribute the load equally to each tire. A complete description of the basic Test Facility is available in a previous WES report[17].

Test Tire

In order to improve the correlation between the multiwheel results and previous single wheel testing, the tire size was chosen to be the 7:00-6, 6 PR Type III tire which was used in the single wheel testing program. Table 8 gives the tire geometry data for the two 7:00-6 tires used in this program.
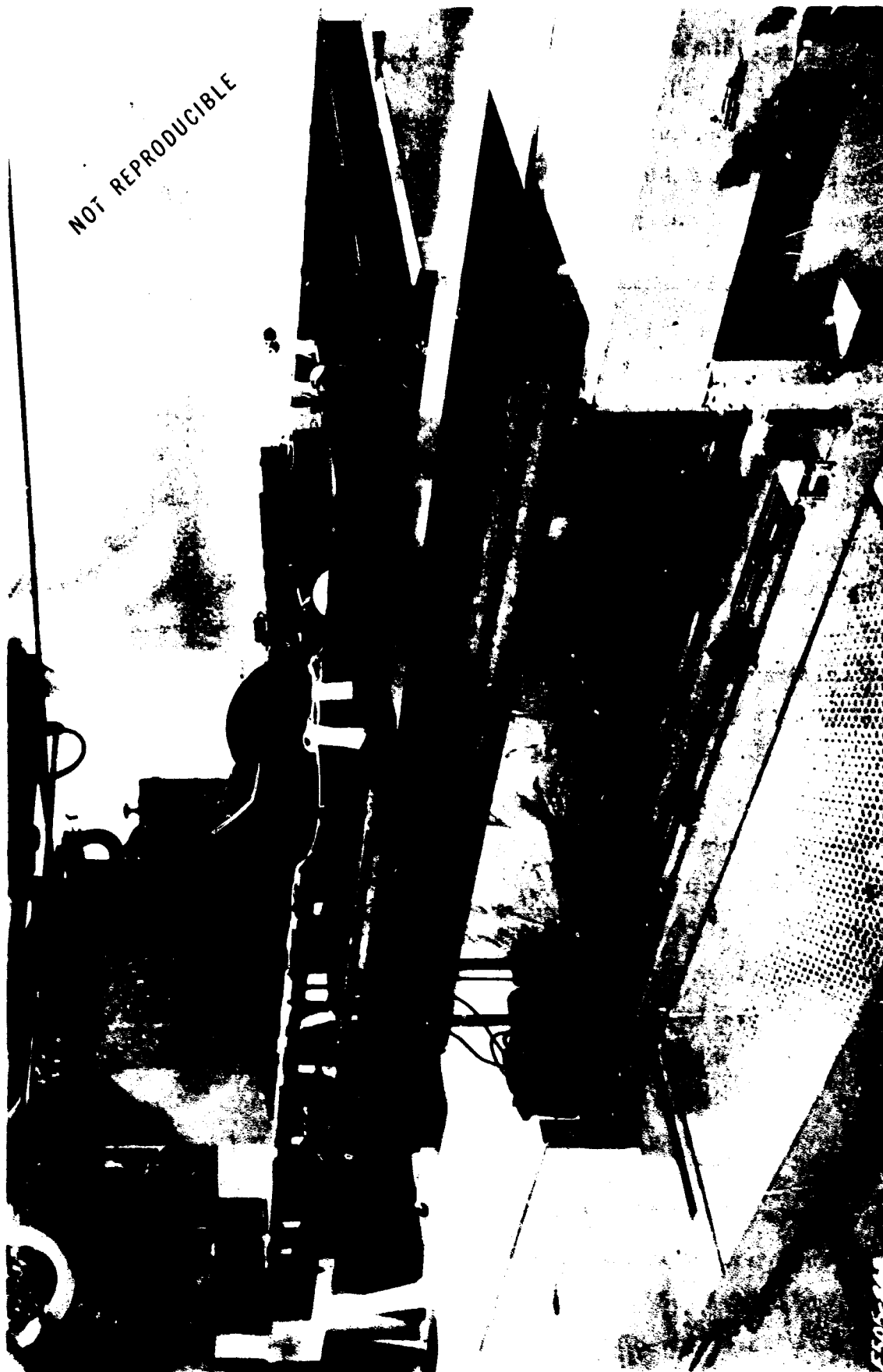
Figure 25. Carriage in Twin Configuration
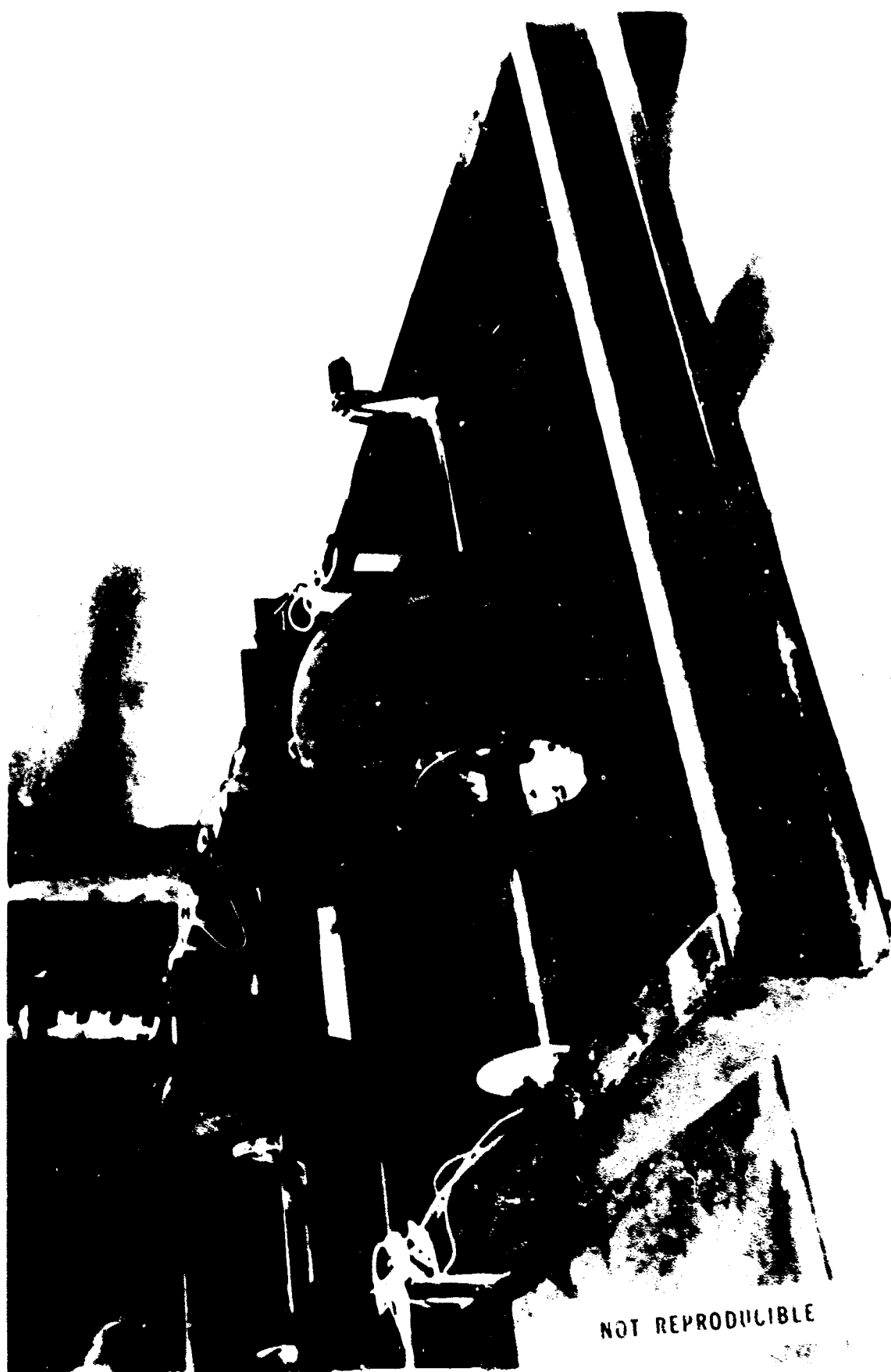
Figure 26. Carriage in Tandem Configuration

NOT REPRODUCIBLE

TABLE 8

Multiwheel Tests - Tire Data

Tire Type	Deflection [%]	Wheel Load P[lbs]	Carcass Dia. D[in]	Contact Area* A[sq.in]	Tire Print			Inflation Pressure		Section Height		Section Width	
					Length* ℓ[in]	Width* b[in]	Deflection* d[in]	Un-loaded [psi]	Loaded [psi]	Un-loaded [in]	Loaded [in]	Un-loaded [in]	Loaded [in]
7.00-6-6PR (west tire for twin tests; rear tire for tandem tests)	35	300	17.58	45.58	9.32	5.50	1.76	2.15	3.05	5.04	3.28	6.72	7.87
"	"	400	17.62	44.02	8.60	5.58	1.77	2.40	4.70	5.06	3.29	6.72	7.88
"	"	500	17.74	43.48	8.71	5.63	1.79	5.25	5.90	5.12	3.33	6.75	7.81
"	"	600	17.78	44.49	8.95	5.70	1.81	7.40	8.30	5.14	3.33	6.75	7.84
"	"	700	17.86	43.24	8.82	5.60	1.81	10.3	11.2	5.18	3.37	6.68	7.55
"	"	800	17.82	44.13	8.86	5.50	1.81	12.0	13.1	5.16	3.35	6.75	7.90
7.00-6-6PR (east tire for twin tests; front tire for tandem tests)	35	300	17.58	47.90	9.60	5.42	1.76	2.20	2.80	5.04	3.28	6.62	7.90
"	"	400	17.68	47.85	9.04	5.55	1.78	3.31	4.40	5.09	3.31	6.75	8.00
"	"	500	17.78	44.72	9.14	5.56	1.80	5.40	6.10	5.14	3.34	6.70	7.88
"	"	600	17.86	44.95	9.00	5.65	1.81	7.60	8.50	5.18	3.37	6.70	7.92
"	"	700	17.90	44.58	9.30	5.45	1.82	10.40	11.35	5.20	3.38	6.70	7.98
"	"	800	17.90	44.95	9.00	5.72	1.82	12.50	13.50	5.20	3.38	6.71	7.87

* Data taken with tire loaded on rigid surface. All other data is for unloaded inflated tire.

48

Soil Tests and Preparation

The two soil types chosen for these multiwheel tests were buckshot clay and mortar sand, both of which were used in the previous single wheel testing. Two purposes were fulfilled by the soil tests conducted, first to insure an accurate description of the test soil and its uniformity; second to allow possible correlation to other tire-soil interaction theories by collecting as much information concerning the soil as possible. The soil tests that were conducted are moisture and density determination, mobility cone penetration resistance (CI), and the California Bearing Ratio (CBR). A complete description of each soil test is given in Appendix IV. The summary of the moisture-density determinations are in Table 9. The summary of the correlation data taken to relate CRB and CI_{avg} is presented in Table 10.

TABLE 9

MOISTURE-DENSITY DATA

Soil Type	Design Soil Strength CI_{avg} (0 to 6")	Average Conditions	
		Dry Density γ_d(pcF)	Moisture Content W, (%)
Buckshot Clay	20	75.6	42
Mortar Sand	40	101.6	less than 1.0

TABLE 10

TEST BED SOIL CONDITIONS

Soil Type	Design Soil Strength CI_{avg} (0" to 6")	CI_{avg} 0" to 6"	CBR CBR 0.1"
Buckshot Clay	20	22.3	0.70
Mortar Sand	40	40.4	2.36

Undrained triaxial tests were also run on undisturbed samples of clay and bulk samples of sand taken from the soil carts to determine the cohesion and friction components of the soil strength. These test results, which are described in detail in Appendix IV, are summarized below in Table 11.

TABLE 11

TRIAXIAL TEST RESULTS

Soil Type	Design Soil Strength CI_{avg} (0-6")	Triaxial Results c (psf)	ϕ deg	Moisture Content W %
Buckshot Clay	20	1.79	-	42
Mortar Sand	40	-	36.5	less than 1.0

Test Results - Buckshot Clay

The finalized test results for the 28 tests run in buckshot clay are presented in Table 12. The data presented represents the parameters that were recorded for permanent records in both computer tape format and oscillograph charts. The following comments clarify the column headings and notations. Three tests (numbers 4, 6, and 7) are considered to be void due to excessive sinkage and basic instability of the test carriage during the test run. The spacings listed in the third column represent actual test spacings based on the tire's nominal diameter (D) of 18" and its nominal width (b) of 6.8". The soil strength (CI_{avg}) represents the average of at least five before traffic tests, and is given in terms of the average penetration resistance over the first six inches of soil profile in psi. Soil strength measurements taken in the tire ruts after one pass are given in Appendix IV. Note that the east-west, and front-rear designations have been used consistently to designate the relative position of each tire to the test section.

50

TABLE 12

Multiwheel Drag-Sinkage Data, Clay Soil

Test No.	Type Test	Tire Spacing	Soil Strength (CI_avg)	Vertical Assembly Load P (lbs)	East or Front Rut Depth Z_R (in)	West or Rear Rut Depth Z_R (in)	East or Front Wheel Sinkage Z (in)	West or Rear Wheel Sinkage Z (in)	East or Front Wheel Drag R (lbs)	West or Rear Wheel Drag R (lbs)	Total Wheel Drag R (lbs)	Multiwheel Drag Ratio $(R/P)_M$
1	T	1.5b	24.2	809	0.20	0.20	0.20	0.20	-	-	107.6	.133
2	TT	4.0D	19.7	1014	-	1.04	-	1.24	89.3	114.3	203.6	.201
3	TT	3.0D	21.7	1007	-	0.72	-	1.04	68.7	92.7	161.4	.160
4	TT	3.0D	22.4	1398	-	2.44	-	2.44	207.3	254.3	461.6	.330
5	TT	2.0D	22.6	1011	-	0.42	-	0.53	57.3	79.3	136.6	.135
6	TT	2.0D	23.4	1401	-	1.88	-	2.43	157.9	220.9	378.8	.270
7	TT	4.0D	22.5	1397	-	2.55	-	2.55	226.3	231.6	457.9	.328
8	TT	1.5D	21.1	1007	-	0.86	-	1.11	81.6	96.6	178.2	.177
9	TT	1.5D	22.8	1202	-	1.36	-	1.66	122.4	129.4	251.8	.209
10	TT	2.0D	23.1	1214	-	1.53	-	2.05	108.7	144.7	253.4	.209
11	TT	3.0D	21.2	1202	-	1.91	-	2.31	133.5	171.5	305.0	.254
12	TT	4.0D	23.6	1211	-	1.16	-	1.50	96.8	124.8	221.6	.183
13	T	1.5b	23.0	996	0.35	0.43	0.55	0.71	-	-	142.5	.143
14	T	1.5b	20.8	1179	0.80	1.02	1.11	1.62	-	-	385.6	.327
15	T	2.0b	19.9	1009	0.41	0.45	0.71	0.95	-	-	184.7	.183
16	T	2.0b	20.7	1188	0.93	1.02	1.09	1.32	-	-	341.4	.287
17	T	3.0b	19.9	999	0.45	0.56	0.83	1.00	-	-	182.3	.182
18	T	3.0b	22.9	1198	0.56	0.69	0.97	1.01	-	-	241.6	.202
19	T	4.0b	22.1	1200	0.61	0.76	1.12	1.16	-	-	270	.225
20	T	4.0b	21.5	1006	0.30	0.44	0.56	0.72	-	-	167.4	.166
21	NTT	2.0b, 2.0D	21.9	1412	1.49	1.14	1.91	1.50	234.6	266.6	501.2	.355
22	NTT	3.0b, 2.0D	22.6	1401	1.20	1.11	1.75	1.47	190.7	222.7	413.4	.295
23	NTT	3.0b, 3.0D	23.5	1385	0.94	1.08	1.33	1.56	183.8	175.8	359.6	.260
24	NTT	2.0b, 3.0D	23.8	1181	1.16	1.01	1.62	1.46	177.2	208.2	385.4	.279
25	T	1.5b	22.6	813	0.08	0.08	0.24	0.30	-	-	114	.140
26	T	1.5b	21.1	1003	0.27	0.28	0.68	0.15	-	-	192.5	.192
27	T	2.0b	24.6	825	0.13	0.18	0.42	0.21	-	-	56.4	.068
28	T	2.0b	25.9	1016	0.07	0.20	0.23	0.23	-	-	72.1	.071

Data questionable due to operational problems

TT - Tandem Tracking

T - Twin

NTT - Tandem-Nontracking

S - Single Wheel

D - Tire Outside Diameter

b = Tire Section Width

Z = Instantaneous Soil Sinkage

Rut Depth = Elevation of Surface Prior to Test Less Elevation of Soil in the Tire Path After a Test

The rut depth measurements given represent the difference between the original soil profile and the soil profile after the passage of the test carriage. The sinkage values presented were calculated as a given percentage of the rut depth based on evaluation of the rebound measured by deflection pins buried in the tire paths. A description of the deflection pins is given in Appendix IV. Soil uniformity measurements and an outline of the basic test procedure is also presented in Appendix IV.

Using the analysis techniques established during development of preliminary multiwheel theories, the verification data was reduced and plotted as shown in Figures 27, 28, and 29, to indicate the multiwheel performance relative to spacing for the twin, tandem-tracking and tandem-nontracking configurations. This multiple wheel performance is evaluated by a comparison of drag ratios as shown in Equation 11.

$$M_M = (R/P)_S / (R/P)_M \tag{11}$$

where:

$(R/P)_S$ = single wheel drag ratio

$(R/P)_M$ = multiple wheel drag ratio

M_M = multiple wheel drag modifier

In order to plot this data, a value of the single wheel drag ratio for each specific condition was required. The single wheel drag ratio, $(R/P)_S$, used in this comparison, was arrived at by using the data collected and verified during the single wheel test program[1] and not the value that would be obtained by use of the single wheel nomograph[1]. The reason for this selection is the close control and accuracy associated with the single wheel tests previously conducted which used the same soil and test tires, whereas the nomograph represents an averaged result of numerous tests with and without test controls.

In general, the multiwheel data for twin and tandem-tracking tests grouped by the magnitude of the tire sinkage. Thus, it appears

52

Figure 27. Twin Tire Drag Performance on Clay–Multiwheel Tests

Figure 28. Tandem-Tracking Tire Drag Performance on Clay-Multiwheel Tests

54

⊙ Buckshot Clay
△ Mortar Sand

b = Tire Section Width

M_M = Multiple Wheel Drag Modifier

$$M_M = \left(\frac{\text{Tandem Nontracking Tire Drag Ratio}}{\text{Single Tire Drag Ratio}} \right)$$

Ratio of Tandem-Nontracking Spacing (Wheel Center to Wheel Center) to $\sqrt{b^2 + D^2}$

Figure 29. Tandem-Nontracking Tire Drag Performance on Sand and Clay-Multiwheel Tests

that a series of sinkage ranges exist in which the M_M value will be constant for a given sinkage at a given spacing. The sinkage ranges are approximately from 0 to 0.5", 0.5" to 1.0", and 1.0" to 4.0", called low, intermediate and high sinkage ranges, respectively. Reference to Figure 27 shows two data points plotted far below the rest of the data. No explanation for this phenomena exists although those two tests were run in a clay section different from all other clay tests. Note also that in Figure 29, the tandem-nontracking data for both sand and clay have been plotted together, as the trends in this data indicate very little if any effect of tandem-nontracking configurations for the spacings used. It should also be noted that due to limited funding the low sinkage tandem-nontracking test condition was not run, and therefore, could not be evaluated. The curves labeled "high" and "low" sinkage in the multiple wheel test data plots are an attempt to bracket the test data while reflecting the effects of different magnitudes of sinkage.

Test Results - Mortar Sand

The test results for the 29 multiwheel tests run in the mortar sand are presented in Table 13. The following comments explain the column headings used in Table 13. The spacings listed in the third column represent actual test spacings based on the tire's nominal diameter (D) of 18" and its nominal width (b) of 6.8". The soil strength (CI_{avg}) represents the average of at least five tests before traffic, and is defined as the average penetration resistance over the first six inches of soil profile. Soil strength measurements taken in the tire ruts after one pass are given in Appendix IV. The east-west, and front-rear designations have again been used to designate the relative position of each tire to the test section. The sinkage listed is actually the measured rut depth, yet is considered to be the total sinkage composed of both elastic deformation (very small in mortar sand) and the permanent deformation since sands exhibit only minimal rebound. The soil uniformity measurements and an outline of the basic test procedure is presented in Appendix IV.

56

TABLE 13

Multiwheel Drag-Sinkage Data-Sand Soil

Test No.	Type Test	Tire Spacing	Soil Strength (CI_avg)	Vertical Assembly Load P (lbs)	Sinkage Z (in)	East or Front Sinkage Z (in)	West or Rear Sinkage Z (in)	East or Front Wheel Drag R (lbs)	West or Rear Wheel Drag R (lbs)	Total Wheel Drag R (lbs)	Multiwheel Drag Ratio $(R/P)_M$
1	TT	4.0D	42.2	583	-	-	0.28	32.1	33.1	65.2	.112
2	TT	4.0D	42.4	1373	-	-	1.06	115	132	247	.180
3	TT	3.0D	48.1	583	-	-	0.18	25.2	32.2	57.4	.098
4	TT	3.0D	37.5	1380	-	-	1.22	124.0	150.0	274.0	.199
5	TT	2.0D	45.8	600	-	-	0.30	32.2	39.2	71.4	.119
6	TT	2.0D	48.3	1424.8	-	-	1.14	116.2	146.0	262.2	.184
7	TT	1.5D	46.7	635	-	-	0.26	32.6	31.6	64.2	.106
8	TT	1.5D	37.8	1416	-	-	1.32	136.0	150	286	.202
9	T	1.5b	44.5	834	-	0.10	0.08	-	-	93.2	.112
10	T	1.5b	41.9	1629	-	0.49	0.55	-	-	291.9	.179
11	T	2.0b	42.3	1618	-	0.45	0.59	-	-	260.0	.161
12	T	2.0b	39.6	760	-	0.13	0.18	-	-	85.7	.113
13	T	3.0b	40.3	831	-	0.24	0.20	-	-	109.8	.132
14	T	3.0b	39.3	821	-	0.24	0.28	-	-	107.3	.131
15	T	3.0b	40.7	1610	-	0.95	1.00	-	-	401.7	.250
16	T	4.0b	42.2	827	-	0.18	0.25	-	-	93.3	.113
17	T	4.0b	38.0	1596	-	0.87	1.26	-	-	417.2	.261
18	NTT	2b, 3D	39.2	1409	-	0.99	0.64	127.5	167.5	295.0	.209
19	NTT	3b, 3D	38.3	1409	-	0.76	1.03	118.6	169.6	288.2	.205
20	NTT	3b, 2D	40.0	1407	-	0.73	1.17	121.2	183.2	304.4	.216
21	NTT	2b, 2D	40.6	1395	-	0.50	1.16	125.8	193.8	329.6	.236
22	NTT	2b, 1.5D	40.6	1407	-	0.31	1.05	108.5	158.5	267.0	.190
23	NTT	3b, 1.5D	39.1	1403	-	0.75	1.08	131.2	156.2	287.4	.205
24	TT	1.5D	28.7	599	-	-	0.67	41.8	38.8	80.6	.134
25	TT	3.0D	24.4	602	-	-	0.88	49.8	48.8	98.6	.164
26	S	-	42.8	712	0.68	-	-	-	-	138	.194
27	S	-	39.0	415	0.24	-	-	-	-	46.7	.113
28	T	3.0b	38.5	1614	-	0.67	0.73	-	-	330.5	.205
29	T	1.75b	42.3	1620	-	0.59	0.52	-	-	276.7	.171

TT = Tandem Tracking
T = Twin
NTT = Tandem-Nontracking
S = Single Wheel

D = Tire Outside Diameter
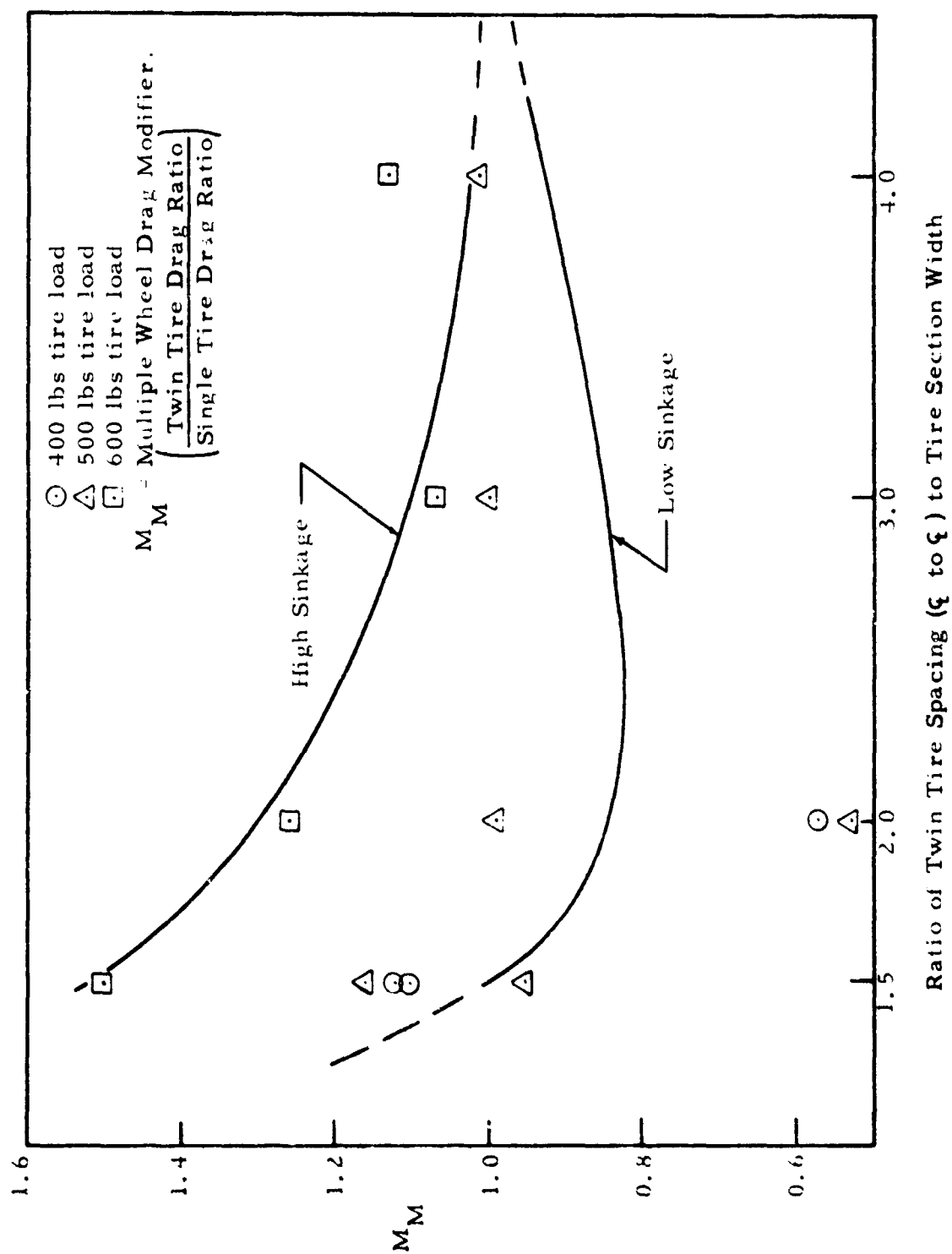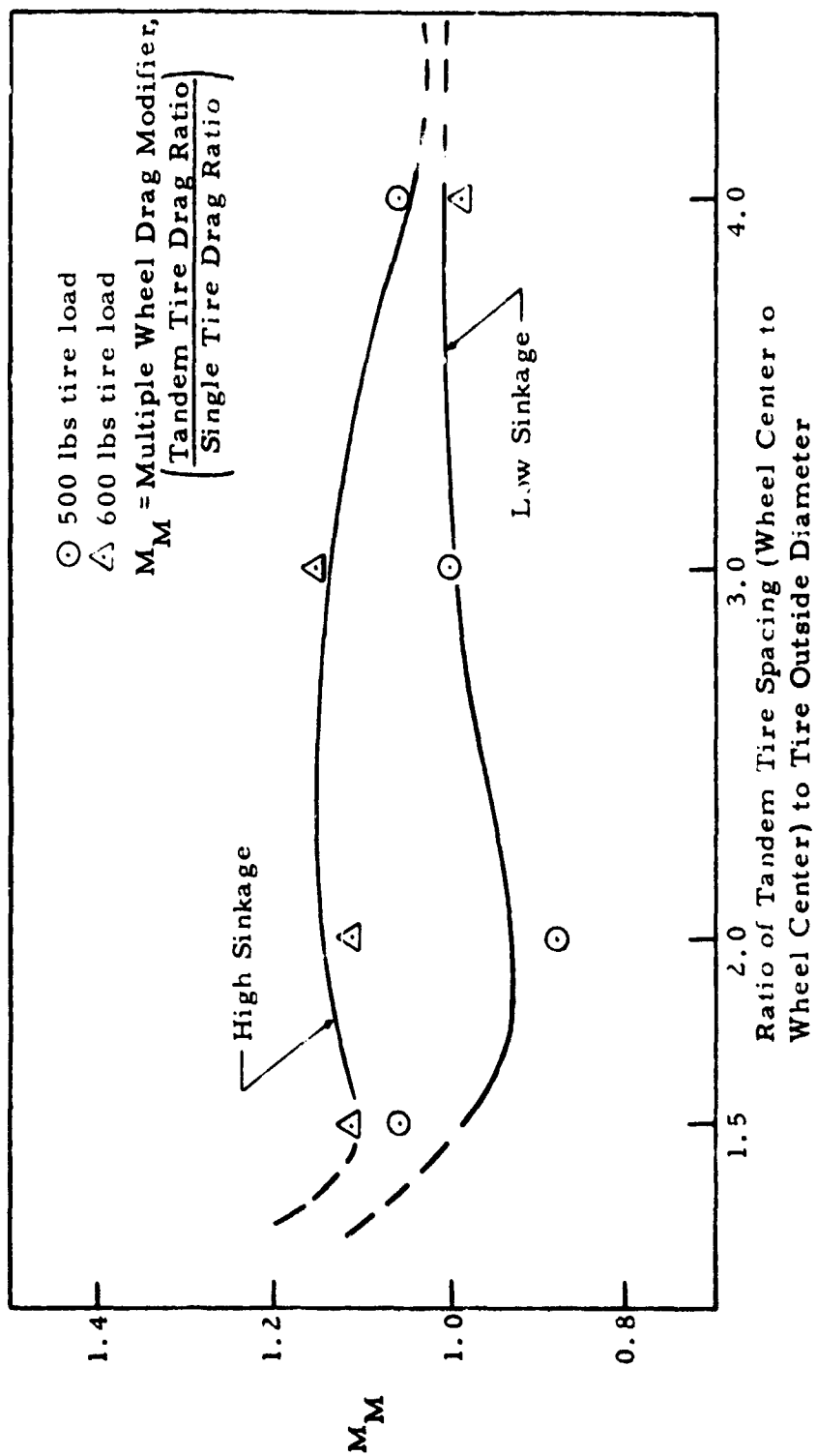b = Tire Section Width
Z = Instantaneous Sinkage

57
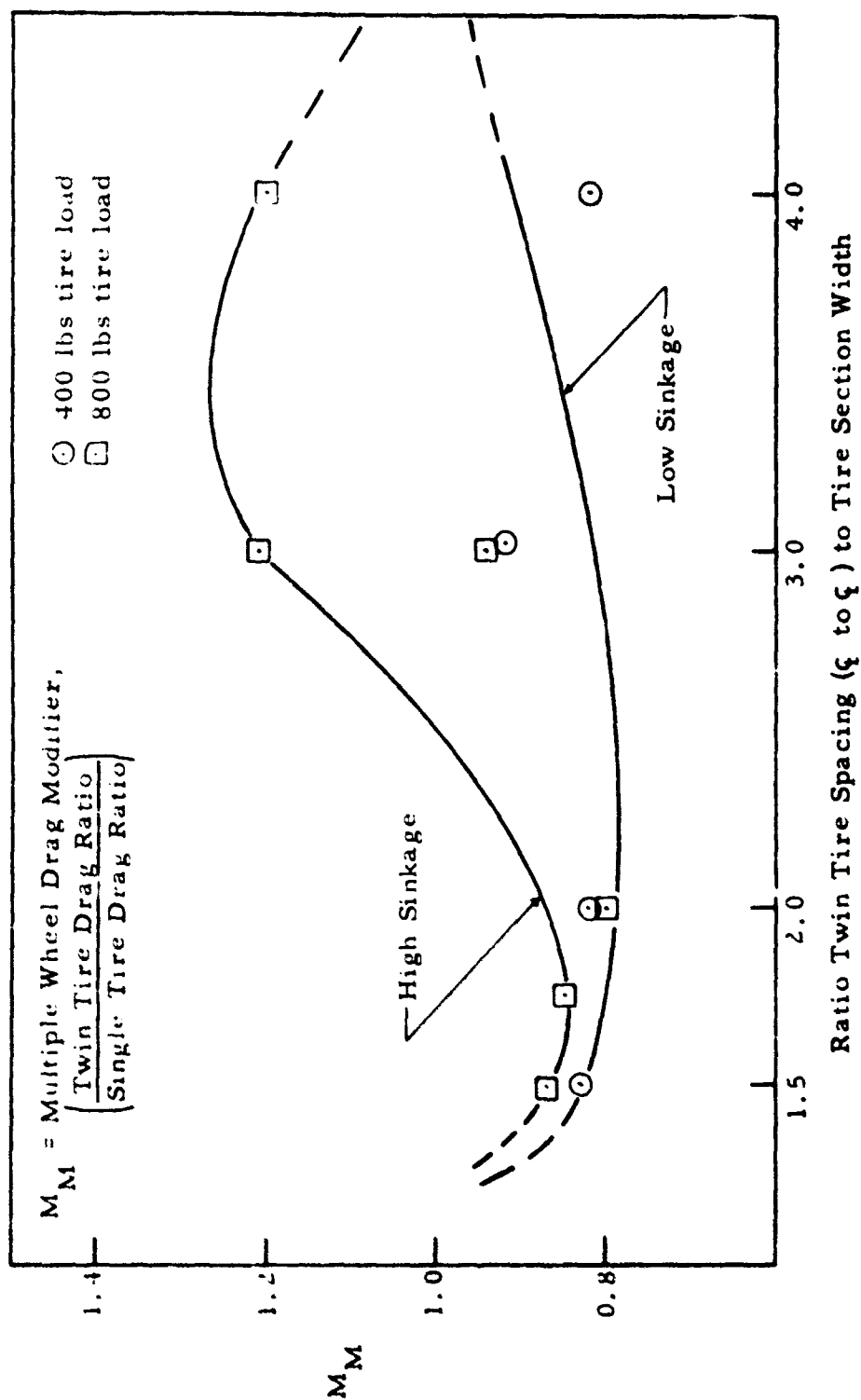
Figure 30. Twin Tire Drag Performance on Sand-Multiwheel Tests

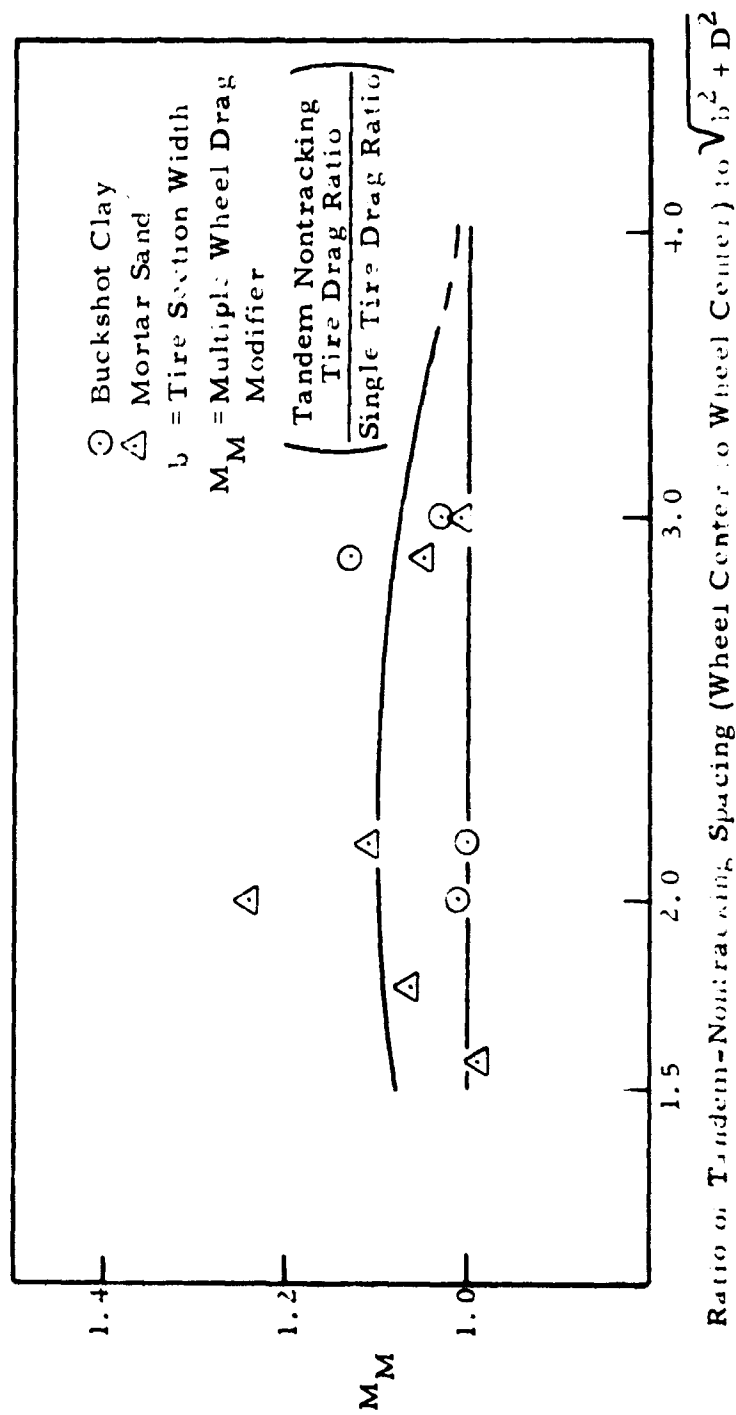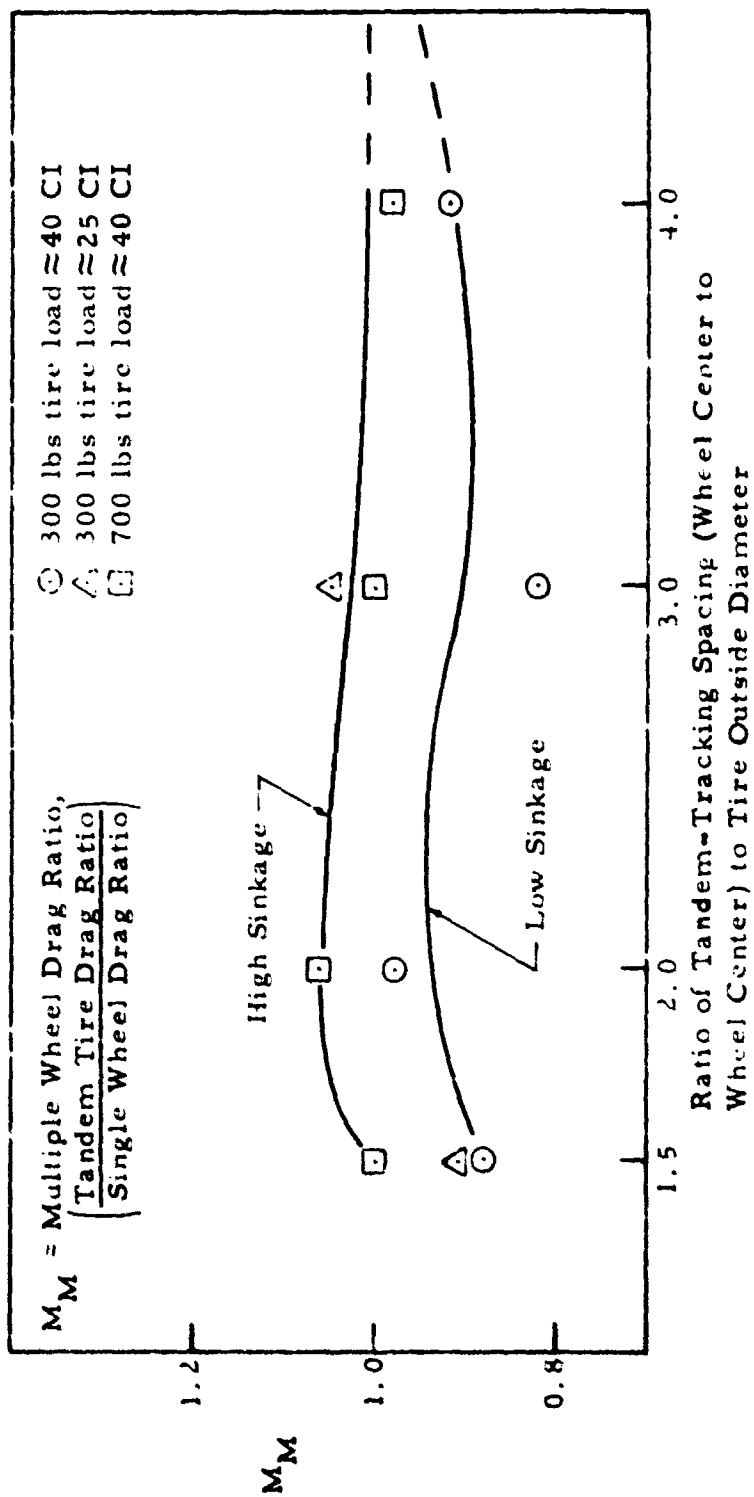Figure 31. Tandem-Tracking Tire Drag Performance on Sand-Multiwheel Tests

The sand data was evaluated based on drag performance and plotted as shown in Figures 30 and 31 to indicate the multiwheel performance relative to wheel spacing. The value of the single wheel drag ratio was obtained from the data taken during the single wheel testing program as explained previously. As for clay, the results show that the data tends to group by the magnitude of sinkage and the same three ranges generally apply. Two of the tandem-tracking tests were run on a much weaker strength soil as shown in Figure 31. Some additional twin wheel performance data on sand was obtained from unpublished work by WES. This data although somewhat scattered, tended to substantiate the trends shown in the twin wheel results of Figure 30.

Summary

Although the multiwheel tests presented here are not in themselves conclusive due to the limited test program, the basic trends shown by this data when combined with the plate test results and the analytical results will permit the development of design and operational criteria for multiwheel configurations. The test results generally indicate that the spacing of twin wheels is critical in minimizing drag for multiwheel configurations but that tandem-tracking spacing and tandem nontracking spacing are less critical in influencing multiwheel drag. The results of the multiwheel analysis and its application to multiwheel flotation criteria are presented in Section IV.

6. Summary of Multiwheel Drag and Sinkage Performance

The results of the review of existing twin tire test data (Figure 3), the Twin Plate Tests (Figure 13), the analytical results (Figure 19), and the Multiwheel (Twin) Verification Tests (Figures 27 and 30) generally show that for the proper twin wheel spacing, a reduction in the drag ratio (and sinkage ratio) over that for single wheels will occur for low to moderate sinkages of twin tires operating on both sand and clay. For high sinkages, the twin tire drag ratio will generally exceed the single wheel drag ratio for twin tires in clay soil but remain less than the single wheel drag ratio for sand soils.

Although the analytical results for tandem-tracking tires are not yet available, the results of the review of existing data (Figure 4), and the Multiwheel (Tandem) Verification Tests (Figures 28 and 31) show a slightly improved performance (≈15%) over single wheel performance in sand soil but an increase in drag ratio (≈10%) on clay soil for most tandem-tracking tire spacings.

The results of the analytical and experimental studies conducted to date on multiple wheel tire/soil interaction effects permit the following preliminary conclusions.

TWIN WHEEL - CLAY SOIL - Slight reduction (≈10%) in the rolling drag ratio (R/P) in clay soils for twin tires is gained over that for isolated single wheels by proper spacing of the tires for low sinkage situations. For high sinkage situations, increases occur (≈15%) in rolling drag ratio over that for single isolated wheels. The proper twin wheel spacing lies between 2.0 b and 3.0 b where b is the tire width.

TWIN WHEEL - SAND SOIL - Reductions in the rolling drag ratio (R/P) for the proper spacing are possible in sand type soil for twin wheel configurations in comparison to single wheels for all sinkages. Potential reductions in the drag ratio of 10% to 20% are evident. The proper twin wheel spacing lies between 1.5 b and 2.5 b.

TANDEM-TRACKING - CLAY SOIL - The operation of tandem-tracking tires in clay soil will yield some reduction (≈10%) in the drag ratio (R/P) for the proper tire spacing in low sinkage situation when compared to single wheel performance but higher drag ratios (≈15%) for high sinkage conditions. Available evidence suggests a desirable tandem-tracking spacing of 1.5 D to 2.0 D.

TANDEM-TRACKING - SAND SOIL - The operation of tandem-tracking tires in sand type soils will yield slight benefits (up to 10%) in reducing the drag ratio over that of a single wheel for proper twin wheel spacing. The spacing of the tandem-tracking tires does not appear to influence the magnitude of the drag ratio.

61

TANDEM-NONTRACKING - CLAY AND SAND SOIL - Although the number of tandem-nontracking tests conducted in clay and sand type soil was limited, this preliminary data suggests that tandem-nontracking configurations have little influence on sinkage and drag interaction between aircraft tires for the normally encountered tire spacings.

As indicated above, the results indicate that multiple wheel geometric configuration (dual, tandem, spacing, etc.) is an important parameter in determining the rolling drag performance of aircraft tires on soil and should receive increased consideration in aircraft design when soil operational performance is a requirement.

SECTION III
BRAKING SINKAGE AND DRAG ANALYSIS

Although the flotation requirements for aircraft landing gear design
and aircraft tire selection should be based primarily on the minimization of
rolling wheel drag (minimization of sinkage) during takeoff operations, the
braked tires on soil effects are an important factor in defining the maximum
drag loads on landing gears and in determining aircraft stopping distances
on unprepared runways. The braked tire on soil problem is considerably
different from rolling tire action since a resultant shear force will exist at
the tire/soil interface for braked tires. The major variables present for
braked tire conditions, in addition to those considered for rolling tires, are
tire slip and the shearing stresses at the interface. Large increases in
drag and in some cases sinkage occur for braked tires over that for rolling
tires.

The major portion of research efforts on studying the tire/soil
response for slip conditions has been conducted on powered wheels. Very
little theoretical or experimental work has been accomplished for braked
tires at speeds and conditions peculiar to aircraft operations. Those
studies[2, 7] which have been accomplished to date have been restricted
to field efforts directed at determining experimental braking coefficients
for limited conditions. The present state of the art of soil mechanics
precludes the development of a theoretical braking analysis due to the lack
of an adequate equation of state describing the stress-strain-time charac-
teristics of soil. For these reasons, a dual approach is being taken to
developing a more complete understanding of braked tire/soil interaction
phenomena. The semi-analytical braking theory described below is an
attempt to provide a useable theory, partially verified by existing experi-
mental data, for defining braked tire/soil interaction. The finite element

63

braking analysis currently in progress is also summarized in this section and is an attempt to take a long range theoretical look at the braking problem.

1. Semi-Analytical Braking Theory

The braked tire condition creates a force-slip condition where the degree of braking is defined by the tire slip, which is given as

$$S = (\frac{V_w}{V_a} - 1) \, 100 \tag{12}$$

where

S = percent tire slip

V_w = peripheral speed of wheel, and

V_a = horizontal velocity of the axle.

The slip is considered to be positive when the wheel is in a powered condition and negative under braked conditions. A fully braked (locked) wheel is a condition of 100 percent negative slip.

A number of references[2, 7, 18-23] were used in developing the braking drag expression. The significant variables included in the analysis were:

Loads

P = vertical tire load

R_B = braked tire drag force

Tire Geometry

b = tire section width

D = tire outside diameter

ℓ = tire footprint length on rigid surface

Soil Strength

c = soil cohesion

ϕ = soil friction angle

CI_{avg} = average cone index over 0" to 6"

G_b = slope of cone index versus depth profile in sand

64

<u>Other</u>

S = percent tire slip

V = aircraft horizontal velocity

The braking drag resistance as shown in Equation (13) is based on the premise that the total drag resistance can be treated as the sum of two components:

$$R_B = R_R + R_T \tag{13}$$

the horizontal soil resistance to forward motion exclusive of soil shear resistence during braking (R_R), plus the horizontal component (R_T) of the net shearing force resistance (T) between the tire and the soil as a function of slip. Figure 32 shows the loading and interface conditions for a braked tire. Justification exists for the use of Equation (13) in that form. Schuring[19] has stated that the rolling resistance (R_R) is independent of slip and that the coefficient of friction (related to R_T) is a function of slip alone. McCrae[21] has also assumed that for driven wheels at any slip, the term R_R can be determined from a rolling resistance formula. Both R_R and R_T are influenced by the magnitude of sinkage. R_R is influenced through use of the rolling drag equation (also see Equation 1)

$$\frac{R_R}{P} = f(Z/D) \tag{14}$$

while R_T varies with sinkage since the size of the shear stress contact area at the tire/soil interface is influenced by the magnitude of the sinkage. A review of some existing information[18] for braked tires on soil indicates that sinkages increase only slightly for all percents slip on clay soil while sinkages increase markedly for braked tires on cohesionless soils. This phenomena is shown very clearly in Figures 33 and 34.

R_R Term, Clay and Sand Type Soil

As indicated previously, the horizontal resistance to forward motion exclusive of shear resistence is independent of slip and can be approximated

65

P = vertical drag

R_B = braking drag

B' = braking torque

R_R = forward motion soil drag

P_s = vertical soil reaction

T = tangential shear force

ℓ_Z = equivalent plane of contact

Figure 32. Braked Tire/Soil Interface Conditions
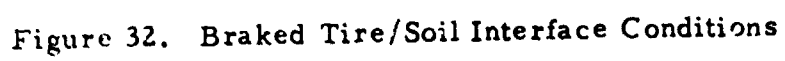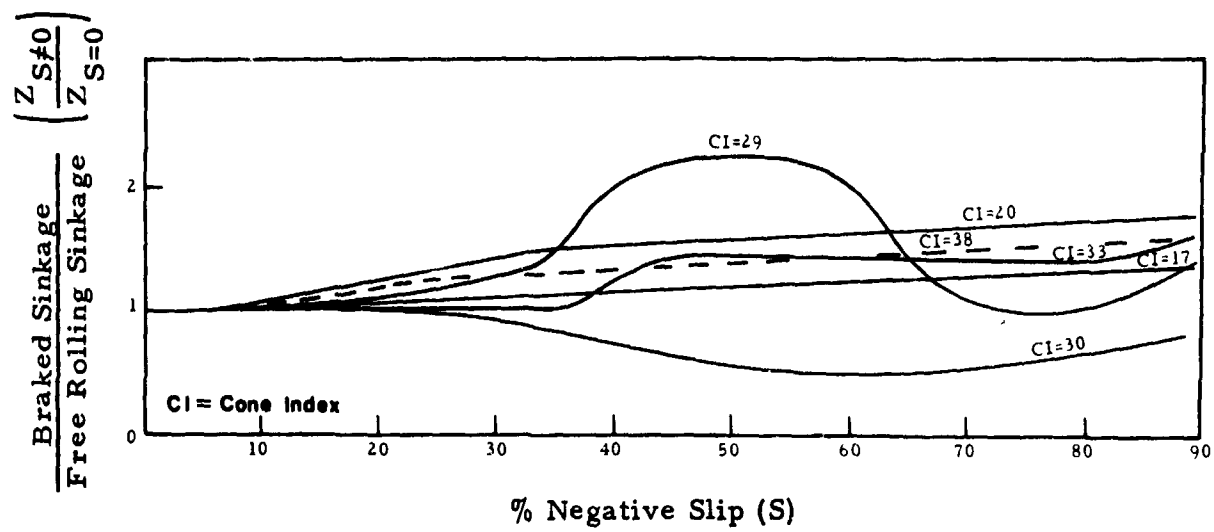
Figure 33. Influence of Negative Slip on Sinkage, Clay Soil
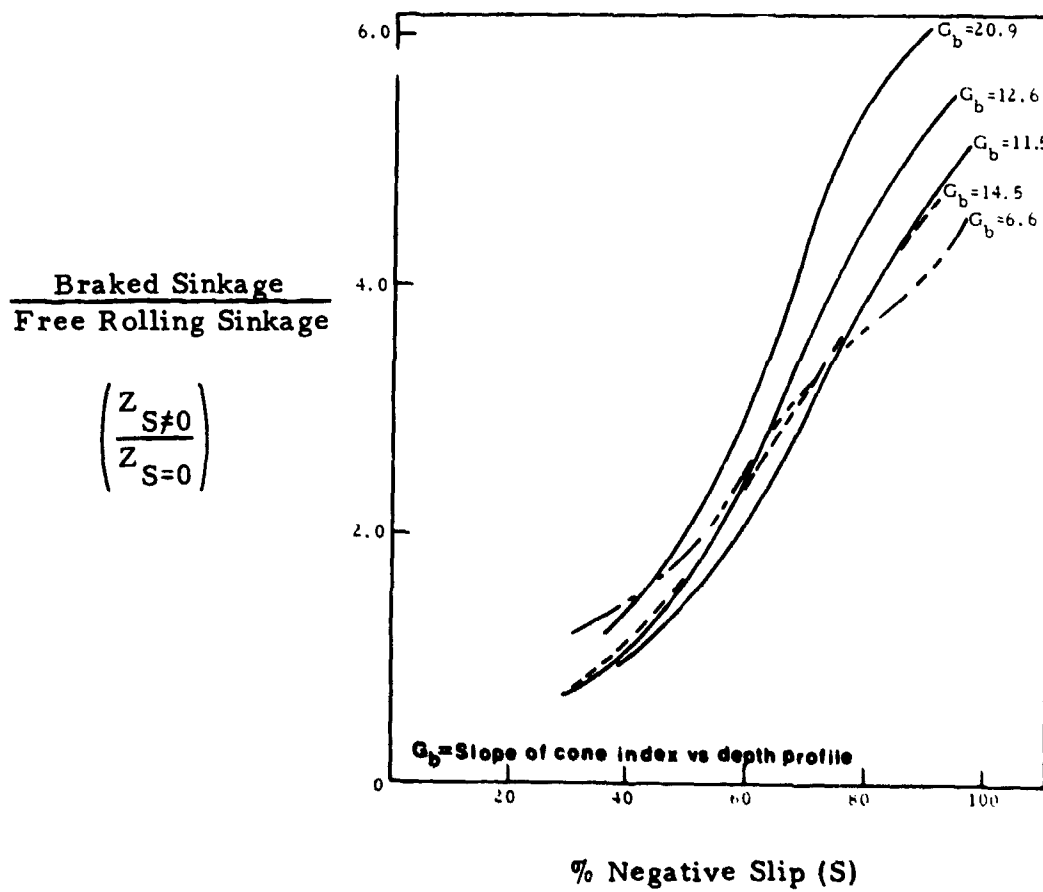
Figure 34. Influence of Negative Slip on Sinkage, Sand Soil

67

from the rolling drag equation for cohesive soils[1] as.

$$\frac{R_R}{P} = 3.85 \, (Z/D) \tag{15}$$

Since sinkages in clay soil increase only slightly throughout the negative slip range, the R_R term is assumed to remain essentially constant. This conclusion is partially verified as shown in Figure 35 by the results of an experimental effort[20] in which R_R was measured separately from R_T.

In sand type soils, the R_R term will increase in magnitude since sinkages increase with increasing negative slip. A change in R_R caused by braking, however, should correspond to the same change in drag (R) for rolling tires for an equivalent change in sinkage. A comparative study[20] of this phenomena is shown in Figure 36 and tends to substantiate the use of the rolling drag equation for sand. The rolling drag equation for sand[1] is given by

$$\frac{R_R}{P} = 0.048 + 2.77 \, (Z/D) \tag{16}$$

It should be noted that R_R for sand will increase throughout the negative slip range thus

$$(R_R)_{S \neq 0} = (R_R)_{S=0} + \Delta R_R \tag{17}$$

where

$$\Delta R_R = f \, (\Delta Z)$$

R_T Term, Clay and Sand Type Soil

The tangential force (T) at the tire/soil interface is the integral of the shear stresses over an equivalent plane of contact as shown in Figure 32. The horizontal component of T is the term R_T and contributes significantly to the total braked drag resistance R_B. If Coulombs law for determining

68

$$\left(\frac{(R_R)_{S \neq 0}}{(R_R)_{S = 0}}\right)$$

R_R = Horizontal Resistance to Forward Motion Exclusive of Shear Resistance

1.2

1.1

1.0

0.9

0   10   20
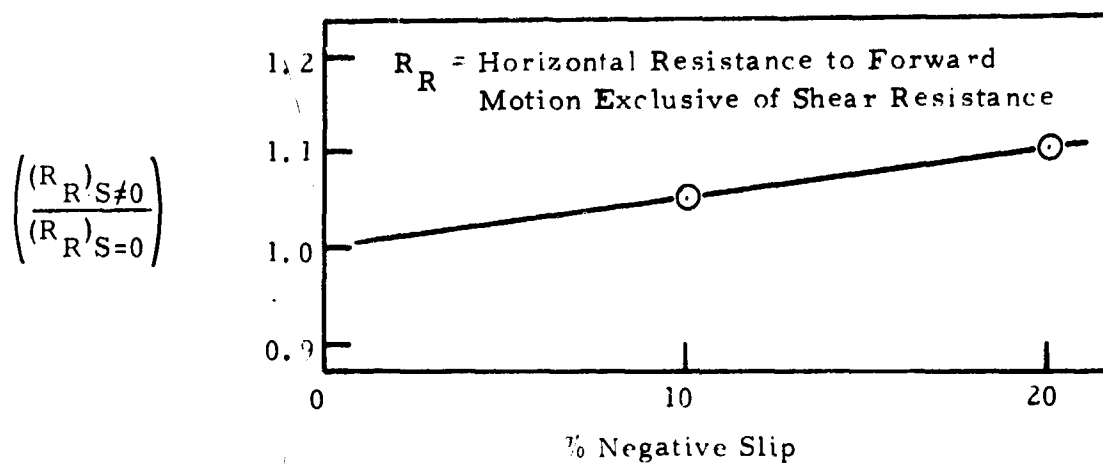
% Negative Slip

Figure 35. Influence of Negative Slip on R_R, Clay Soil

$$\frac{\left(\frac{\Delta R_R}{P}\right)_{braked}}{\left(\frac{\Delta R}{P}\right)_{rolling}}$$

ΔR = Change in Rolling Drag

ΔR_R = Change in Forward Motion Resistence Exclusive of Shear Resistence

1.6

1.4

1.2

1.0

0.8

0.6

0   .02   .04   .06   .08

Z/D
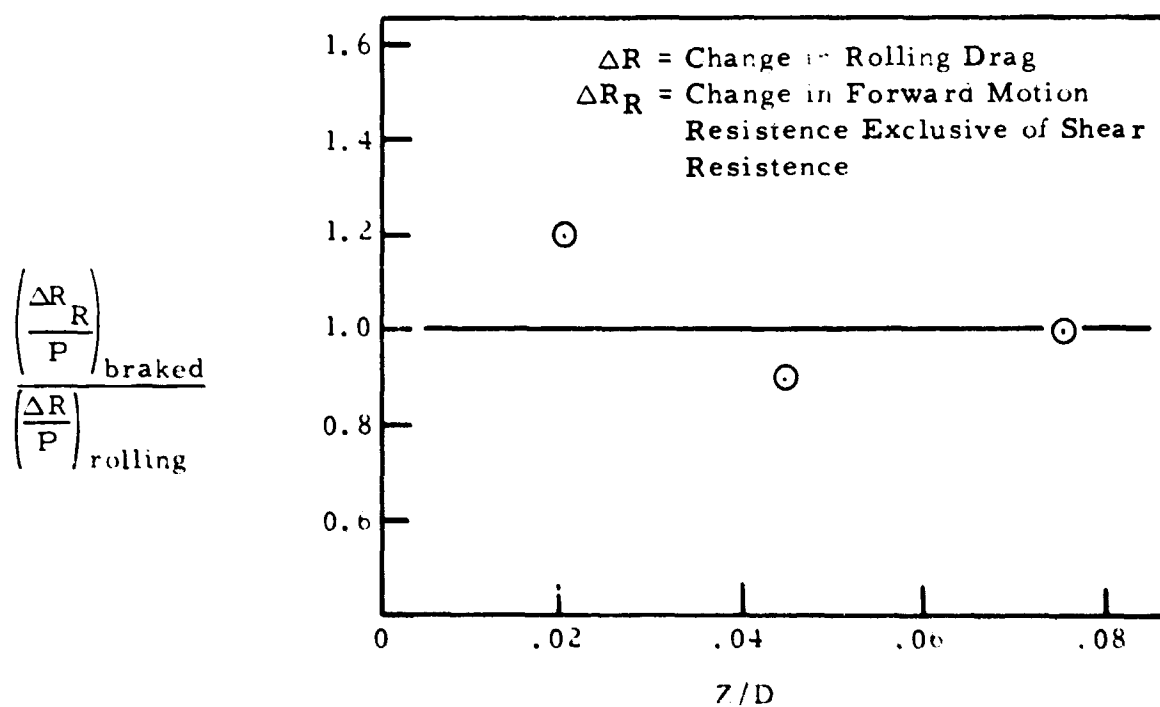
Figure 36. Comparison of Braked R_R With Rolling Tire Drag for Increasing Sinkage, Sand Soil

69

shear force at the interface is valid, the shearing resistance at the interface could be computed as a function of slip as

$$\tau = (c + \overline{\sigma} \tan \phi) \, \mu(S) \tag{18}$$

where

τ = shearing stress

$\overline{\sigma}$ = effective normal stress

$\mu(S)$ = nonlinear function which varies with slip

For the rolling tire case for which the braking torque, B', is zero, experimental evidence indicates that although there are shearing stresses at the tire/soil interface, the net shearing force, T, is zero, and the resultant of the vertical and horizontal soil reaction passes through the center of the tire. As a braking torque is applied continuously to the tire, the negative slip increases creating additional shear stresses at the interface. These shearing stresses result in a net shearing force as given by

$$T = A_Z (c + \overline{\sigma} \tan \phi) \, \mu(S) \tag{19}$$

where

A_Z = area of equivalent plane of contact at sinkage Z.

The resultant force at the interface no longer passes through the tire center, but acts through an eccentric point creating a moment equivalent to the braking torque, B', for a steady state braking condition. The horizontal component of T is given by

$$R_T = A_Z (c + \overline{\sigma} \tan \phi) \, \mu(S) \cos \theta \tag{20}$$

Reference to Figure 32 indicates that the angle θ defining the equivalent plane of contact is given as

$$\theta = 90^\circ - [\sin^{-1}(1 - \frac{2Z}{D}) + 1/2 \cos^{-1}(1 - \frac{2 \ell Z}{D^2})] \tag{21}$$

70

The use of Equation (20) necessitates the accurate description of the tire/soil contact area as a function of sinkage. For certain clay type soils this A_Z term would have to include sidewall contact areas. Using simplifying assumptions, expressions have been developed by others[3, 21] which analytically define the footprint length (l_Z) and footprint width (b_Z) from which A_Z^l could be determined if sidewall effects are ignored. Analysis of these expressions indicates that for tires operating in their normal deflection range ($\pm 10\%$ of their normal deflection), that the contact area can be written as a functional expression in the following manner

$$f(A_Z, Z, D) \tag{22}$$

or

$$\frac{A_Z}{D^2} = f(Z/D) \tag{23}$$

The results of a controlled braking study conducted by WES[18] for the Air Force were used to examine Equations (20) and (23) leading to the development of an R_T expression for cohesive and cohesionless type soils. These tests were conducted using two different tires (D = 14" and 28-1/2"), one tire deflection (D = 25%), various soil strengths and vertical loads in both sand and clay, and negative slips ranging from 0 to 100%.

$\underline{R_T, \text{ Cohesive Soil}}$

For cohesive soils, the $\tan \phi$ is zero in Equation (20) and the cohesion, c, can be replaced by the average cone index, CI (or CI_{avg}). Equations (20) and (23) can then be combined to give the dimensionless expression

$$\frac{R_T}{CI \cdot D^2 (Z/D)^n} = J(S) \cos \beta \tag{24}$$

The clay test results[18] were plotted based on Equation (24) and Figure 37 shows that a reasonable convergence of the data exists for the case n = 1/2.

71

R_T values were determined by subtracting a calculated R_R value based on the magnitude of the instantaneous sinkage, Z (see Equation 15). The data used in developing Figure 37 is summarized in Appendix V. Based on Figure 37 then, the braked tire horizontal shearing force at the interface can be approximated by

$$R_T = 0.11 \ CI \cdot D^2 (Z/D)^{1/2} u(S) \qquad (25)$$

$\underline{R_T, \text{ Cohesionless Soil}}$

In cohesionless soils, the cohesive term, c, in Equation (20) is zero. Replacing $\bar{\sigma}$ in Equation (20) by $\alpha = P/A$, where A is the rigid surface tire contact area, Equation (20) and (23) can be combined as

$$\frac{R_T}{D^2 (Z/D)^n} = \alpha \ \tan\phi \cdot u(S)\cos\rho \qquad (26)$$

Initial analysis of the sand data[18] indicated that the R_T term in sand was only a weak function of Z/D (n is very small) and consequently within acceptable accuracy limits, Equation (26) can be written as

$$\frac{R_T}{D^2} = \alpha \ \tan\phi \cdot u(S)\cos\rho \qquad (27)$$

Observations of braked tire performance in soil shows that considerable sand flow takes place at the tire soil interface. This sand disturbance and flow very likely causes the shearing strength to be determined by some large deformation equilibrium void ratio condition in sand rather than the initial soil shear strength. If this phenomena is true, analysis of Equation (27) should show R_T to be approximately constant for all values of initial shear strength for sand for all other factors remaining constant. Figure 38 which includes soil strength changes up to an order of magnitude of three, shows that the initial soil strength does not have a significant influence on the magnitude of R_T for braked tires on sand. Analysis of Figure 38 in conjunction with Equation (27) leads to the expression

$$R_T = \frac{\alpha D^2}{29} u(s) \qquad (28)$$

72
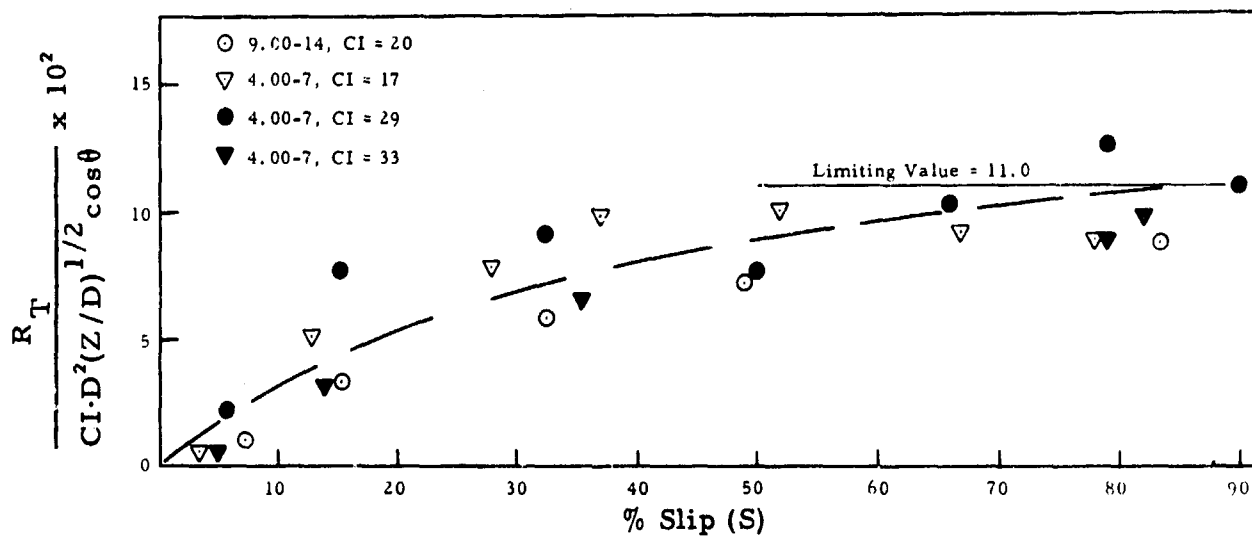
Figure 37. Horizontal Shear Component Evaluation, Clay Soil
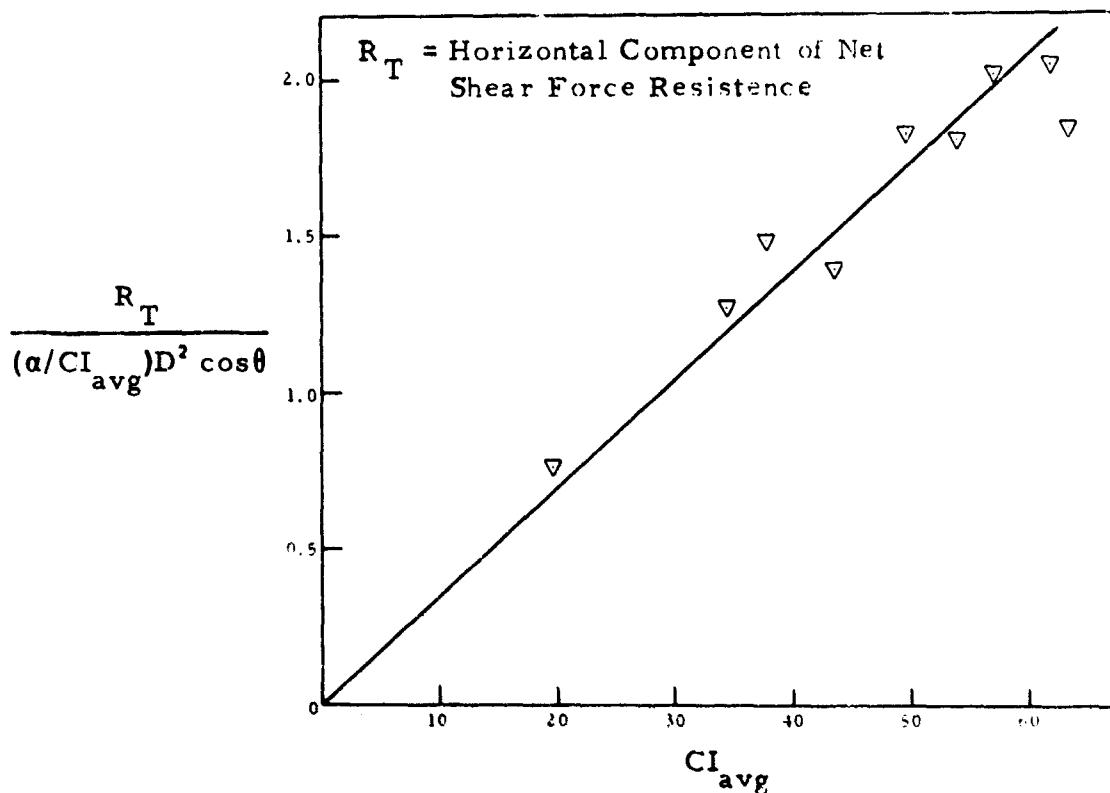
Figure 38. Horizontal Shear Component Evaluation, Sand Soil

73

As for the clay data analysis, R_T values were determined by subtracting a calculated R_R value based on the magnitude of the instantaneous sinkage, Z (see Equation 16). The data used in developing Figure 38 is summarized in Appendix V.

Variance of R_T With Slip

As the negative slip increases, the R_T value in both sand and clay increases in magnitude. This increase in R_T with increasing slip occurs in a nonlinear manner as shown in Figure 39. Although Figure 39 shows some differences in the growth of $R_T/R_{T_{max}}$ with slip for sand and clay, as a first approximation, the quantity $\mu(S)$ in Equation (25) and (28) can be written as

$$\mu(S) = \frac{R_T}{R_{T_{max}}} = (\frac{S}{100})^{1/3} \tag{29}$$

Variance of Sinkage With Slip, Cohesionless Soil

Due to the large increases in sinkage for braked tires on sand type soils, these sinkages must be known since it significantly influences the resulting drag, R_B. By comparing the sinkage at 100% slip $(Z_{S \neq 0})$ to the sinkage at zero slip $(Z_{S=0})$ for the test data from the WES study[18], Figure 40 was developed which shows that the initial load–strength ratio (σ/CI_{avg}) is critical in determining this ratio. Although considerable research remains to be accomplished in order to accurately define the growth of sinkage for braked tires on sand, Figure 40 can be used to estimate the sinkage at S = 100% in the following manner:

1. Calculate the sinkage for a rolling tire (S=0) using the previously developed sinkage prediction equations for sand[1]. This sinkage is $Z_{S=0}$ in Figure 40.
2. Determine α/CI_{avg} for the braked tire and use Figure 40 to find $(Z_{S \neq 0})_{max}/Z_{S=0}$. From this value the maximum braked tire sinkage $(Z_{S \neq 0})_{max}$ in sand can be determined.
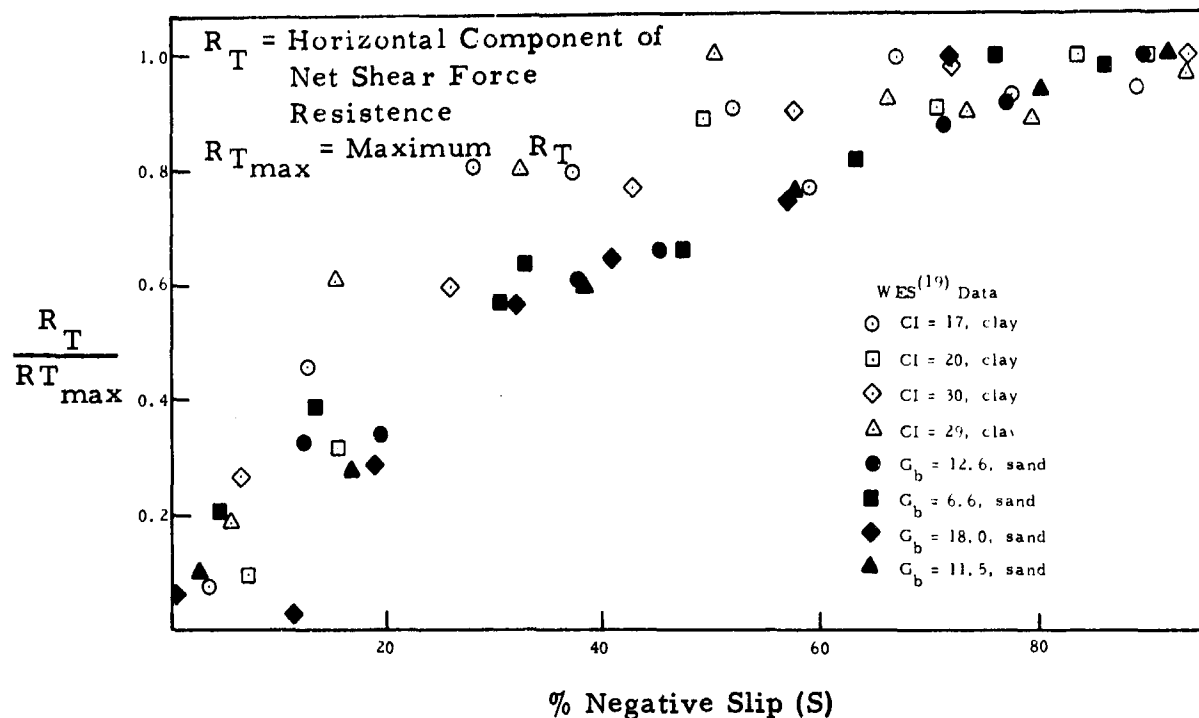
Figure 39. Increase in Braked Shear Force at the
Tire/Soil Interface, Sand and Clay
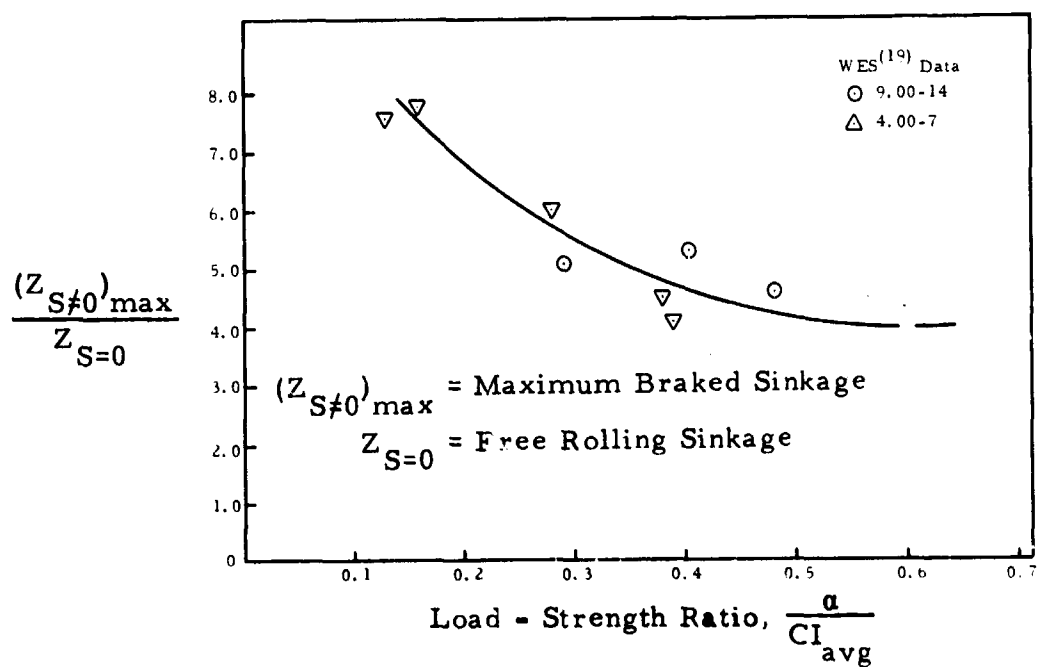
Figure 40. Variation of Braked Sinkage Ratio With
Load-Strength Ratio, Sand Soil

75

Braking Equations - Summary

Cohesive Soil

$$\frac{R_B}{P} = \frac{R_R}{P} + \frac{R_T}{P} = 3.85\left(\frac{Z}{D}\right) + \frac{0.11\ CI \cdot D^2}{P}\left(\frac{Z}{D}\right)^{1/2}\mu(S) \tag{30}$$

Cohesionless Soil

$$\frac{R_B}{P} = \frac{R_R}{P} + \frac{R_T}{P} = 0.048 + 2.77\left(\frac{Z}{D}\right) + \frac{\alpha D^2}{29P}\ \mu(S) \tag{31}$$

where $\mu(S)$ is given by Equation (29).

2. Comparative Study Using Semi-Analytical Braking Theory

Limited experimental efforts have been sponsored by the Air Force to conduct braked tire on soil tests on a full scale basis. Douglas[7], Boeing[7], and Lockheed[2] have conducted these test programs. The results of these tests provided an opportunity to compare the braking drag analysis equations developed from controlled laboratory testing to the results of these field operations. Equations (30) and (31) together with other information was used in developing a computer program to conduct this comparative study. The results of the study are summarized below.

Lockheed Tests

The Lockheed Corporation[2] in 1968, conducted a series of rolling and braked tire tests at the NASA/Langley test track using a 29 inch diameter, Type III tire. Braked tire tests were conducted on both buckshot clay and a beach sand common in the Langley area. The soil strength, vertical load, and tire deflection for each test are summarized in Table 14 and Table 15 for clay and sand respectively. Braked drag predictions in the clay soil (Buckshot clay) were based on sinkage by adding to the measured rut depth a rebound deflection. This rebound deflection was

76

TABLE 14

Braking Test Variables, Lockheed Clay Tests

Test No.	CI Cone Index	P Vertical Load (lbs)	d Tire Deflection
1	67.5	6166	0.51
2	67.5	7020	0.56
3	67.5	6466	0.53
4	67.5	6315	0.52
5	67.5	6003	0.49
6	67.5	6201	0.42
7	67.5	4900	0.35
8	67.5	6131	0.41
9	67.5	6389	0.43
10	67.5	6339	0.42
11	67.5	7277	0.36
12	67.5	6350	0.32
13	67.5	7000	0.35
14	67.5	5500	0.28
15	67.5	5965	0.31
16	103.5	4839	0.42
17	103.5	5280	0.45
18	103.5	4900	0.43
19	103.5	6500	0.53
20	103.5	5150	0.45
21	103.5	4599	0.33
22	103.5	3941	0.29
23	103.5	5506	0.38
24	103.5	4860	0.35
25	103.5	4389	0.24
26	103.5	3747	0.22
27	198	4828	0.34
28	198	4945	0.35
29	198	5006	0.35
30	198	5047	0.35
31	198	5150	0.36

TABLE 15

Braking Test Variables, Lockheed Sand Tests

Test No.	CI Cone Index	P Vertical Load (lbs)	d Tire Deflection
1	163	6467	0.51
2	163	6077	0.49
3	163	6621	0.52
4	163	8121	0.59
5	163	5700	0.45
6	163	5513	0.46
7	163	5442	0.46
8	163	5500	0.38
9	163	6800	0.46
10	163	6600	0.45
11	163	6100	0.42
12	163	5779	0.4
13	163	6114	0.42
14	163	5504	0.38
15	163	5100	0.27
16	163	4950	0.26
17	163	7258	0.36
18	163	7223	0.36
19	163	6300	0.32
20	163	6310	0.32

estimated based on data from previous tests conducted at WES[1] (also in Buckshot clay) where both rebound and rut depth were measured. Table 16 presents the measured rut depth and the corrected rut depth (sinkage) using the results of the Phase II study[1] while Table 17 gives the measured rut depths for the sand tests. Very little rebound occurs in sand type soils and consequently the rut depths were used as sinkages.

The results of the braked drag predictions are summarized in Table 18 for the clay soil tests and in Table 19 for the sand soil tests. Comparisons between the predicted braking drag using Equations (30) and (31) and the measured braking drag (results of Table 18 and 19) are shown in Figures 41 and 42 for clay and sand respectively. In both Figures, ±20% lines are shown in order to provide an estimate of the accuracy of the prediction technique. Considering the limitations which exist in preparing uniform soil test beds and the accuracy with which tests measurements on soil can be taken, the results as shown in Figures 41 and 42 are quite favorable.

Boeing Tests

The Boeing Company[7] in 1964, carried out a series of aircraft field tests including both rolling and braking tire conditions using a Boeing 367-80 (KC-135 prototype) aircraft. The tests were conducted on a lean clay lake bed located at Harpers Lake, California. The aircraft was equipped with a high flotation landing gear (basic 707 type bogie) with 46 x 16, Type VII tires. Only one braking test was conducted on soil and a summary of the test variables and the resulting measured braking coefficient (R_B/P) as well as the predicted braking coefficient are shown in Table 20.

Douglas Tests

Douglas Aircraft Company also ran a series of aircraft on soil field tests in 1964-65 using a C-5A prototype landing gear configuration.

TABLE 16

Braking Rut and Sinkage Data,
Lockheed Clay Tests

Test No.	z Measured Rut Corrected (sinkage), in.	z_a Measured Rut (in.)
1	2.23	2.08
2	1.82	1.39
3	1.31	0.72
4	1.00	0.42
5	1.05	0.46
6	2.35	2.32
7	2.94	2.94
8	2.33	2.27
9	1.48	0.92
10	1.41	0.83
11	2.44	2.5
12	2.44	2.5
13	2.25	2.12
14	1.85	1.44
15	1.95	1.59
16	0.91	0.35
17	0.92	0.36
18	0.53	0.12
19	0.75	0.24
20	0.75	0.24
21	1.42	0.85
22	1.76	1.3
23	1.13	0.54
24	1.00	0.42
25	1.34	0.75
26	2.09	1.83
27	0.25*	-
28	0.25*	-
29	0.25*	-
30	0.25*	-
31	0.25*	-

TABLE 17

Braking Rut Data,
Lockheed Sand Tests

Test No.	z_a Measured Rut (in.)
1	6.24
2	2.75
3	3.08
4	2.69
5	0.87
6	0.87
7	0.79
8	7.0
9	4.8
10	3.3
11	1.4
12	1.35
13	0.98
14	1.12
15	4.06
16	4.44
17	2.65
18	2.46
19	1.6
20	1.3

TABLE 18

Braking Drag Comparison, Clay Soil

Test No.	Measured Experimental Drag (lbs)	Predicted Drag (based on sinkage) (lbs)
1	4145	3549.66
2	3488	3258.83
3	2986	2443.45
4	2396	1988.44
5	2544	2010.05
6	4045	3711.99
7	3700	3883.11
8	2775	3659.08
9	2754	2659.57
10	2466	2550.70
11	3693	4176.00
12	3800	3869.27
13	3150	3829.66
14	2710	2921.53
15	497	3153.03
16	2574	2257.44
17	2128	2333.04
18	1950	1624.19
19	2100	2175.47
20	2300	2037.06
21	3075	2957.53
22	3292	3242.55
23	2429	2694.96
24	2625	2394.81
25	3443	2801.86
26	3527	3568.44
27	3566	1819.15
28	2073	1823.10
29	3411	1825.16
30	1977	1826.54
31	2000	1830.02

TABLE 19

Braking Drag Comparison, Sand Soil

Test No.	R_B Measured Experimental Drag (lbs)	R_B Predicted Drag (based on Rut Depth) (lbs)
1	4299	5686.24
2	4160	3315.27
3	4640	3771.39
4	4201	4200.98
5	2393	2141.28
6	2317	2051.90
7	2431	1983.16
8	4450	5510.25
9	3756	5128.30
10	3689	4038.15
11	2727	2676.54
12	2710	2558.87
13	2063	2433.10
14	2043	2368.75
15	3907	4080.05
16	4257	4199.17
17	3410	4284.01
18	3263	4129.97
19	2579	3245.43
20	2367	3066.59

R_B = Braked Tire Drag Force
P = Vertical Load

29 x 11-10 Tire,
Buckshot Clay
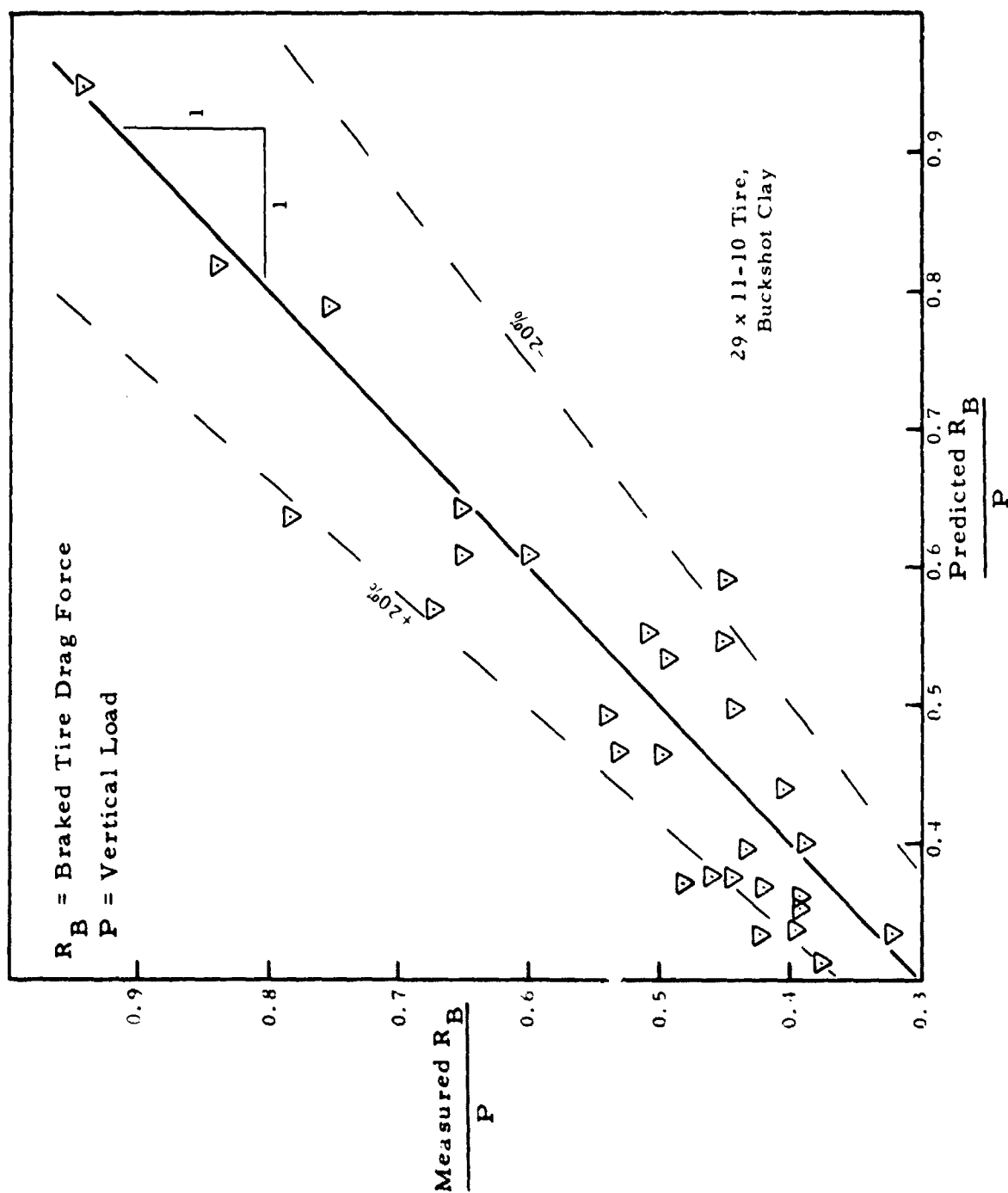
Figure 41. Measured Drag vs. Predicted Drag, Clay Soil

81
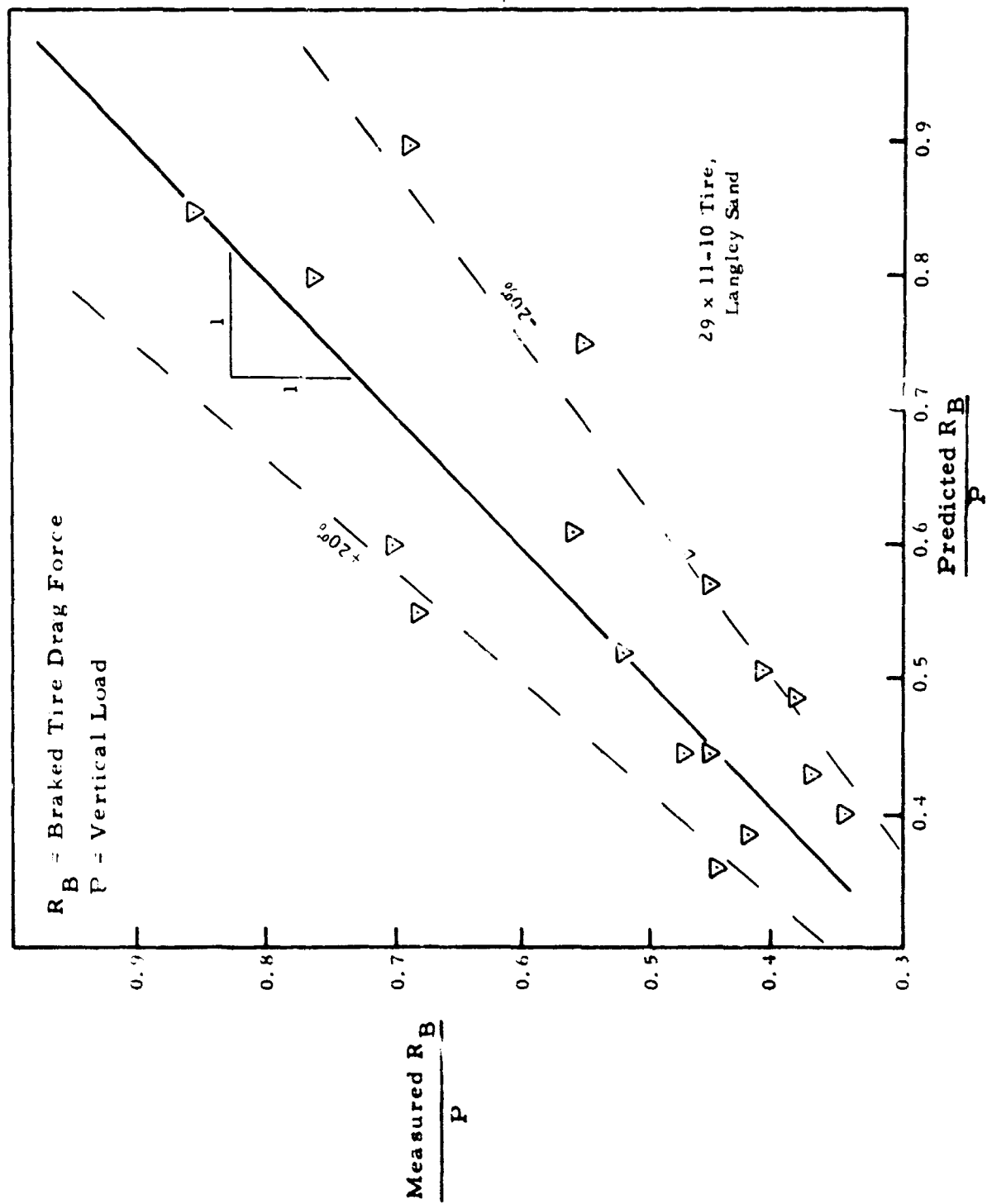
Figure 42. Measured Drag vs. Predicted Drag, Sand Soil

82

Table 20. Comparative Braking Study Results--Boeing Data

Tire	Inflation Pressure (psi)	Vertical Load P(lbs)	Soil Strength (CBR)	Sinkage, Z (estimated)	$(\frac{R_B}{P})$ measured	$(\frac{R_B}{P})$ predicted*
46 x 16, Type VII	30	8575	5.5	1/2" to 1"	0.68	0.74

* Using clay prediction equations.

Table 21. Comparative Braking Study Results--Douglas Data

Tire	Inflation Pressure (psi)	Vertical Load P(lbs)	Soil Strength (CBR)	Sinkage, Z (estimated)	$(\frac{R_B}{P})$ measured	$(\frac{R_B}{P})$ predicted*
40 x 14, Type VII	80	10,200	16	1/4" to 3/4"	0.58	0.77
40 x 14, Type VII	110	10,200	16	1/2" to 1-1/2"	0.69	0.89

* Using clay prediction equations.

83

The test program which was also conducted at Harpers Lake, California, included rolling aircraft tests and a limited number of braking tests on a soil runway. Although tire data was not specified, the tires were very likely 40 x 14, Type VII tires. The braking tests were conducted on a lean clay with a CBR rating of 16. Analysis of soil strength data, however, indicates that the rated CBR 16 runway had CBR values ranging from 8 to 34 which certainly influenced the resulting measured braking coefficients. A summary of the test variables and the resulting comparisons using the braking prediction equations is given in Table 21.

The results as given in Table 21 show the predicted braked drag ratio to be significantly higher than the measured. These differences are likely related to the magnitude of the sinkages used in the prediction equations. Due to the variability in soil strength at the test site, the estimated sinkages shown in Table 21 could be considerably in error.

Based on the results of the comparative study, the braked drag prediction equations developed herein can be used as a first approximation for determining aircraft braking performance on soil runways. These braking equations which were developed for sand and clay type soil can also be used to bracket the braked drag ratios for intermediate type soils.

3.   Finite Element Braking Analysis

As indicated previously, the interaction of aircraft tires and soil runways while an aircraft is being braked is a complex phenomenon. In actuality, braking does not occur independently of other equally complicated effects such as the rolling action of the tires, the speed of the aircraft, and turning. Additionally, the proximate tires interact, the behavior is three-dimensional, the composition and material properties of soils are usually uncertain, etc.

The purpose of this section is to outline the numerical approach currently under development for the prediction of the sinkage of aircraft

tires during braking. In order to study the effects of braking on sinkage, braking is isolated from other effects such as those mentioned above. It may be appropriate at a later time to attempt to include as many factors as possible in a single analysis; however, the approach outlined below has been adopted to obtain an initial, "first-cut", grasp of the braking phenomenon.

The remainder of this section is presented in four principal parts. (1) The first part contains a description of the specific problem which will be considered. The problem definition includes: a listing of the physical, geometric, and material assumptions which are made (e. g., isolation of braking effects, plane strain, etc.); a description of the simulated loading; a description of the region of half-space in which a solution will be obtained; and a discussion of the assumed boundary conditions at the extremities of the region of solution. (2) The second part contains a brief description of the mathematical model which is intended to represent the behavior of an idealized sample of soil subjected to simulated weight and brake loadings. This discussion contains: the proposed finite element; the assumed displacement state for the finite element; the resulting stiffness matrix; and a possible finite element modeling of the soil sample. (3) The third part contains a description of the solution procedure which is proposed (load-incrementation technique). (4) The last part contains a brief summary of the current progress of the development of the finite element braking analysis.

PART 1 - Problem Definition

The idealized problem considered is defined below by listing the assumptions and discussing the loading, region of solution, and boundary conditions.

Assumptions

- A single wheel is in contact with the sample of soil under consideration.

85

- Only the effects of vertical loading and braking are considered (the aircraft is not turning, the soil surface is smooth, etc.).

- The deformation of the soil material under the loading considered results in a state of plane strain. This is equivalent to assuming that the tire is infinite in width. Sidewall shear is, therefore, neglected; however, this is most likely a secondary effect. Consequently, the problem is reduced to two dimensions.

- The loading is assumed to be applied slowly so that acceleration effects of the soil can be neglected.

Loading

Figure 43 shows the portion of the half-plane which is loaded by a uniform vertical pressure, p_n, and a uniform shear distribution, p_s. The indicated loading is intended to represent a very simplified simulation of the effect of an aircraft tire during braking. The shear distribution, p_s, is a function of the contact area between the tire and the soil, the cohesion, the friction angle, and the percent slip between the tire and the soil. The loading is assumed to remain constant during the deformation.

Region of Solution

Thus far the problem has been reduced to a loaded half-space. In order to effect a solution by numerical means, however, the extent of the region affected by the load must be restricted to be finite. Figure 44 shows two possible approaches. In Figure 44a, a rectangular area has been designated as the region of solution while a semicircular area is indicated in Figure 44b. In each case, an attempt is made to select the dimensions of the region so that the load has negligible influence on the displacements at the extremities of the region.

Boundary Conditions

- Under the load the normal stress is equal to the uniform vertical pressure (p_n) and the shear stress is equal to the uniform shear distribution (p_s) (Figure 44).

86

ℓ = Tire Footprint Length

p_n = Uniform Vertical Pressure

p_s = Uniform Shear Distribution
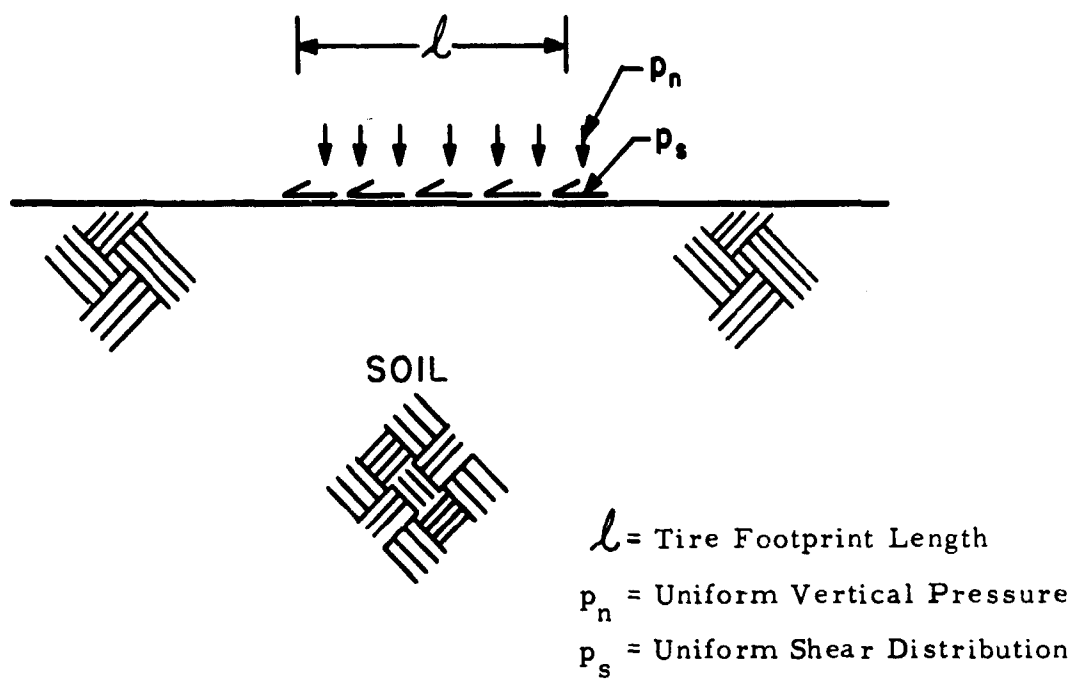
SOIL

Figure 43. Simulated Loading During Braking
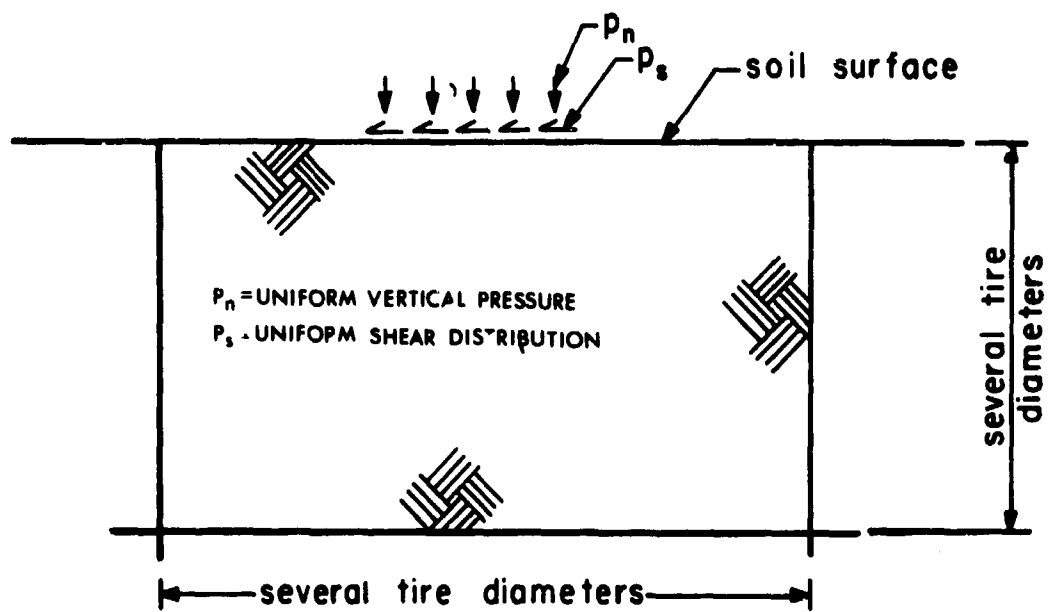
(a)
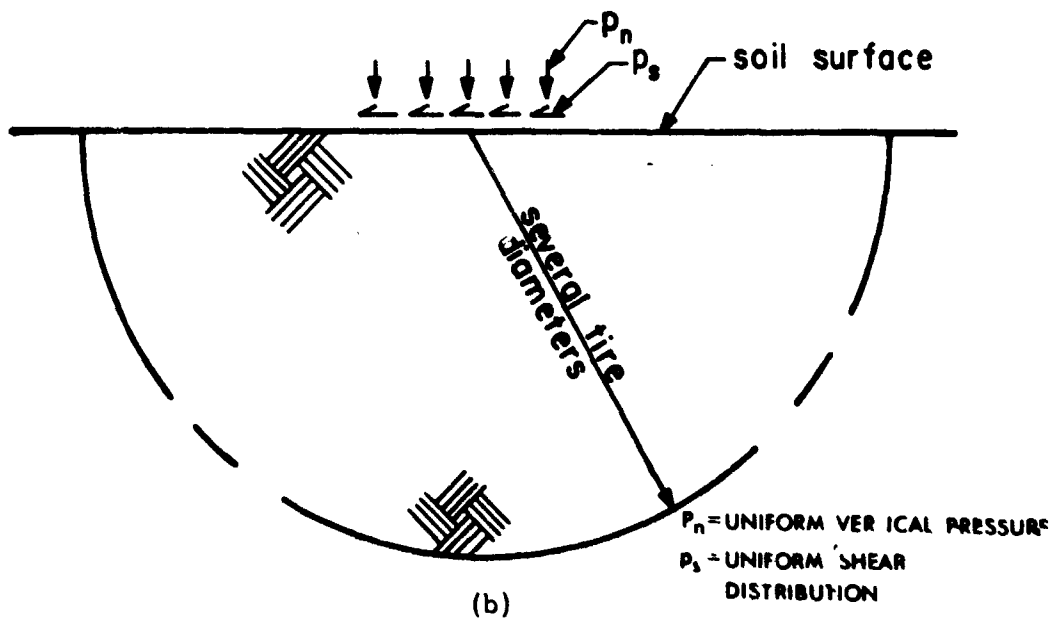
(b)

Figure 44. Region of Solution for Finite Element

88

- The shear and normal stresses are zero on the remainder of the soil surface.

- The displacements are zero on the artificial boundaries which limit the extent of the soil medium (Figure 44).

PART 2 - Mathematical Model

The technical literature pertaining to the elastic-plastic analysis of structures by the finite element method has been reviewed and evaluated. A comparative study of the most pertinent sources appearing in the literature through 1967 is given by Marcal[24]. It has been determined that the best existing approach to the prediction of elastic-plastic response is the technique presented in Reference 24 and explained in greater detail in Reference 25 . Essentially, the method involves applying the loading in small increments and performing a linearized direct stiffness analysis at each stage of the load incrementation. The mathematical model is the incremental potential energy of an assembled set of finite elements. The discretized stiffness equations are based on assumed finite element displacement approximations since a potential energy formulation is basically a displacement formulation. The primary disadvantage of Marcal's technique is that the predicted stress state is discontinuous between the individual elements; this situation is common to all displacement approaches, however. One valuable attribute of the method is that it is equally applicable to both perfectly plastic and work hardening materials.

It is believed that an improved method for solving elastic-plastic problems can be developed by using an incremental Reissner energy[26] expression rather than an incremental potential energy formulation as the mathematical model. The Reissner energy treats both displacements and stresses as primary variables. Therefore, the discretized stiffness equations will be based on assumed finite element stress and displacement states rather than just assumed element displacement states. Consequently, it will be possible to obtain continuous stresses as well as continuous

89

displacements with a Reissner energy formulation. Some of the principal characteristics of the method to be used for predicting the sinkage of braked aircraft tires are outlined below.

Finite Element

Two different finite elements are considered as possible candidates for the modeling of the region of solution: a rectangular element (Figure 45) and a triangular element (Figure 46). The displacement and stress approximations within each of the two types of finite elements are taken as bilinear functions of the spatial variables in the form:

$$f^{(r)}(x, y) = c_1 + c_2 x + c_3 y + c_4 xy \tag{32}$$

$$f^{(t)}(x, y) = d_1 + d_2 x + d_3 y \tag{33}$$

where the superscripts r and t refer to the rectangular and triangular elements, respectively. The function $f(x, y)$ represents any of the displacement and stress variables u, v, σ_x, σ_y, σ_{xy}. Both forms of the approximating functions given in Equations (32) and (33) contain sufficient generality to insure continuous displacements and stresses across the common boundaries of interfacing elements.

As in the normal application of the finite element method, the displacement and stress approximations can be expressed in terms of the nodal values by evaluating Equations (32) and (33) at the nodes (Figure 45 or 46) and solving for the constants c_i, i=1, 2, 3, 4 or d_i, i=1, 2, 3 depending on which element type is utilized. For example, the displacement and stress states of a rectangular finite element can be put in the form

$$\begin{Bmatrix} u \\ v \\ \sigma_x \\ \sigma_y \\ \sigma_{xy} \end{Bmatrix}^{(r)} = \lfloor P(x, y) \rfloor \{\delta\} \tag{34}$$

90
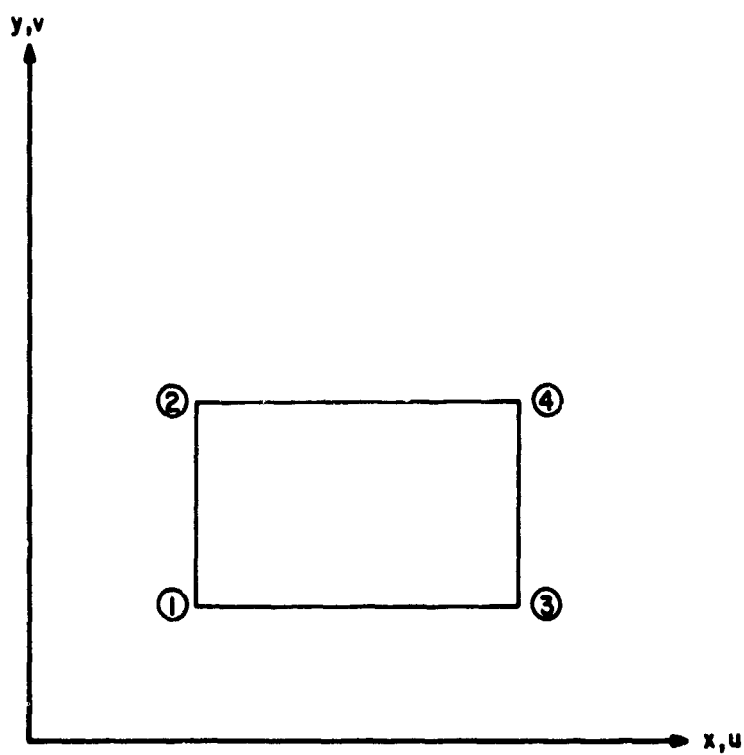
Figure 45.   Rectangular Element
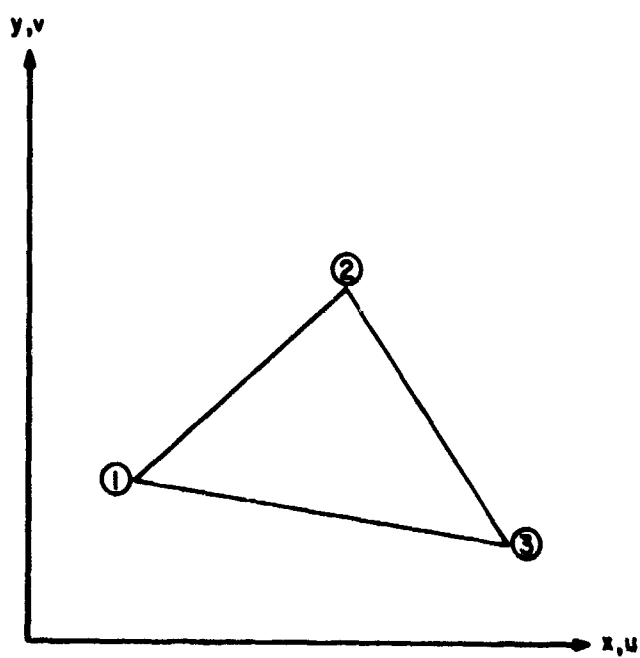
Figure 46.   Triangular Element

91

where $\{\delta\}$ is a vector which contains the nodal values of the stresses and displacements and $\{P(x,y)\}$ is a vector of bi-linear functions of x and y. The vector of nodal variables, $\{\delta\}$ contains 20-elements since there are 4-nodal values (in the case of the rectangular element) for each of the 6-variables u, v, σ_x, σ_y, and σ_{xy}.

Stiffness Matrix

The Reissner energy for a typical finite element in plane strain which is situated within the interior of an assemblage of finite elements can be written as

$$\pi_R = \int\int_A \{\sigma_x u_{,x} + \sigma_y v_{,y} + \sigma_{xy}(u_{,y} + v_{,x}) - \frac{1}{2E}[(1-\nu^2)(\sigma_x^2 + \sigma_y^2)$$

$$- 2\nu(1+\nu)\sigma_x\sigma_y + 2(1+\nu)\tau_{xy}^2]\}\,dx\,dy \tag{35}$$

Substituting the assumed displacement and stress states given by Equations (32) and (33) into the Reissner energy expression and performing the indicated integrations over the element area results in a quadratic form in the nodal variables

$$\pi_R = \frac{1}{2}\lfloor\delta\rfloor[k]\{\delta\} \tag{36}$$

where $[k]$ is the stiffness matrix associated with the Reissner energy.

The total Reissner energy of an assembled set of finite elements can be written as

$$\pi_R = \frac{1}{2}\lfloor\Delta\rfloor[K]\{\Delta\} - \lfloor\Delta\rfloor\{P\} \tag{37}$$

where $\{\Delta\}$ is a vector containing the independent, non-imposed nodal variables, $[K]$ is the assembled stiffness matrix, and $\{P\}$ is a vector of imposed nodal displacements or stresses. The first term in Equation (37) is the total Reissner energy of an assemblage of elements and the second term is interpreted as the external work associated with imposed stresses and displacements (boundary conditions).

Invoking the stationary Reissner energy principal, Equation (37) implies that

$$[K]\{\Delta\} = \{P\} \qquad (38)$$

from which the unknown nodal displacements and stresses can be determined by

$$\{\Delta\} = [K]^{-1}\{P\} \qquad (39)$$

Typical Finite Element Modeling

Figure 47 shows a typical finite element modeling of the region of solution of Figure 44b using triangular elements. In this case, the material in the vicinity of the loading has been modeled with small elements while increasingly larger elements are used toward the extremity of the region. Typical modeling of the region in Figure 44a is not shown here since it is more or less obvious. Note that the uniform normal and shear distributions have been converted into equivalent concentrated node forces. The eventual solution to the problem may or may not require a more refined modeling than the one shown.

PART 3 - Solution

If the soil material were completely elastic in nature, the solution could be obtained by applying Equation (39) a single time. The material, however, is assumed to be elastic-plastic. Therefore, if the stresses in an element are of such a magnitude that plastic deformation occurs the stiffness matrix for that element depends on the stress state and is no longer constant. Clearly, this makes the assembled stiffness matrix nonconstant also. Consequently, the solution procedure will be to express the Reissner energy in terms of incremental stresses and displacements and derive an "incremental stiffness matrix" which includes the effects of plastic flow as well as initial stresses and displacements. The loading applied to the soil surface will then be applied in small increments and at

93

P_n = Uniform Vertical
Pressure
P_s = Uniform Shear Distribution
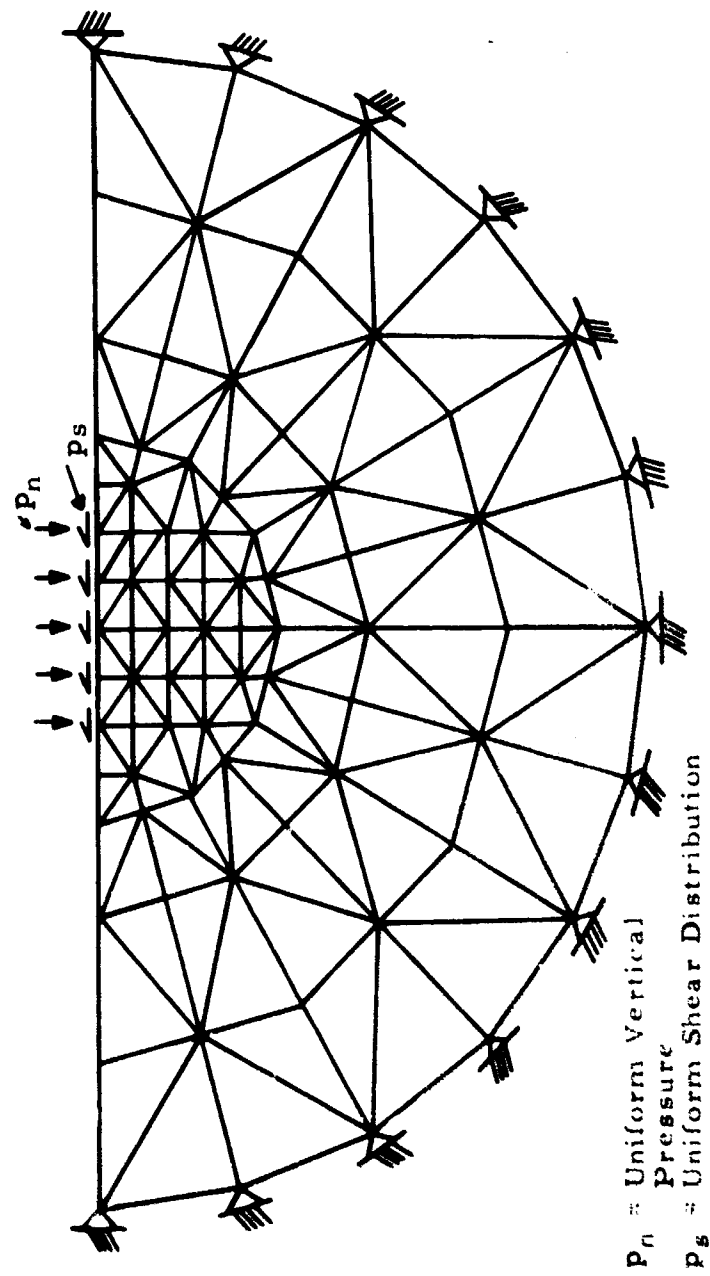
Figure 47. Sample Finite Element Modeling

each stage of the loading the stiffness matrices will be updated for those elements which have yielded. The total deformation and stress states caused by the applied loading will be obtained by summing the incremental stresses and displacements obtained during each load increment. The residual displacement state (sinkage) and stress state which remains after unloading will be obtained by the solution described above minus a completely elastic solution.

PART 4 - Progress-to-Date

- An appropriate incremental Reissner energy expression for two-dimensional, plane strain, elastic-plastic problems has been derived.

- Finite element stiffness relations based on the Reissner energy principle have been derived for rectangular elements with bilinear, assumed stress and displacement states. The bilinear variation is sufficient to assure interelement stress and displacement continuity and solution accuracy can be controlled by varying the number and size of the finite elements used to model the region of solution.

- A test computer program has been nearly completed. No example cases have been treated as yet.

4. Braked Wheel Verification Tests

The simplifying assumptions made in the development of the braking analysis equations (Equations 30 and 31) as well as the results of the comparative study certainly points to the need for additional braked tire on soil performance data from both controlled laboratory testing and full scale field tests. Currently scheduled as a part of this continuing research effort are a series of Braked Wheel Verification Tests. These tests will begin in early February, 1971 and the results of these tests will very likely lead to some modification in Equations (30) and (31).

SECTION IV

ADDITIONAL STUDIES IN TIRE/SOIL INTERACTION

1.   Single Wheel Comparative Study

Under Phase II of the research program, a single wheel simulation computer program was developed for predicting sinkages in sand and clay soil of moving aircraft tires. The results from the development of this program which used a lumped parameter approach are available elsewhere[1]. Subsequent to this computer program development, a number of comparisons were made between predicted sinkages as determined from the computer program usage and the experimentally determined sinkages from the Single Wheel Verification Tests of Phase II[1]. The results of this comparative study are given below.

The results of the comparisons are shown in Table 22 for Tests No. 8, 9, 10, 12, and 19 in clay soil of the Single Wheel Verification Tests[1]. Loading and soil parameters used in the sinkage prediction were taken from data developed from these tests[1]. Reference to Table 22 indicates that in 3 cases the predicted sinkages were within 16% of the measured sinkages. Differences in the other two cases compared ranged up to approximately 40%.

In order to study the influence of varying such parameters as cohesion, Young's modulus, and duration of pulse while holding other parameters constant, an additional series of runs were made using the single wheel simulation computer program. A summary of the additional cases is shown in Table 23.

The results of varying the cohesion and Young's modulus are shown in Figure 48. In this graph, the sinkage characteristic (defined as the instantaneous sinkage divided by the footprint length) is plotted against

96

TABLE 22

SINKAGE PREDICTION BY STATIONARY PULSE LOAD COMPUTER
PROGRAM COMPARED WITH EXPERIMENTAL RESULTS
(CLAY SOILS)

Test No.	Vertical Load (lbs) P	Peak Pressure p(psi) P_{max}	E (psi)	c (psf)	ϕ (deg)	Experi- mental Sinkage Z, (inch)	Analytical Sinkage Z, (inch)
High Strength Clay							
8	2019	21.3	575	560	1	0.39	0.33
9	1000	17.9	575	560	1	0.30	0.17
10	1494	25.1	575	560	1	0.52	0.68
Low Strength Clay							
12	995	10.5	178	230	1	0.91	1.03
19	503	9.6	178	230	1	0.60	0.68

TABLE 23

ADDITIONAL SINKAGE PREDICTION CASES - CLAY SOIL

Test No.	Soil Type	Vertical Load P(lbs)	Contact Area A(in^2)	Peak Pressure p P$_{max}$(psi)	E (psi)	c (psf)	φ (deg)	Time Duration (sec)
8	Clay	2019	94.8	21.3	575	450	1	0.1
"	"	"	"	"	"	500	"	"
"	"	"	"	"	"	560	"	"
"	"	"	"	"	425	"	" ╱	"
9	"	1000	55.8	17.9	575	450	"	"
"	"	"	"	"	"	500	"	"
"	"	"	"	"	"	560	"	"
10	"	1494	59.5	25.1	"	450	"	"
"	"	"	"	"	"	560	"	"
11	"	2016	57.9	34.8	"	450	"	"
12	"	995	95.0	10.5	178	230	"	"
"	"	"	"	"	"	"	"	0.05
"	"	"	"	"	"	"	"	0.01
"	"	"	"	"	"	255	"	0.1
"	"	"	"	"	"	280	"	"
"	"	"	"	"	"	350	"	"
19	"	503	52.3	9.6	"	230	"	"
"	"	"	"	"	"	255	"	"
"	"	"	"	"	"	280	"	"
"	"	"	"	"	"	350	"	"

98

Figure 48. Analytically Predicted Sinkages Compared With Experimental Results

99

the load-strength ratio (defined as the average tire contact pressure, α, divided by the average cone index of the soil). Shown in the same graph are experimental data previously compiled from the literature. The analytically predicted results show a trend of dependence on the dimensionless parameter, α/E, where E is Young's modulus of elasticity. For lower values of load strength ratio (<0.5), the analytically predicted sinkage ratios are quite close to the experimental results. This indicates that the computer program simulation is satisfactory. But for higher load strength ratios, the predicted sinkages are larger than their corresponding experimental results, and the trends are indicated by the solid line curves. This trend of higher sinkage occurs because a non-strain hardening soil model was used and for $\alpha/CI_{avg} > 0.5$, the pressures were many times greater than the limiting yield strength.

The results of varying the time duration of the load pulse are shown in Figure 49. In this graph, the time duration of the load pulse was converted to horizontal ground velocity of the aircraft based on the relationship given in Reference 13. The sinkage decreases as the velocity increases. The known increase of sinkage in the Region III velocity range does not occur in this instance because the stationary load sinkage prediction computer program cannot account for the plowing and hydroplaning effects of the high speed forward motion.

100
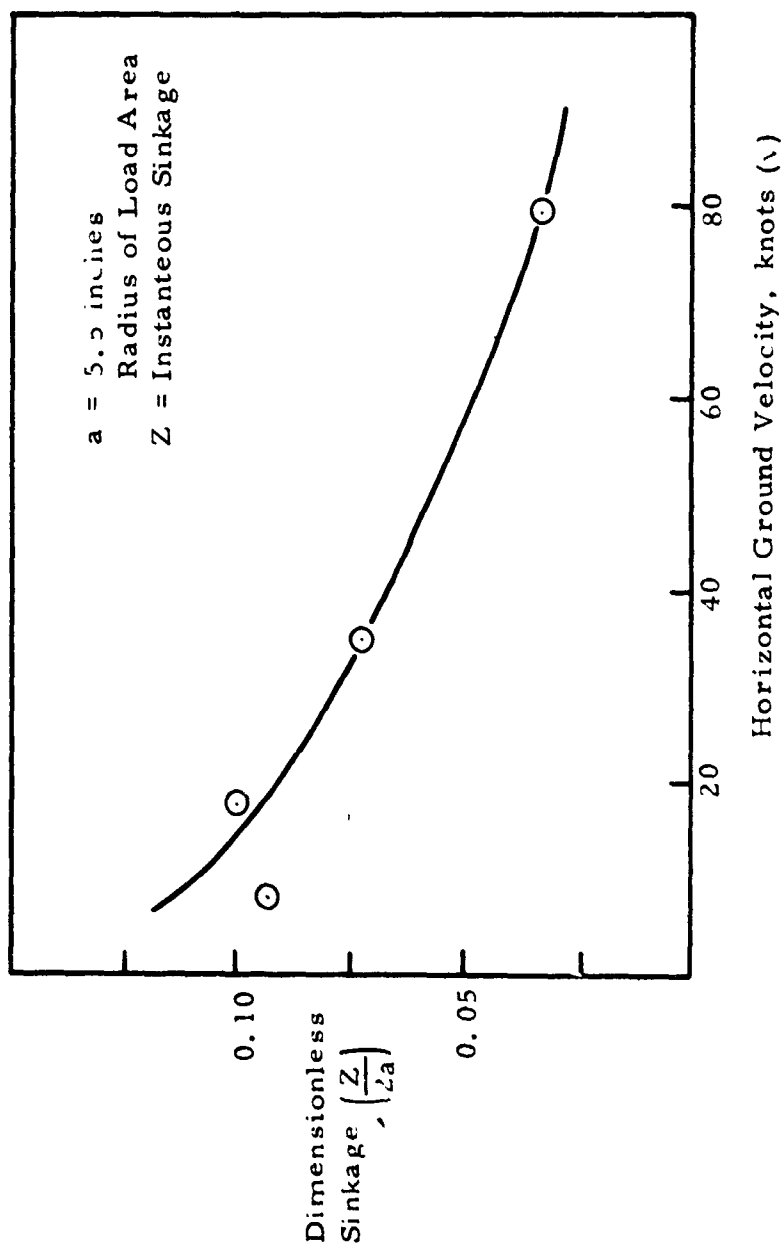
Figure 49. Analytically Predicted Sinkage vs. Horizontal Ground Velocity

SECTION V

MULTIWHEEL FLOTATION CRITERIA AND RESEARCH PLANNING

1. Multiwheel Flotation Criteria

The multiwheel flotation criteria described herein is an extension of the previously developed single wheel flotation criteria[1]. The multiwheel criteria permits the evaluation of aircraft flotation performance rather than single tire performance. It also will permit aircraft designers to determine optimum landing gear configuration (twin, tandem, spacing, etc.) for aircraft leading to drag minimization.

The basis of the multiple wheel drag criteria is the previously defined multiple wheel dra; modifier (see Section II, Part 4) which leads to the definition of the multi-wheel drag ratio as

$$(FI)_M = (\frac{R}{P})_S M_M \tag{40}$$

where

$(\frac{R}{P})_S$ = single wheel drag ratio

M_M = multiple wheel drag modifier

By using the following definition of terms,

N = total number of wheels per landing gear

N_n = number of wheels (of N) in a twin situation

N_m = number of wheels (of N) in a tandem-tracking situation

N_r = number of wheels (of N) in a tandem-nontracking situation

K_n = drag modifier for twin wheel situation (see Figure 50)

K_m = drag modifier for tandem-tracking situation (see Figure 51)

K_r = drag modifier for tandem-nontracking situation (see Figure 52)

the drag variations due to multiple wheel configurations are given by

102

$N_n(R-K_n R)$ = drag increase or decrease due to twin wheel effects

$N_m(R-K_m R)$ = drag increase or decrease due to tandem-tracking wheel effects

$N_r(R-K_r R)$ = drag increase or decrease due to tandem-nontracking wheel effects.

where

R = single wheel drag.

The resulting multiwheel drag per tire is then given as

$$(R)_{\text{multiwheel per tire}} = R\left[1 - \left\{\frac{N_n}{N}(1-K_n) + \frac{N_m}{N}(1-K_m) + \frac{N_r}{N}(1-K_r)\right\}\right] \quad (41)$$

and the multiwheel drag ratio becomes

$$\left(\frac{R}{P}\right)_M = \left(\frac{R}{P}\right)_S\left[1 - \left\{\frac{N_n}{N}(1-K_n) + \frac{N_m}{N}(1-K_m) + \frac{N_r}{N}(1-K_r)\right\}\right] \quad (42)$$

The multiple wheel drag modified becomes then

$$\frac{\left(\frac{R}{P}\right)_M}{\left(\frac{R}{P}\right)_S} = M_M = \left[1 - \left\{\frac{N_n}{N}(1-K_n) + \frac{N_m}{N}(1-K_m) + \frac{N_r}{N}(1-K_r)\right\}\right] \quad (43)$$

The results of the multiwheel drag analysis presented in Section II were used to develop the drag modifier relationships, $(1-K_n)$, $(1-K_m)$, and $(1-K_r)$ shown in Figures 50, 51, and 52. The curves shown in Figures 50, 51, and 52, reflect the results of all the work conducted to date on multiple wheel interaction effects and represent an attempt to bracket these results while still trying to indicate high and low sinkage magnitudes. High sinkages are defined as greater than approximately one inch while low sinkages generally are less than one-half inch. In order to facilitate the determination of M_M, Equation 43 was put into nomographic form as shown in Figure 53.

The current multiple wheel drag criteria is defined for the Region II velocity range. Extensions of this criteria to Regions I and III will be made as analytical and experimental results become available. Based on

103
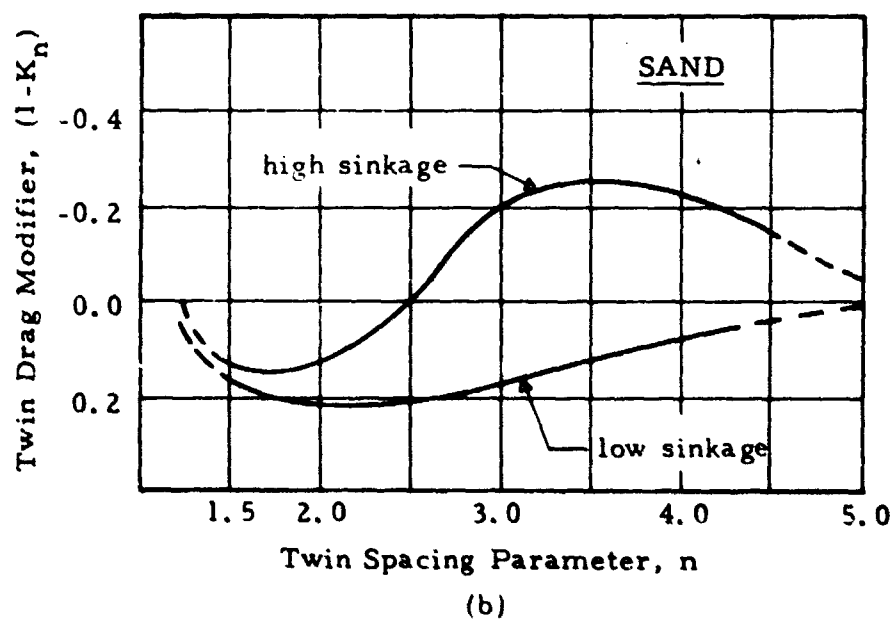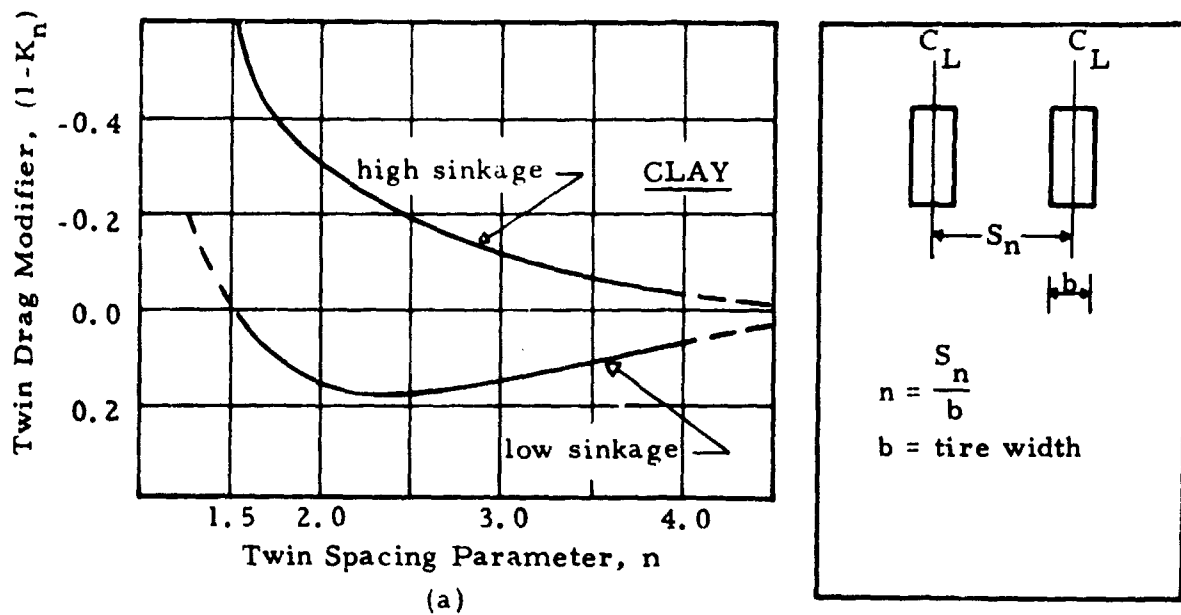
Figure 50. Drag Modifiers for Twin Wheel Situations

104
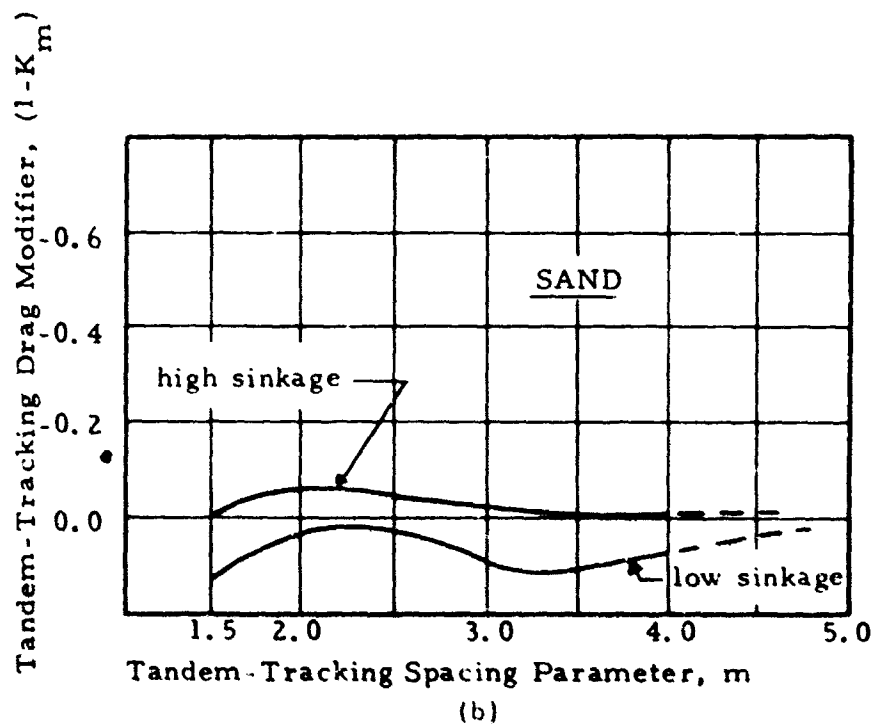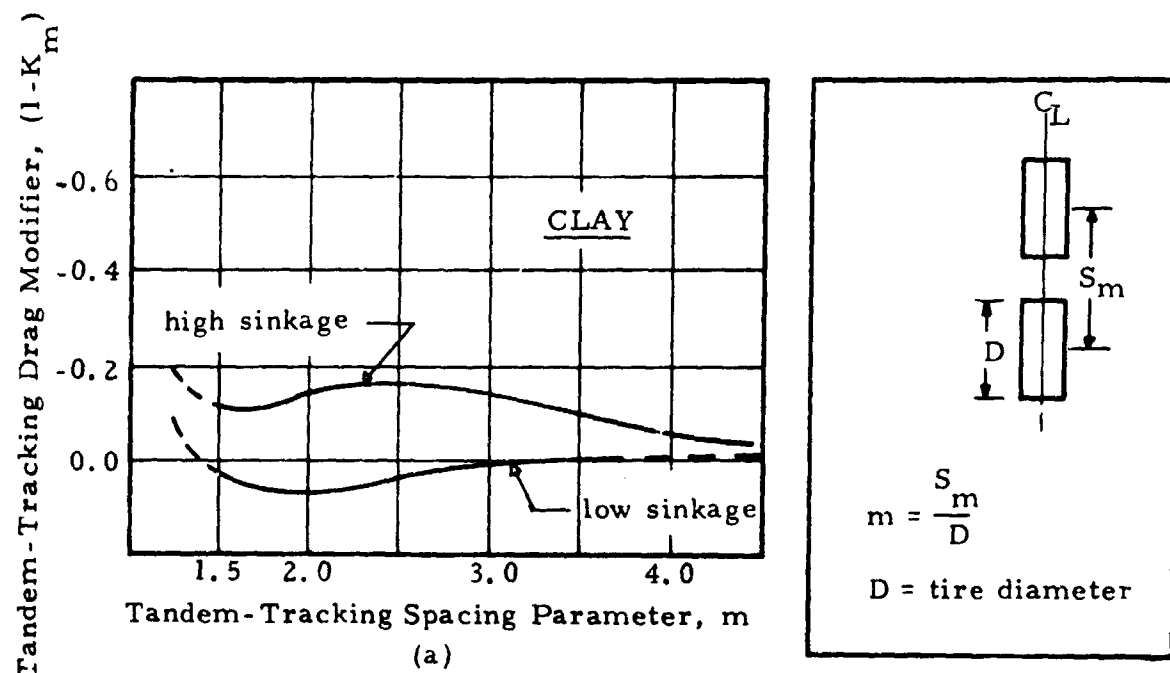
Figure 51. Drag Modifiers for Tandem-Tracking Situations

Figure 52. Drag Modifiers for Tandem-Nontracking Situations

The figure's y-axis is labeled "Tandem-Nontracking Drag Modifier, $(1-K_r)$" with values -0.6, -0.4, -0.2, 0.0. The x-axis is labeled "Tandem-Nontracking Spacing Parameter, r" with values 1.5, 2.0, 3.0, 4.0. The plot is labeled "SAND & CLAY".

The right panel shows a diagram with C_L, L, C_L, S_m, S_n, and:

$$r = \frac{L}{\sqrt{b^2 + D^2}}$$

where

$$L = \sqrt{(S_m)^2 + (S_n)^2}$$

106
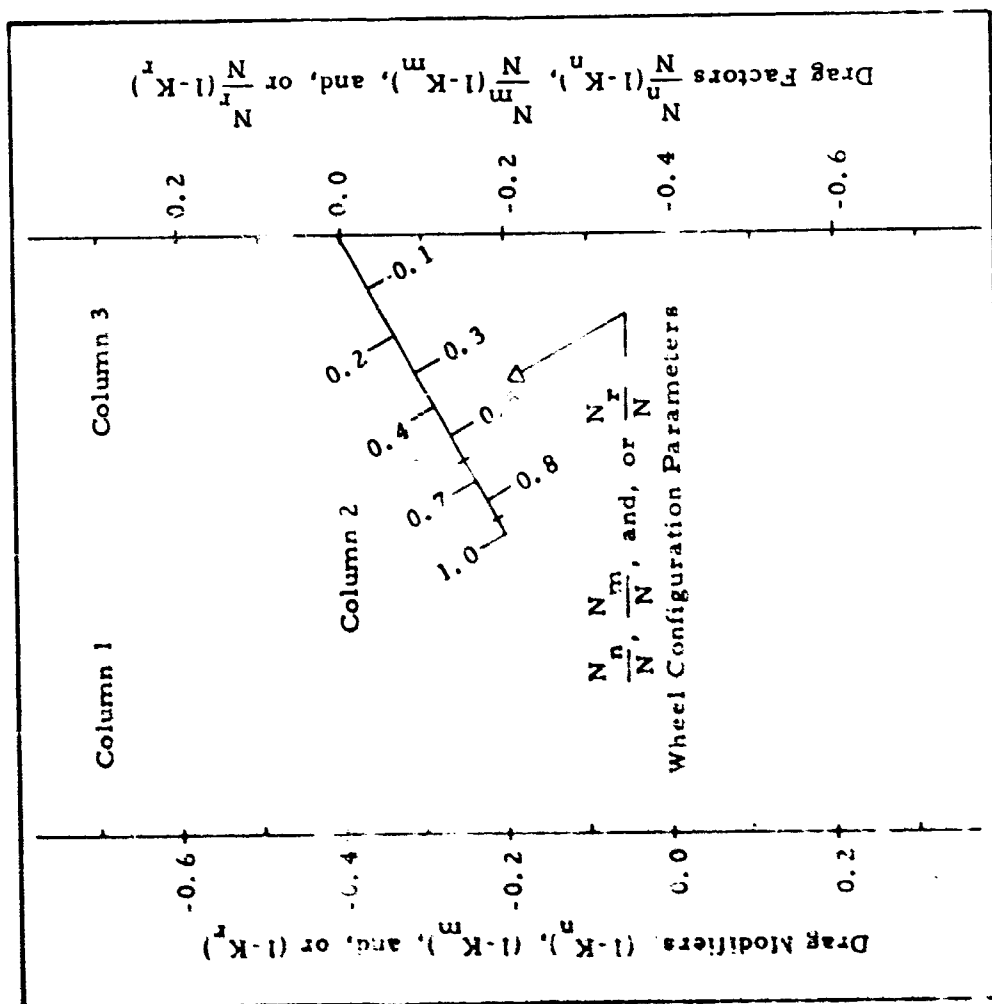
Instructions:

- Determine the drag modifiers from Figures

- Enter nomograph from left column and draw a straight line between Column 1 and Column 2, crossing the appropriate drag modifier with the respective wheel configuration parameter.

- Read the drag modifiers from Column 3.

- The multiwheel modifier (M_M) is then equal to one (1) minus the sum of the drag modifiers.

$$M_M = 1 - \left[\frac{N_n}{N}(1-K_n) + \frac{N_m}{N}(1-K_m) + \frac{N_r}{N}(1-K_r) \right]$$

N = total number of wheels
N_n = no. of wheels that are twin
N_m = no. of wheels in tandem-tracking situation
N_r = no. of wheels in tandem-nontracking situation

Note: This chart should not be used for actual problems. An exact nomograph can be requested from AFFDL/FED, Wright-Patterson AFB, Ohio 45433

Figure 55. Multiple Wheel Modifier Nomograph

available evidence, it is unlikely that the relative flotation capacity as defined for Region II will change when considering Regions I and III (although the absolute drag ratios will change).

2. Multiple Wheel Flotation Criteria Example

In order to illustrate the use of the multiple wheel flotation index, $(FI)_M$, an example was prepared using the C-5A aircraft. In order to arrive at $(FI)_M$, the single wheel flotation index, $(FI)_S$, as determined from Figure 54 is required.

C-5A FLOTATION RATING

Given the C-5A aircraft, calculate the Multiwheel Drag Ratio, $(R/P)_M$, for the normal landing weight and tire deflection on a CBR 8 (250 CI) clay soil.

Known Information

- Clay Soil, $CI_{avg} \approx 250$
- C-5A landing gear configuration (Figure 55)
- Tire size is 49 x 17-26 PR Type VII
- Load distribution to Main Gear (max) is 94.2%,

$$P(\text{per tire}) = \frac{641,200 \times 0.942}{24} = 25,200 \text{ lbs.}$$

- Normal tire deflection is 35%
- Normal landing weight is 641,200 lbs.

Solution

A. Using Reference 27, all tire data and parameters can be calculated for the main gear.

Tire diameter, D	= 48.4 in.
Tire width, b	= 16.7 in.
Tire deflection, d	= 4.36 in.
Tire print length, l	= 13.86 in.
Tire contact area, A	= 240 sq. in.
Tire load, P	= 25.2 kips

108

Note: Not to scale. To obtain accurate answers
request a nomograph from AFFDL/FEM,
Wright-Patterson AFB, Ohio 45433.
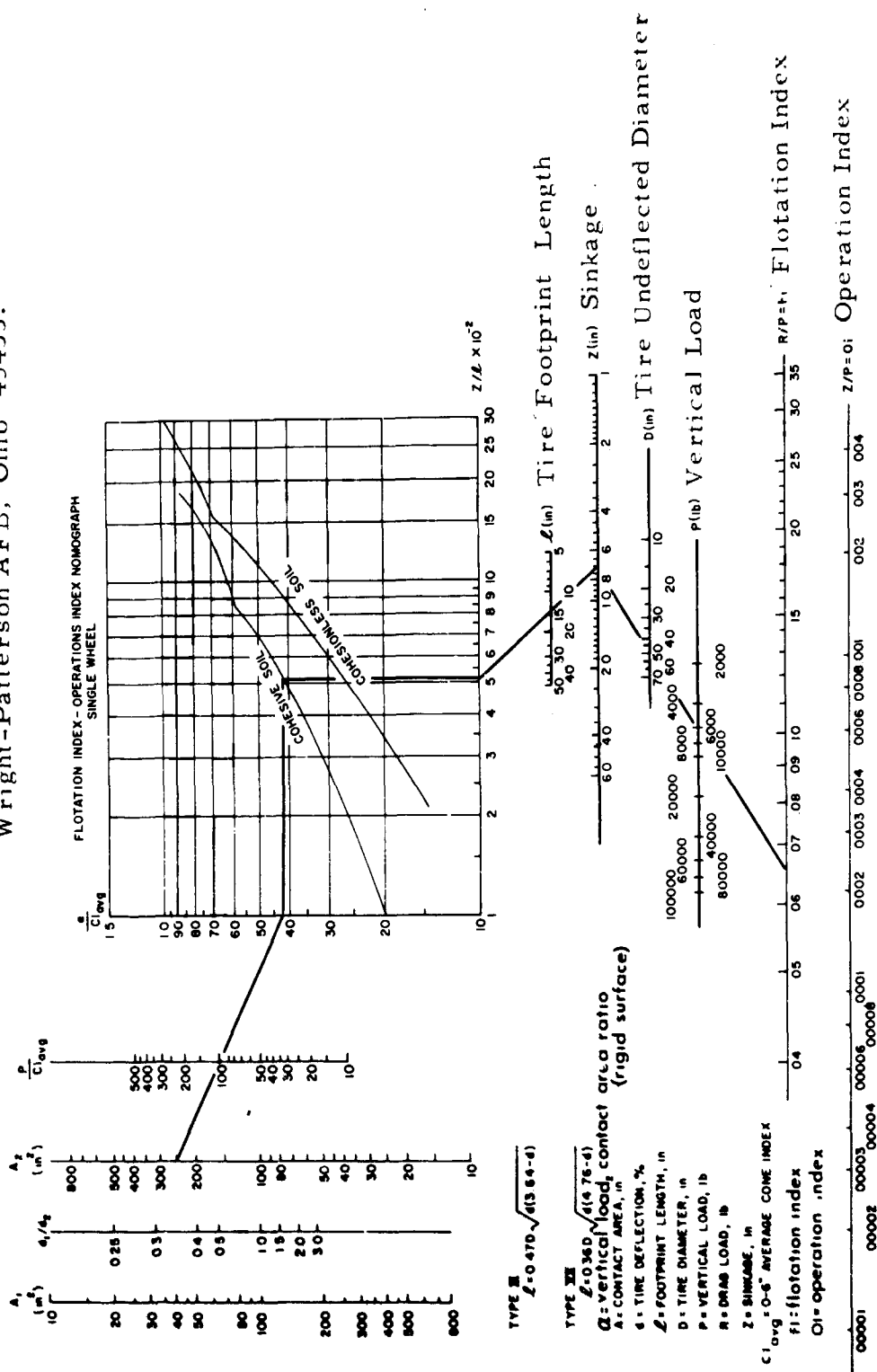
FLOTATION-OPERATIONS INDEX NOMOGRAPH

Figure 54. Single Wheel Flotation Index Nomograph

one unit
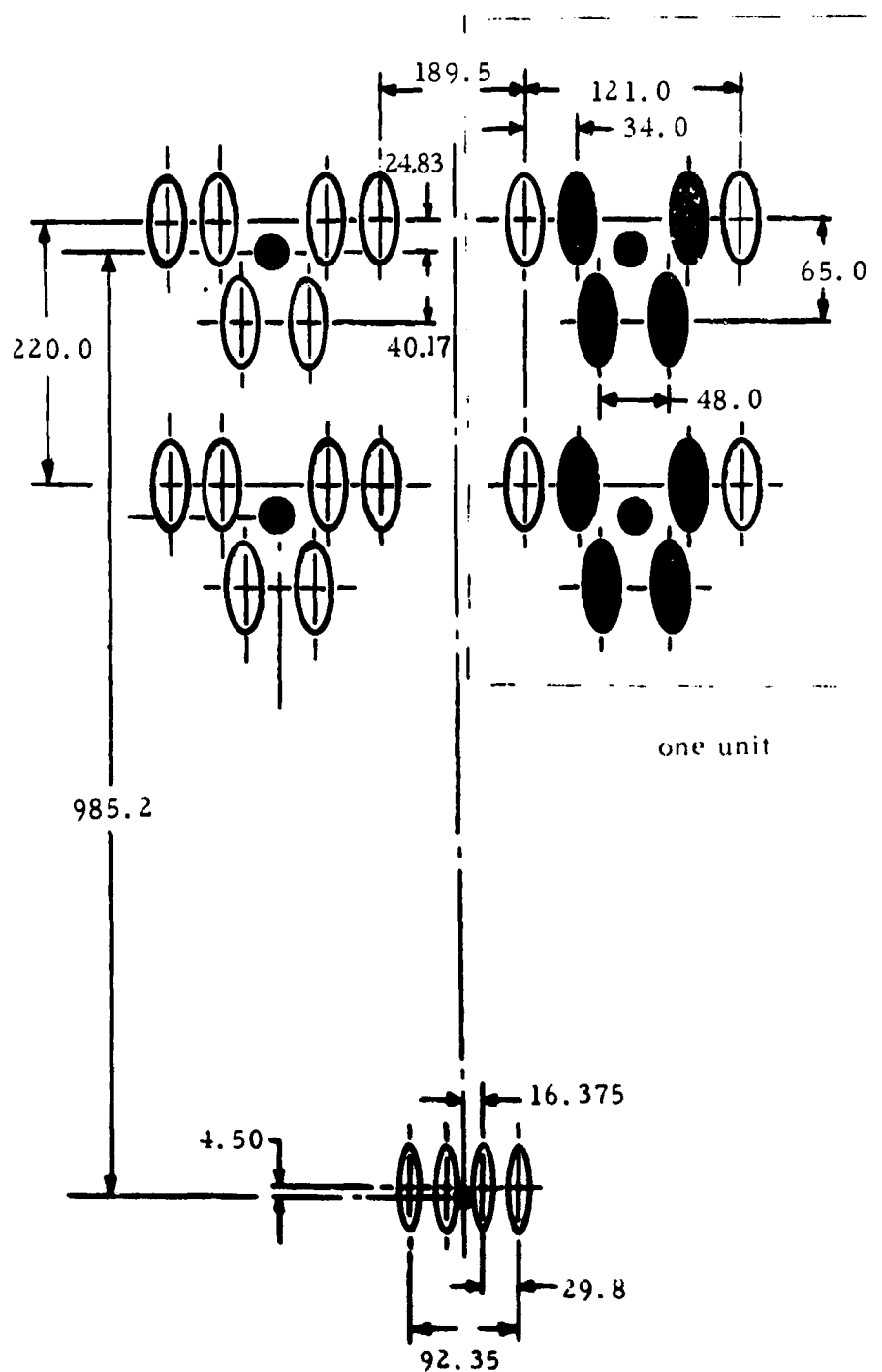
MAIN LANDING GEAR CONFIGURATION - TWIN DELTA TANDEM
NOSE LANDING GEAR - TWIN - TWIN

Figure 55. C-5A Landing Gear Configuration

B. Using the nomograph in Figure 54, calculate the single wheel performance:

a. Calculate $P/CI_{avg} = \dfrac{25200}{250} = 101$

b. Intersect 240 sq. in. (A_2) with $P/CI_{avg} = 101$, which gives $\alpha/CI_{avg} = 0.42$

c. Move horizontally to intersect the cohesive (clay) line and down vertically to get $Z/\ell = 5.0 \times 10^{-2}$

d. Intersect $Z/\ell = 5 \times 10^{-2}$ with $\ell = 13.9$ to get $Z = 0.7''$

e. Intersect $Z = 0.7''$ with $D = 48.4''$ to get
$(FI)_S = (R/P)_S = 0.065$

C. Using Figures 50, 51, 52 and 53, calculate the Multiwheel Modifier, M_M:

a. Calculate the spacing parameters m, n, and r. As the multiwheel criteria is limited in its scope, some simplifying assumptions must be made to rate all aircraft landing gear configurations. The C-5A main landing gear consists of two identical units of 12 tires each as indicated in Figure 55. The M_M for either unit is identical and the calculations will be based on the following assumptions.

ASSUMPTIONS

- Assume that all eight center tires in the indicated unit (shaded in Figure 55) act as tandem-tracking tires at $S_m = 65''$.
- Assume that all 12 tires in the indicated unit act as twin tires at $S_n = 42''$ even though the actual S_n ranges from 34'' to 53''.
- Interaction effects due to tandem-nontracking tires are negligible (see Figure 52).

Then:

$$m = \frac{S_m}{D} = \frac{65''}{48.4''} \approx 1.4 \qquad n = \frac{S_n}{b} = \frac{42''}{16.7''} \approx 2.5$$

111

b. Determine the Drag Modifiers:

- From Figure 50, for clay soil, move vertically from n=2.5 to a point between the two lines. The upper line represents the relation for sinkages of 1" or greater, the lower line represents sinkages of 0.5" or less. Therefore, for Z = 0.7" (see above) the point should be ≈1/2 the distance between the lines. Now move horizontally to read $(1-K_n) = 0.0$.

- From Figure 51, for clay soil, move vertically from m=1.4 to a point between the two lines keeping in mind the relative values of the sinkages. Move horizontally from the extrapolated value to read $(1-K_m) = -0.10$.

c. Determine the wheel configuration parameters

$$\frac{N_n}{N} = \frac{12}{12} = 1.0$$

$$\frac{N_m}{N} = \frac{8}{12} = 0.67$$

d. Enter Figure 53 and determine M_M:

$$\frac{N_n}{N}(1-K_n) = 0.0$$

$$\frac{N_m}{N}(1-K_m) = \underline{-0.067}$$

$$\text{Total } -0.067$$

$$M_M = 1 - (-0.067) = 1.067$$

'. Determine the Multiwheel Drag Ratio

$$(R/P)_M = M_M(R/P)_S = 1.067 \times 0.065 = 0.069$$

112

Note that this value is slightly different from that which would be calculated if the exact equations were used versus the general equations used to construct the single wheel nomograph[1].

3.   Current Aircraft Flotation Ratings

The procedure as detailed above was used to evaluate the currently used cargo type military aircraft as to their relative flotation capacity. The ratings are based on the Multiwheel Drag Ratio, $(R/P)_M$, using the specific conditions listed in Figure 56 which also shows the resulting ratings in a chart format. The most commonly used aircraft type tires have been previously rated for flotation capacity and their ratings can be found in Reference 1.

4.   Summary of Flotation Criteria

A summary of the current state of the art in aircraft flotation criteria is presented in Table 24. This table is an attempt to present in a summary fashion all of the current flotation criteria as developed by both UDRI and others.

5.   Research Planning

As a part of the continuing research program by the Air Force, research planning in knowledge deficient areas has been conducted as a part of the current effort. The planning efforts to date have been in the areas of braking, multipass, and speed. The results of these planning efforts are currently under review by AFFDL/FEM.

6.   Current Research Results and Reports

In order to provide an up to date overview of the current research work being conducted in the areas of aircraft flotation and vehicle mobility, the University has established a research library. Efforts are continually made to obtain the results of past and on-going research programs from governmental and private agencies. The library system

113

AIRCRAFT FLOTATION RATINGS

(R/P)

M

0.00

C-123K — C-119G

0.05

C-131E — C-5A

0.10 — C-130E

C-133B

0.15 — C-135A

— KC 97G

0.20

C-141A

0.25

0.30

Increased Flotation Capability

The aircraft listed are rated based on data taken from References 27, 28, and 29, using the conditions listed below:

Soil Strength ≈ 8 CBR
   (250 CI)
Normal Landing Wt.[28]
Normal Tire Deflection[27]
Clay Type Soil
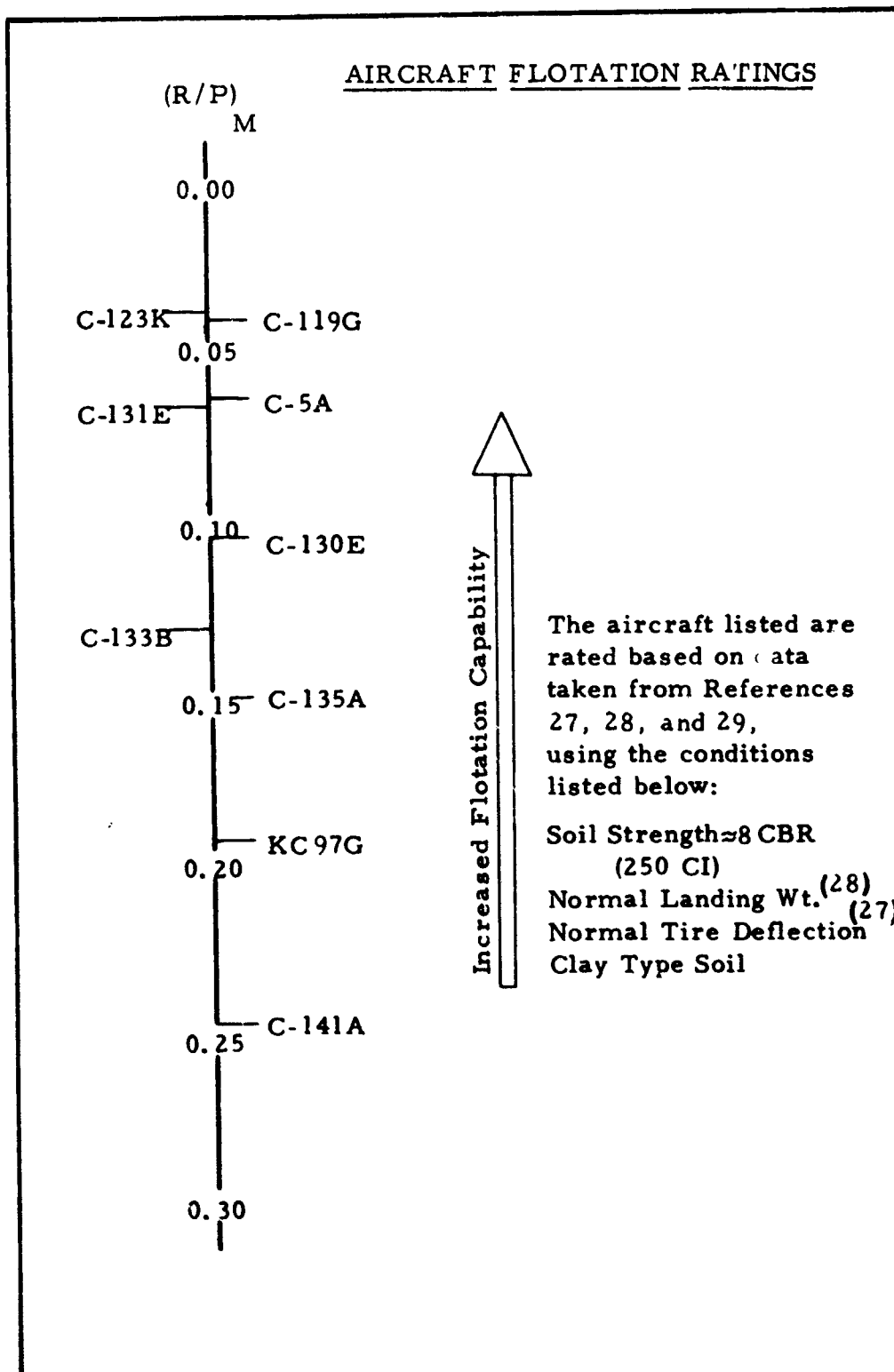
Figure 56. Cargo Type Aircraft Flotation Ratings

TABLE 24

Currently Available and Proposed Aircraft Flotation/Operation Criteria

	FLOTATION VARIABLE	CRITERIA	INDEX	LIMITING SPECIFICATION	LIMITATIONS ON USE	ACCURACY	USER ORGANIZATION
PRIMARY FLOTATION VARIABLES	DRAG	Rolling drag ratio, R/P	Flotation Index, FI_S, for single wheel; Flotation Index, FI_M, for aircraft (multiple wheels)	None required, design or analysis based on comparative procedures in minimizing R/P.	Region II velocity range (5 to 40 knots). Relative rating unlikely to change in Region I and III.	Estimated ±20% within 90% confidence limits. Not established	UDRI; WES, Boeing, Governmental
	SINKAGE	Limiting magnitude of sinkage, Z, permanent or elastic	Permanent, Z_R; Elastic, Ze	3 inches; 1.5 inches	Region I Velocity range Clay soil only	Conservative	--
		Sinkage Ratio, Z/D	None	Z/D = 0.10	Proposed Criteria	Not established	
		Sinkage per unit load, Z/P	Operations Index, OI	None required, design or analysis based on comparative procedures in minimizing Z/P after design based on FI	Region II velocity range (5 to 40 knots)	Estimated ±40% within 90% confidence limits	UDRI
	BRAKING	Braking drag ratio, $R_B/P(S)$	Drag Index, DI	None required, design or analysis based on comparative procedures in maximizing R_B/P after design based on FI	Proposed criteria	Not established	--
		MIL-A-8862(ASG)	None	Load Factors	None	Not established	Governmental
	MULTI-WHEEL	Multiple Wheel Drag Ratio	Multiple Drag Modifier, M_M	Same as for drag	Region II velocity range (5 to 40 knots) Relative rating unlikely to change in Regions I and III.	Not established	UDRI
SECONDARY FLOTATION VARIABLES	ROUGHNESS	Proposed MIL-A-8862A Power Spectral Density (PSD)	Constant C in equation $P(C) = C_i^{-N}$, (n=2.0)	$C = 5.0 \times 10^{-3}$ ft	Proposed Criteria	Not established	Governmental
		Ground Induced Loads	Acceleration in g's	Vertical acceleration = ±0.4g at pilots station	Accuracy of simulation models	Unknown	Governmental
	MULTIPASS	Aircraft coverages based on failure criteria AFSC DH 2-1	Coverages (no symbol used)	Permanent rutting of 3.0 inches or elastic sinkage of 1.5 inches	Region I velocity Range Clay type soil	Conservative	WES, Boeing, Governmental, Lockheed
	TURNING	MIL-A-8862(ASG)	None	Load Factors	None	Not established	Governmental
	LANDING IMPACT	MIL-A-8862(ASG)	None	Load Factors	None	Not established	Governmental
	SPEED	Drag	Region I - None; Region II - FI_S & FI_M; Region III - based on soil inertia effects	Same as for drag	None; Impingement drag coefficient not known	Estimated ±20%; Poor	UDRI; Boeing, Lockheed

currently has over 1000 documents on file. Due to the increasing volume of technical reports and literature reviewed and stored in the library system, it became necessary to expedite the indexing and retrieval process through an information system. The system selected is referred to as the KWIC index system and its development is available through services provided by Wright-Patterson Air Force Base. The KWIC index is a machine generated printed listing of documents which uses the keywords in the document's title as the retrieval key. The KWIC index displays on continuous computer printout sheets (which are bound in book form) each significant word of the title alphabetically in the center of the page. The KWIC index also identifies the author on the same line as the title. All flotation related research articles are then stored alphabetically by the author names. Those articles having no identified author are numbered consecutively and located by this number since it also appears in the KWIC index.

SECTION VI
CONCLUSIONS AND RECOMMENDATIONS FOR RESEARCH

1.   Conclusions

The results of the landing gear/soil interaction research effort have shown that:

1.   The effects of geometric configuration (twin, tandem, etc.) are a significant factor in defining the multiple wheel drag ratio, $(R/P)_M$.

2.   Results from the plate tests, analytical solution, and the multiple wheel tests are in general agreement as to load and sinkage interaction effects.

3.   Proper twin spacing is more critical than tandem spacing in minimizing rolling drag.

4.   Large increases in sinkage occur for braked tires on sand while only slight increases in sinkage occur for braked tires on clay.

5.   The braking prediction equations were partially verified and are suitable to use on a preliminary basis for predicting braked tire on soil drag ratios.

6.   The analytical sinkage prediction equation is a reliable prediction technique for clays in the lower sinkage range. High sinkage situations cannot be predicted accurately because of the lack of strain hardening in the current soils model.

7.   The single wheel drag ratio, $(FI)_S$, has been modified to a multiple wheel drag ratio, $(FI)_M$. This multiple wheel drag ratio can now be used to determine the flotation performance of aircraft during takeoff operations.

2.   Recommendations for Research

Immediate efforts for landing gear/soil interaction and flotation criteria research should be directed at the following areas.

117

1. High speed (Region III) sinkage and drag performance for rolling tires.

2. Additional verification of the braking sinkage and drag analysis equations.

3. Incorporation of strain hardening in the currently used soils model.

Long range flotation research efforts should include:

1. Multiple pass (operations) effects as related to runway deterioration and operational capability.

2. Landing gear loads in turning operations.

3. Effects of roughness on the flotation performance of aircraft on soil runways.

REFERENCES

1. Kraft, David C., Luming, H., and Hoppenjans, J. R., "Aircraft Landing Gear-Soils Interaction and Flotation Criteria, Phase II," AFFDL-TR-69-76, Air Force Flight Dynamics Laboratory, Wright-Patterson AFB, Ohio, November 1969.

2. Crenshaw, B. M., Lockheed Georgia Co., Marietta, Ga., "Aircraft Landing Gear Dynamic Loads from Operation on Clay and Sandy Soil - Preliminary Data," March 1969.

3. Richmond, L. D., et al., "Aircraft Dynamic Loads from Substandard Landing Sites," AFFDL-TR-67-145 Air Force Flight Dynamics Laboratory, Wright-Patterson AFB, Ohio, September 1968.

4. Ladd, D., et al., "Aircraft Ground Flotation Investigation," AFFDL-TR-66-43, Air Force Flight Dynamics Laboratory, Wright-Patterson AFB, Ohio, August 1967.

5. Kraft, David C., "Analytical Landing Gear-Soils Interaction, Phase I," AFFDL-TR-68-88, Air Force Flight Dynamics Laboratory, Wright-Patterson AFB, Ohio, May 1968.

6. Freitag, Dean R. "Wheels on Soft Soils, an Analysis of Existing Data," Tech. Report No. 3-670, U.S. Army Engineers Waterways Experiment Station. Vicksburg, Miss., January 1965.

7. Richmond, L. D., et al., "Aircraft Dynamic Loads from Substandard Landing Sites," AFFDL-TR-67-45, Part II, Air Force Flight Dynamics Laboratory, Wright-Patterson AFB, Ohio, September 1968.

8. Barker, J. V. L., "Sinkage of a Dual Aircraft Wheel Assembly," Report No. 925, Military Engineering Experimental Establishment, Christchurch, England, October 1965.

9. Holm, I. C., "Multipass Behavior of Pneumatic Tires," Journal of Terramechanics, Volume 6, No. 3, 1969.

10. Terzaghi, K., *Theoretical Soil Mechanics*, John Wiley and Sons, 1956.

11. Luming, H., "Analytical Landing Gear-Soil Interaction, Phase III, Rolling Single Wheel Analytical Sinkage Prediction Technique and Computer Program," AFFDL-TR-70-142, Wright-Patterson AFB, Ohio, September 1970.

12. Thompson, A. B. and Smith, M. E., "Stresses Under Moving Vehicles: Wheeled Vehicles," U.S. Army Engineer Waterways Experiment Station, Technical Report No. 3-545, 1960.

13. Peattie, K. R., "A Fundamental Approach to the Design of Flexible Pavements," *Proceedings of the Interaction Conference on Structural Design of Asphalt Pavements*, University of Michigan, August 1962.

14. Drucker, D. C. and Prager, W., "Soil Mechanics and Plastic Analysis of Limit Design," *Quarterly Applied Mathematics*, Vol. 10, No. 2, 1952.

15. Christian, J. T., *Two-Dimensional Analysis of Stress and Strain in Soils*, Report No. 3, "Plane-Strain Deformation Analysis of Soil," Reports to DASA, Contract DA-22-079-eng-471, MIT, December 1966.

16. Luming, H., "Multiwheel Landing Gear/Soil Interaction - Phase III, Multiwheel Vertical Pulse Load Analytical Sinkage Prediction Technique and Computer Program," Technical Report No. UDRI-TR-70-22, University of Dayton Research Institute, May 1970.

17. McCrae, J. L., Powell, C. J., and Wismer, R. D., "Performance of Soils Under Tire Loads, Test Facilities and Techniques," Technical Report No. 3-66, U.S. Army Engineers Waterways Experiment Station, Vicksburg, Miss., January 1965.

18. Smith, Jerry L., "A Study of the Effects of Braking on Drag Force and Sinkage," unpublished report, Army Corps of Engineers, U.S. Army Engineers Waterways Experiment Station, Vicksburg, Miss.

19. Schuring, D. J., "Analysis and Simulation of Dynamical Vehicle-Terrain Interaction," CAL No. VJ-2330-G-56, Cornell Aeronautical Laboratories, Inc., Buffalo, New York, May 1969.

20. Pymm, F. H., and Uffelmann, F. L., "An Experimental Determination of the Force Existing Between the Soil and Rim of a Rigid Wheel Under Both Towed and Driven Conditions on Clay and Sand," Report No. B.R. 195, Fighting Vehicles Research and Development Establishment, Chertsey, Surrey, England, July 1967.

21. McCrae, J. L., "Theory for a Towed Wheel in Soil," in Journal of Terramechanics, Vol. 1, No. 4, The International Society for Terrain Vehicle Systems, 1964.

22. Reece, A. R., "Principles of Soil-Vehicle Mechanics," Automobile Division Proceedings of Institution of Mechanical Engineers, Vol. 180, London, England, 1965.

23. Hegedus, Ervin, "Pressure Distribution Under Rigid Wheels," American Society of Agricultural Engineers, General Edition, No. 3, 1965.

24. Marcal, P. V., "A Comparative Study of Numerical Methods of Elastic-Plastic Analysis," AIAA J., Vol. 6, No. 1, 1967.

25. Marcal, P. V., "Finite Element Analysis with Material Non-linearities--Theory and Practice," paper presented at U.S.-Japan Seminar on Matrix Methods of Structural Analysis and the JSSC Symposium on Matrix Methods and Structural Analysis, Tokyo, August 1969.

26. Washizu, K., Variational Methods in Elasticity and Plasticity, Pergamon Press, Oxford, 1968.

121

27.   "Aircraft Tires - Engineering Data," Third Edition, B. F. Goodrich
       Aerospace and Defense Products, Akron, Ohio.

28.   Hay, D. R., "Aircraft Characteristics for Airfield Pavement Design
       and Evaluation," Technical Report AFWL-TR-69-54, Air
       Force Weapons Laboratory, Kirtland AFB, New Mexico,
       October 1969.

29.   "Weight and Blast Data Relative to Runway Design," Systems
       Engineering Group (SEPIE), Research and Technology Division,
       Wright-Patterson AFB, Ohio, May 1964.

APPENDIX I

TWIN PLATE-VERTICAL LOAD TEST PROGRAM,
SOIL TESTS PREPARATION,
PROCEDURES, AND UNIFORMITY TESTS

Soil Classification

The two soils selected for testing were sand (mixture of mortar sand and Yuma sand) and buckshot clay. The grain size distribution for the sand is given in Figure 5:, and the grain size distribution and limits properties for the buckshot clay are given in Figure 58. The intent of the soil placement was to provide a uniform soil test section. The cone penetrometer could then evaluate the soil strength. The results of the moisture-density determinations for the test sections are summarized in Table 25.

TABLE 25

MOISTURE-DENSITY DATA

Soil Type	Average Conditions	
	Dry Density v_d (pcf)	Moisture Content W (%)
Sand (1S to 12S)	= 95.4	1.5
Clay 1C	87.7	27.5
2C	82.3	29.0
3C	85.9	27.0
4C	75.5	29.1
5C	82.1	27.3
6C	97.4	27.5
7C	82.6	28.3
8C	85.2	29.3
9C	92.0	27.8

Soil Preparation

a. Sand

A standard sand soil placement and density preparation technique was used in an effort to develop an acceptable uniformity of
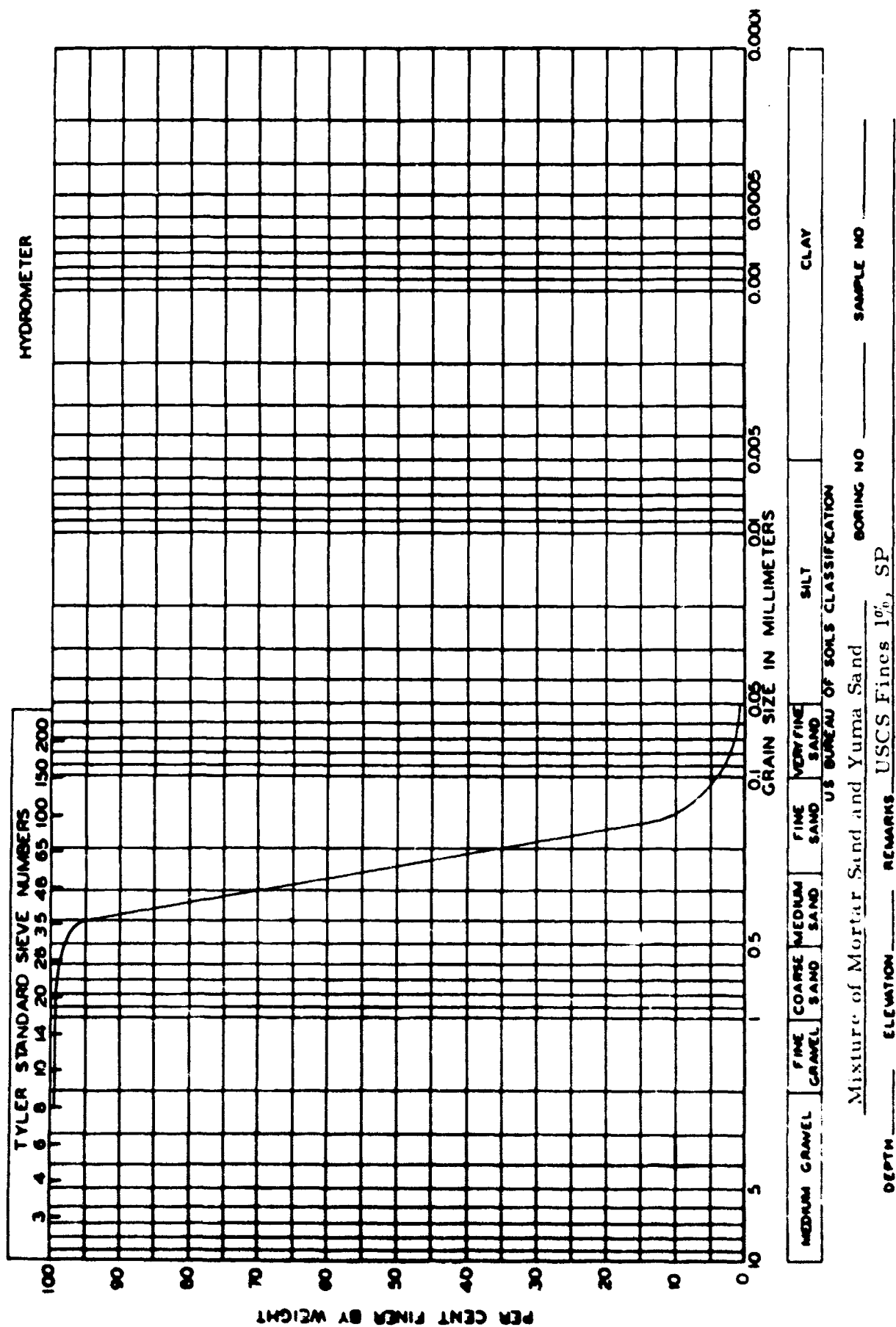
Figure 57. Grain Size Distribution, Mixture of Mortar Sand and Yuma Sand
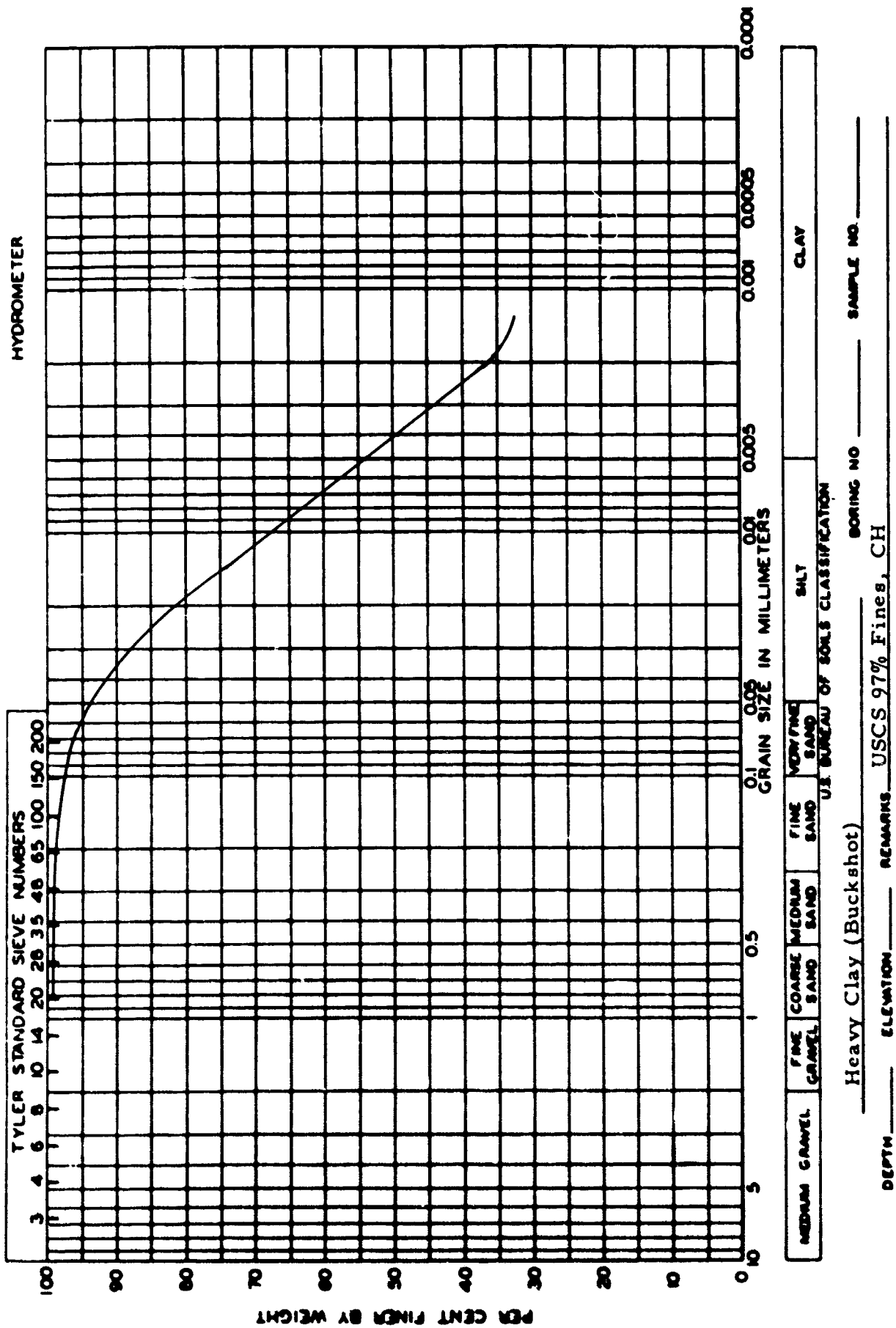
Figure 58. Grain Size Distribution, Buckshot Clay

soil section for testing. After placement of the sand in the test box, a 1/4" thick steel plate was placed on the soil surface as a uniform surcharge completely covering the soil surface.

The box with the surcharge load was then placed on the load platform in the MTS load frame. An aluminum block was centered on the steel plate and a small pressure was applied by actuating the MTS hydraulic loading system. Once this small pressure was applied, the MTS load system was programmed to vibrate the sand under a sawtooth type load with a peak intensity of 150 lbs. at a frequency of 7 cps until 0. 2 of an inch downward movement of the soil surface occurred (determined by observing the sinkage trace on the Visicorder). The application of an initial pressure insured that contact was maintained by the load piston throughout the vibration process. A number of trial and error procedures were used in arriving at the peak intensity and frequency selected for compacting the soil. Each time the sand was to be vibrated, the sand was thoroughly mixed to bring it back to a loose condition.

b. Clay

Buckshot clay, a fine grained soil found in the Vicksburg, Mississippi region, was shipped to the University in a premixed condition at a moisture content of approximately 27% to 28% in sealed containers by the U.S. Army Corps of Engineers (WES) located in Vicksburg. The selection of buckshot clay which exhibits a consistent water content-strength relationship was made to permit comparisons with previous and future tests conducted by the University on the same soil.

Before compaction, the test box was lined with a plastic sheet to reduce moisture loss. An approximate 2-1/2 inch layer of loose soil was placed in the box and compacted by 100 blows from a standard Proctor hammer. A total of 4 layers were so placed, which constituted the test section. Each layer was scarified before the placement of the next layer. The soil surface was leveled and suitable measurements made to define the wet density of the placed soil.

127

The top of the test box was then covered with a plastic sheet and stored in a moist room for 3 days prior to testing. Moisture content determinations were made on each test specimen after the loading tests. Two moisture content samples were taken from each test specimen.

Test Procedure

a. Sand

Once the sand soil test section had been prepared, either a cone penetration test or a plate test was conducted. For those test sections for which only cone penetration tests were performed, three penetrations were made: one at the center of the section, and one toward each end of the section approximately 5" from the center. Both sinkage and load were recorded as a function of time to a penetration of 2-1/2".

For the single plate tests, the plate loading was applied at the center of the test section, with the sinkage and load recorded as a function of time. The plate was penetrated at a constant rate of 12.5"/sec. to a depth of 1-1/4". After this plate test, three penetration tests were conducted: one toward each end of the section approximately 5-1/2" from the center, and one where the single plate had penetrated. The purpose of the penetration test in the previously loaded plate region was to obtain information on the modified soil properties.

In the twin plate testing, three different spacings between plates were used, as described previously. In each twin plate test, both plates were penetrated simultaneously, with sinkage and load (total load on both plates) recorded as a function of time on the Visicorder. After the twin plate test, one plate was removed from the test frame and the remaining plate was used to conduct a single plate test in one of the previous plate load regions. A cone penetration test was then conducted in the other previously loaded plate region. Two cone penetration tests were also performed toward each end of the test section approximately 5-1/2" from the center.

Calibration checks on load and sinkage were made prior to and after testing on each test section. This calibration was accomplished by substitution of a known resistance into the circuitry of the MTS system.

b. Clay

After the test box was placed on the MTS platform, cone penetration tests were first run in each of the four corners of the box (cone test Nos. 1, 2, 3, and 4), approximately 2" from the edge. The plate loading test (either single or twin) was then conducted at the center of the test section. After each plate test (single or twin), a cone penetration test (cone test No. 5) was conducted in the previously-loaded plate region. For all the twin plate tests, one plate was removed and a subsequent plate test was conducted within the remaining previous plate test region. Finally, an additional cone penetration test (cone test No. 6) was made in a relatively undisturbed region.

Both sinkage and force were recorded as a function of time on the Visicorder. For twin plate tests, the recorded force was the total force on both plates.

Uniformity Tests

a. Sand

The results of the cone penetration tests are given in Table 26, with the penetration resistances given at depths of 1-1/4", 1-3/4", and 2-1/4" as determined from the Visicorder traces. The average soil cone penetration resistance for each penetration test was defined as

$$CPR_N + (CPR_{@ 1-1/4"} + CPR_{@ 1-3/4"} + CPR_{@ 2-1/4"}) / 3 \qquad (A-1)$$

where $N = 1, 2, 3$.

129

TABLE 26

Sand Tests - Cone Penetration Test Results
(Initial Loading)

Test Sequence No.	Comments	Test Cone No.	Resistance (CPR) in lbs. at 1-1/4"	1-3/4"	2-1/4"	CPR_N (lbs)	CPR_{avg} (lbs)	Date
1S	Cone Test	1	5.8	8.1	11.3	8.4		
	Only	2	5.1	7.6	10.6	7.8	(8.0)	4-3-70
		3	5.4	7.4	10.3	7.6		
2S	1st Single	1	◄— in plate area —►					
	Plate Test	2	5.8	8.8	12.8	9.1	(8.2)	4-3-70
		3	4.8	6.9	9.9	7.2		
3S	2nd Single	1	◄— in plate area —►					
	Plate Test	2	6.5	10.2	15.4	10.7	(11.1)	4-3-70
		3	7.8	11.2	15.5	11.5		
4S	Cone Tests	1	7.5	11.4	17.5	12.1		
	Only, *Box	2	9.1	13.3	19.2	13.9	(13.7)	4-3-70
	Jiggled	3	10.3	15.0	20.3	15.2		
5S	3rd Single	1	◄— in plate area —►					
	Plate Test	2	6.3	9.0	12.3	9.2	(9.7)	4-3-70
		3	6.4	9.8	14.3	10.2		
6S	Cone Test	1	6.3	8.6	11.3	8.7		
	Only	2	5.0	7.1	10.0	7.4	(8.2)	4-3-70
		3	5.4	8.3	11.8	8.5		
7S	1st Twin	1	◄— in plate area —►					
	at 1-1/2D	2	6.2	9.5	13.5	9.7	(9.0)	4-3-70
		3	5.3	8.4	11.3	8.3		
8S	2nd Twin	1	◄— in plate area —►					
	at 1-1/2D	2	5.8	8.1	10.7	8.2	(9.4)	4-3-70
		3	7.4	10.5	14.0	10.6		
9S	Cone Test	1	4.7	6.6	9.8	7.0		
	Only	2	4.6	6.3	8.7	6.5	(7.6)	4-3-70
		3	6.6	9.1	11.8	9.2		
10S	1st Twin	1	◄— in plate area —►					
	at 2-1/2D	2	4.4	7.3	10.8	7.5	(8.4)	4-3-70
		3	6.7	9.4	11.7	9.3		
11S	2nd Twin	1	◄— in plate area —►					
	at 2-1/2D	2	3.6	5.1	7.1	5.3	(5.4)	4-3-70
		3	3.9	5.4	7.4	5.6		
12S	1st Twin	1	◄— in plate area —►					
	at 4D	2	5.5	7.8	10.6	8.0	(7.0)	4-3-70
		3	4.2	6.0	8.1	6.1		

③ ① ②   Typical Cone Test Locations

The average soil strength (or resistance) for each test section in which plate tests were conducted, the results of which were used in the analysis, was given by

$$CPR_{avg} = \frac{CPR_2 + CPR_3}{2} \qquad (A-2)$$

In general, the results of the penetration tests in sand show that each test section exhibited a relatively uniform soil strength, but that significant variations did occur in soil strength between test sections. To allow for these strength variations between test sections, a dimensionless quantity $(F_{avg}/CPR_{avg}$ was used in comparing the results of the plate tests.

   b.   Clay

        The results of the cone penetration tests are given in Table 27, with the cone penetration resistances (CPR) given at depths of 1/2" and 1", in addition to the average cone penetration resistance reached subsequent to the full penetration of the cone tip (CPR_F). The average cone penetration resistance (CPR_{unif}) for each test section, the results of which were used in the analysis, was determined by averaging the uniform penetration resistance reached in cone tests nos. 1, 2, 3, and 4.

        Reference to Table 27 shows the variation in strength between test sections. Note that two different stiffness ranges were selected to insure that the test results would be representative over a strength range.

        Four of the nine prepared clay test sections exhibited a slight ($\simeq 10\%$) loss in strength with depth (Test Sequence Nos. 3C, 5C, 7C, and 9C), and two of the nine test sections exhibited a slight increase in strength with depth (Test Sequence Nos. 1C and 8C). Dimensionless quantities (F_{avg}/CPR_{unif}) were used in all comparative analyses between tests.

131

TABLE 27

Clay Tests - Cone Penetration Test Results
(Initial Loading)

Test Sequence No.	Comments	Test Cone No.	CPR in lb. at 1/2"	1"	CPR$_F$	CPR$_{unif}$ *	**	Date
1C	1st Single Plate Test	1	3.6	13.5	33.4			
		2	4.6	16.9	37.5			
		3	5.1	17.5	35.5	35.0	33.9	4-20-70
		4	4.1	14.5	33.6			
		5	← in plate area →					
		6	---	----	33.9			
2C	1st Twin at 1-1/2D	1	3.0	10.7	22.2			
		2	3.0	8.7	15.7			
		3	---	----	25.0	21.3	21.3	4-20-70
		4	3.0	10.2	22.3			
		5	← in plate area →					
		6			21.3			
3C	1st Twin at 2-1/2D	1	---	----	----			
		2	6.2	19.8	35.6			
		3	4.5	19.3	34.2	35.7	34.4	4-20-70
		4	7.1	21.2	37.4			
		5	← in plate area →					
		6	---	----	34.4			
4C	2nd Single Plate	1	3.4	10.2	19.5			
		2	3.8	10.7	20.1			
		3	3.7	11.0	21.6	21.2	21.7	4-22-70
		4	3.8	12.1	23.4			
		5	← in plate area →					
		6	---	----	21.7			
5C	1st Twin at 4D	1	5.4	17.5	30.6			
		2	3.9	15.0	26.8			
		3	---	----	----	28.2	29.0	4-22-70
		4	5.0	15.2	27.1			
		5	← in plate area →					
		6	---	----	29.0			
6C	2nd Twin at 2-1/2D	1	3.6	13.9	29.0			
		2	4.5	14.8	28.8			
		3	3.6	13.6	36.9	27.9	25.0	4-22-70
		4	4.3	14.3	27.0			
		5	← in plate area →					
		6	---	----	25.0			
7C	3rd Single Plate	1	5.4	17.3	31.8			
		2	6.2	18.9	32.3			
		3	6.2	19.3	30.1	31.2	30.3	4-24-70
		4	5.4	15.7	30.7			
		5	← in plate area →					
		6	---	----	30.3			
8C	2nd Twin at 1-1/2D	1	3.7	10.5	21.0			
		2	6.2	19.4	----			
		3	4.5	13.6	19.4	20.0	19.3	
		4	3.9	12.3	19.5			
		5	← in plate area →					
		6	---	----	19.3			
		1	5.4	17.5	27.8			
		2	---	----	----			
		3	6.8	19.3	25.5	26.1	26.7	
		4	---	----	25.1			
		5	← in plate area →					
		6	---	----	26.7			

Typical Cone Test Location
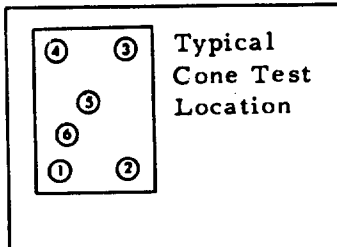
* Average of Cone Test Nos. 1, 2, 3, and 4
** Cone Test No. 6

APPENDIX ii

GOVERNING EQUATIONS AND NUMERICAL PROCEDURES
FOR THE TWO DIMENSIONAL PLANE STRAIN
MULTIWHEEL VERTICAL PULSE LOAD PROBLEM
- TWIN WHEEL SIMULATION

Governing Equations

The equations of continuum elasticity and plasticity used in the lumped parameter iteration method are listed in this section in the form applicable to the lumped parameter model.

a. Dynamic Equations of Motion

$$\rho \ddot{U}(i, j) = \frac{\sigma_\eta(i+1, j+1) - \sigma_\eta(i, j)}{h/\sqrt{2}} + \frac{\tau_{\eta\zeta}(i, j+1) - \tau_{\eta\zeta}(i+1, j)}{h/\sqrt{2}} \qquad \text{(A-3)}$$

$$\rho \ddot{V}(i, j) = \frac{\sigma_\zeta(i, j+1) - \sigma_\zeta(i+1, j)}{h/\sqrt{2}} + \frac{\tau_{\eta\zeta}(i+1, j+1) - \tau_{\eta\zeta}(i, j)}{h/\sqrt{2}} \qquad \text{(A-4)}$$

where

U and V are the displacements in the η and ζ directions, respectively;

σ_η and σ_ζ are the normal stresses and $\tau_{\eta\zeta}$ is the shear stress;

ρ is the density of the soil;

h is the grid size; and

the dots indicate time derivatives.

b. Quadrature Equations

$$U^t = U^{t-\Delta t} + (\Delta t)\, \dot{U}^{t-\Delta t} + \frac{(\Delta t)^2}{6}\left[2\ddot{U}^{t-\Delta t} + \ddot{U}^t \right] \qquad \text{(A-5)}$$

$$V^t = V^{t-\Delta t} + (\Delta t)\, \dot{V}^{t-\Delta t} + \frac{(\Delta t)^2}{6}\left[2\ddot{V}^{t-\Delta t} + \ddot{V}^t \right] \qquad \text{(A-6)}$$

$$\dot{U}^t = \dot{U}^{t-\Delta t} + \frac{\Delta t}{2}\left[\ddot{U}^{t-\Delta t} + \ddot{U}^t \right] \qquad \text{(A-7)}$$

$$\dot{V}^t = \dot{V}^{t-\Delta t} + \frac{\Delta t}{2}\left[\ddot{V}^{t-\Delta t} + \ddot{V}^t \right] \qquad \text{(A-8)}$$

where

Δt is the time increment, and superscript $(t-\Delta t)$ indicates the variables of the previous load increment.

134

c. Drucker-Prager Yield Criterion

The criterion states that if the yield function, f, as defined below is less than zero, the stress point is elastic, and if f is equal to or greater than zero, the stress point has yielded.

$$\text{Yield function} = f = \alpha_1 I + \sqrt{J} - k \qquad (A-9)$$

where

$$I = \sigma_\eta + \sigma_\zeta + \sigma_\xi \qquad (A-10)$$

$$J = \frac{1}{6}\left[(\sigma_\eta - \sigma_\zeta)^2 + (\sigma_\zeta - \sigma_\xi)^2 + (\sigma_\xi - \sigma_\eta)^2 + 6\tau_{\eta\zeta}^2\right] \qquad (A-11)$$

$$\sigma_\xi = \nu(\sigma_\eta + \sigma_\zeta) \qquad (A-12)$$

$$\alpha_1 = \frac{2\sin\phi}{\sqrt{3}\,(3 - \sin\phi)} \qquad (A-13)$$

$$k = \frac{6c\,\cos\phi}{\sqrt{3}\,(3-\sin\phi)} = \text{yield stress in shear} \qquad (A-14)$$

c = cohesion

ϕ = friction angle

d. Incremental Strain-Displacement Relations

$$\Delta\epsilon_\eta(i, j) = \frac{\Delta U(i, j) - \Delta U(i-1, j-1)}{h/\sqrt{2}} \qquad (A-15)$$

$$\Delta\epsilon_\zeta(i, j) = \frac{\Delta V(i-1, j) - \Delta V(i, j-1)}{h/\sqrt{2}} \qquad (A-16)$$

$$\Delta\epsilon_\xi(i, j) = 0 \qquad (A-17)$$

$$\Delta\gamma_{\eta\zeta}(i, j) = \frac{\Delta U(i-1, j) - \Delta U(i, j-1)}{2h/\sqrt{2}} + \frac{\Delta V(i, j) - \Delta V(i-1, j-1)}{2h/\sqrt{2}} \qquad (A-18)$$

where $\Delta\epsilon_\eta$, $\Delta\epsilon_\zeta$, and $\Delta\epsilon_\xi$ are the normal strain increments,

$\Delta\gamma_{\eta\zeta}$ is the shear strain increment,

and

$$\Delta U = U^t - U^{t-\Delta t} \tag{A-19}$$

$$\Delta V = V^t - V^{t-\Delta t} \tag{A-20}$$

e. Incremental Stress-Strain Relations

$$\Delta\sigma_\eta = \lambda\Delta\epsilon + 2G\Delta\epsilon_\eta - \beta Q\left(\frac{\sigma_\eta}{2\sqrt{J}} + B\right)\left(\frac{\Delta W}{2\sqrt{J}} + B\Delta\epsilon\right) \tag{A-21}$$

$$\Delta\sigma_\zeta = \lambda\Delta\epsilon + 2G\Delta\epsilon_\zeta - \beta Q\left(\frac{\sigma_\zeta}{2\sqrt{J}} + B\right)\left(\frac{\Delta W}{2\sqrt{J}} + B\Delta\epsilon\right) \tag{A-22}$$

$$\Delta\tau_{\eta\zeta} = 2G\Delta\gamma_{\eta\zeta} - \beta Q\left(\frac{\tau_{\eta\zeta}}{2\sqrt{J}}\right)\left(\frac{\Delta W}{2\sqrt{J}} + B\Delta\epsilon\right) \tag{A-23}$$

where

$$\Delta\epsilon = \Delta\epsilon_\eta + \Delta\epsilon_\zeta \tag{A-24}$$

$$B = \frac{1+\nu}{1-2\nu}\ \alpha_1 - \frac{I}{6\sqrt{J}} \tag{A-25}$$

$$Q = \frac{4G}{1 + \dfrac{6(1+\nu)\alpha_1^2}{1-2\nu}} \tag{A-26}$$

λ = Lame's constant in Hooke's law = $\dfrac{E\nu}{(1+\nu)(1-2\nu)}$

G = Modulus of rigidity = $\dfrac{E}{2(1+\nu)}$

ΔW = Increment work done

$$= \sigma_\eta\Delta\epsilon_\eta + \sigma_\zeta\Delta\epsilon_\zeta + \tau_{\eta\zeta}\Delta\gamma_{\eta\zeta} \tag{A-27}$$

and $\beta = \begin{cases} 1 & \text{if } f\geq 0 \text{ and } \Delta W > 0 \text{ (loading)} \\ 0 & \text{if } f\geq 0 \text{ and } \Delta W < 0 \text{ (unloading) or } f < 0 \text{ (elastic)} \end{cases}$

136

Then the stresses at time t are:

$$\sigma_\eta^t = \sigma_\eta^{t-\Delta t} + \Delta\sigma_\eta^t \qquad\qquad (A-28)$$

$$\sigma_\zeta^t = \sigma_\zeta^{t-\Delta t} + \Delta\sigma_\zeta^t \qquad\qquad (A-29)$$

$$\tau_{\eta\zeta}^t = \tau_{\eta\zeta}^{t-\Delta t} + \Delta\tau_{\eta\zeta}^t \qquad\qquad (A-30)$$

f. Stress Correction Equations for Perfectly Plastic Yielding

$$\sigma_\eta' = (1-\eta_c)\sigma_\eta + \eta_c\left[(1+6\alpha_1^2)\frac{I}{3} - 2\alpha_1 k\right] \qquad\qquad (A-31)$$

$$\sigma_\zeta' = (1-\eta_c)\sigma_\zeta + \eta_c\left[(1+6\alpha^2)\frac{I}{3} - 2\alpha_1 k\right] \qquad\qquad (A-32)$$

$$\tau_{\eta\zeta}' = (1-\eta_c)\tau_{\eta\zeta} \qquad\qquad (A-33)$$

where

$$\eta_c = \frac{J - (K-\alpha I)^2}{2J + 12\alpha_1^2 (k-\alpha_1 I)^2} \qquad\qquad (A-34)$$

and

σ_η', σ_ζ', and $\tau_{\eta\zeta}'$ are the corrected stresses.

Numerical Procedure for the Development of the Computer Program

For convenience in the numerical calculations, the above governing equations are first expressed in terms of dimensionless variables. The dimensionless variables are formed in the following manner: the variables having a dimension of stress are divided by the yield stress in shear, k (see Equation A-14); variables having a dimension of length are divided by the width, a, of the applied surface pressure strip; and the time is divided by the time duration of the pulse, t_d.

The pulse curve of the applied pressure on the surface on the soil is approximated by linear segments. For each segment, the change in

137

pressure through an increment of time is determined. For each increment of time the stresses at the fictitious stress points in the plane $(j=1)$ are changed based on the pressure increments of the particular linear segment of the approximate pulse curve. Then the following steps are performed starting with the mass point at $(i, j) = (1, 1)$:

(1) The accelerations $\dot{U}$ and $\dot{W}$ at time t are obtained by means of the dynamic equations of motion, Equation (A-3), using the most current stresses that are known at time t (if not known, those at time $t-\Delta t$ are used).

(2) The accelerations at time t and the accelerations, velocities, and displacements at time $t-\Delta t$ are then substituted into the quadrature equations, Equations (A-5 to A-8), to give U, V, $\dot{U}$ and $\dot{V}$ at time t. Then the incremental displacements, ΔU^t and ΔV^t are obtained from Equations (A-19) and (A-20).

(3) The stresses at the two stress points immediately below the mass point (i, j) are recalculated according to the following steps for each stress point:

(i) The yield indicating table is checked to determine if the stress point had yielded. (Initially, the table would indicate all stress points to be elastic).

(ii) The incremental strains at time t are calculated using the incremental strain-displacement relations, Equations (A-15 to A-18).

(iii) The stress increments are then calculated from the incremental stress strain relations, Equations (A-21 to A-23). The stresses at the time t are then calculated by Equations (A-28 to A-30).

(iv) The newly obtained stresses are then substituted into the yield criterion, Equation (A-9), to check if the stress point had yielded. The result is then recorded in the yield indicating table. Stress correction is performed using Equations (A-31 to A-33), if it was required.

(4) Steps 1 through 3 are repeated for the rest of the mass points, proceeding from the axis of symmetry toward the right and then row by row downward.

138

(5) Using the new stresses obtained for all the stress points, steps 1 through 4 are repeated, thus starting the iteration cycle. This is done until the desired accuracy is reached.

(6) Steps 1 through 5 are repeated for the subsequent time increments, in which the applied pressure on the boundary is incremented according to the vertical pulse load curve.

APPENDIX III

MULTIWHEEL VERTICAL PULSE LOAD ANALYTICAL SINKAGE PREDICTION COMPUTER PROGRAM TWIN WHEEL SIMULATION

with

A. Some Preliminary Remarks About the Computer Program

B. Fortran Source Listing of the Computer Program

C. List of Symbols

Some Preliminary Remarks About the Computer Program

a.   The load curve was assumed to be symmetrical, that is, the peak occurs at one-half the time duration and the shape of the loading portion of the curve is the same as that of the unloading portion. Both portions were approximated by 20 equal linear segments. The "basic load curve" in the program has a peak load of 10,000 psf, as shown in Table 28, and the curve is scaled down proportionately in the program for lower peak loads.

TABLE 28
BASIC LOAD CURVE

Dimensionless Time	Applied Pressure in psf
0.0	0.0
0.025	-20.0
0.050	-110.0
0.075	-270.0
0.100	-580.0
0.125	-1050.0
0.150	-1730.0
0.175	-2630.0
0.200	-3750.0
0.225	-4890.0
0.250	-5890.0
0.275	-6770.0
0.300	-7540.0
0.325	-8190.0
0.350	-8730.0
0.375	-9170.0
0.400	-9500.0
0.425	-9740.0
0.450	-9900.0
0.475	-9980.0
0.500	-10000.0

b.   One of the input data items to the program is the time increment, DT. It is calculated previous to use of the program using the stability criterion discussed in the Phase II Final Report[1]. The following procedure should be followed.

- An approximate time increment is obtained by the formula,

$$(\Delta t)_{\text{approx.}} = \frac{h}{2c_1}$$

where h and c_1 are the grid size and the dilatational wave velocity, respectively.

- With the above approximate time increment as a guide, a smaller time increment, Δt, is chosen such that the number of increments in the entire load curve $\frac{t_d}{\Delta t}$ is a multiple of 40. This ensures that each linear segment of the load curve will have an integral number of time increments.

c. Since the computer time required to run through a load curve is quite long, the computer program is written such that portions of the load curve can be run at separate times by using magnetic tape input and output. This can be done by specifying the starting load increment number, LB, and the ending load increment number, LEN, and setting up the appropriate tapes.

d. The computer run is monitored by printing out the vertical normal stresses, the vertical displacements, and the yield indicating table of the region under the load intermittently; the number of load increments skipped is given by the Index ILI. The vertical normal stresses, vertical displacements, and yield indicating table of the rest of the region are also printed out at a less frequent rate, and the number of load increments skipped in this case is given by IEI. The other stresses and displacements are not printed out because the volume of print-out would be prohibitively large; however, at a much less frequent rate all results of a load increment are saved on the output tape. The number of load increments skipped for this case is given by JLI. The indices ILI, IEI, and JLI are all input data specified in the last data card.

142

e. The numerical value of each element of the yield indicating table supplies the following information:

(i) If $-1.0 <$ YIT < 0.0, the stress point is elastic.

(ii) If $-10.015 <$ YIT < -10.0, the yield function is greater than zero but has not exceeded the tolerance for yielding (which is 0.015 in this case), thus the stress point is still considered elastic.

(iii) If $0.0 <$ YIT $< 10,000$, the stress point has yielded and is loading, and no stress correction was applied. The digits to the right of the decimal point give the stress correction factor $(1-r_c)$, which is a number between 0.0 and 1.0. The four digits left of the decimal point gives the value of the yield function which is a number between 0.0 and 1.0.

(iv) If $30000.0 <$ YIT < 40000.0, the yield function has exceeded the tolerances for stress correction, and stress correction has been applied. The digits other than the ten thousand place digit gives the same information as (iii).

(v) If $20000.0 <$ YIT < 30000.0, the yield function is negative but has not gone below the tolerance (-0.015) for becoming elastic again, thus the stress point is still considered plastic. The digits other than the ten thousand place digit give the same information as (iii).

(vi) If $40000.0 <$ YIT < 70000.0, the stress point is plastic and unloading. The digits other than the ten thousand place digit give the same information as (iii).

f. Before making a continuation run of the computer program, with the soil medium being still all-elastic, the value of the cohesion may be changed without affecting the results. However, since the stresses are normalized with respect to the yield stress in shear which is proportional to the cohesion, the values of the stresses must be converted by the conversion factor, CONV, during read-in of the tape data. This is done by specifying the control index ICV; if conversion is desired, ICV=1; if conversion is not desired, ICV=0. The value of the cohesion of the saved data on tape must also be specified as an input data.

143

g. The procedure for running the computer program is as follows:

(1) Specify on the first data card a title of length less than 24 characters including blank spaces.

(2) Specify the next three data cards:

Second card - specify five soil parameters: weight density (pcf), Poisson's ratio, Young's modulus (psi), cohesion (psf), and friction angle (degree):

Third card - specify six load parameters: time duration of load pulse (seconds), width of loaded area (inches), peak pressure of load curve (vertical load/contact area, psf), tolerance for unloading (dimensionless), the i-index of the mass point at which the loaded area starts, the i-index of the mass point at which the loaded area ends.

Fourth card - specify computational parameters: space grid size (inches), time increments (seconds, as explained in Item b), number of grids for depth (use 30), number of grids for width extent.

(3) The next five data cards specify the basic load curve (see Sample Data).

(4) Specify on the tenth data card the value of the cohesion of the saved data on tape if conversion is desired. If conversion is not desired, a blank card must be supplied (see Item f).

(5) Prepare two magnetic tapes; supply tape numbers for the "setup cards". Specify on the second to the last data card these two tape numbers arranged with the one for Unit 9 first.

(6) Specify the last data card: Twelve integer numbers are required. Eight of them must be the following, the other four may be specified accordingly.

144

1 (LEN) (ILI) (IEI) (JLI) 0 0 0 1 9 10 0

LEN is the ending load increment number. It is desirable to have it equal to multiples of JLI. It is also desirable to have JLI being multiples of IEI and IEI being multiples of ILI. It is suggested to use LEN=50, JLI=50, IEI=10, and ILI=5.

(7) To make a continuation run, the last data card is the only card needed to be changed. The information needed to change this card is always printed at the end of the preceding run. Only LEN needs to be supplied by the operator.

FORTRAN SOURCE LISTING OF THE COMPUTER PROGRAM

```
$SETUP 9          (TAPF 10.)
$SETUP 10         (TAPF NO.)
$IBJOB            MAP,ALTIO

$IBFTC MUVLSP   M94,XR7
C   HENRY LUMISG    UD RESEARCH INST.
C   PROGRAM FOR MULTI-WHEEL VERTICAL LOAD SINKAGE PREDICTION
C   MAIN PROGRAM CALLING THE TWO OVERLAID SUBROUTINES.
        COMMON/DUMMY/  VO(38,28), UD(38,28),    V(38,28),  U(38,28),
       1              SX(38,28), SY(38,28), SXY(38,28),
       2              UT(38,28),UDT(38,28),UDDT(38,28), UI(38,28),
       3              VT(38,28),VDT(38,28),VDDT(38,28), VI(38,28),
       4             SXT(38,28),SYT(38,28),SXYT(38,28),YIT(38,28),
       5             SZ(38,28),  W(38,28),PCU(21),PIN(20),VLD(30)
        COMMON/SDAT/ WR,WRM,TM,DT,N,M,N1,M1,IB,IEH,SI,SIK,CO1,HH,DTT,AL,
       1              GG,PO,CO3,P,AP,AAP,LPP,SQR2,LS,NTO,NIN,KT,KU,KN,WOT
        COMMON/CONTR/LB,LEN,ILI,ILP,IEI,IF,JLI,JLL,NT1,NT2,NT3,NTO,NTI,
       1              NIT,NDT
      CALL SDATA (S99)
      CALL SCALC
   99 STOP
      END




THE FOLLOWING IS A MAP SUB-PROGRAM TO DEFINE THE FILES FOR THE TAPE
    UNITS 8, 9, 10.

$IBMAP MVLTAP
         ENTRY     .UN08.
.UN08. PZE       UNIT08
UNIT08 FILE      ,B(1),READY,INOUT,BIN,BLK=256
         ENTRY     .UN09.
.UN09. PZE       UNIT09
UNIT09 FILE      ,B(2),READY,INOUT,BIN,BLK=256
         ENTRY     .UN10.
.UN10. PZE       UNIT10
UNIT10 FILE      ,B(3),READY,INOUT,BIN,BLK=256
         END




$ORIGIN           SEG1
$IBFTC MVLDAT   M94,XR7
C   THIS SUBROUTINE READS IN PARAMETER DATA, READS DATA FROM TAPE, AND
C   DOES OTHER PRELIMINARY CALCULATIONS.
      SUBROUTINE SDATA (*)
        COMMON/DUMMY/  VO(38,28), UD(38,28),    V(38,28),  U(38,28),
       1              SX(38,28), SY(38,28), SXY(38,28),
       2              UT(38,28),UDT(38,28),UDDT(38,28), UI(38,28),
       3              VT(38,28),VDT(38,28),VDDT(38,28), VI(38,28),
```

147

```
      4                 SXT(38,28),SYT(38,28),SXYT(38,28),YIT(38,28),
      5                 SZ(38,28),  W(38,28),PCU(21),PIN(20),NLO(30)
        COMMON/SDAT/ WR,WRM,TM,DT,N,M,N1,M1,Id,IEN,SI,SIK,CO1,HH,DTT,AL,
      1                 GG,PO,CO3,P,AP,AAP,LPP,SQR2,LS,NTO,NIN,KT,KU,KN,WOT
        COMMON/CONTR/LB,LEN,ILI,ILP,IEI,IF,JLI,JLL,NT1,NT2,NT3,NTO,NTI,
      1                 NIT,NOT
        DIMENSION TITLE(4)
C READ IN AND WRITE TITLE OF THE RUN.
        READ (5,129)  TITLE
        WRITE (6,144)  TITLE
C READ IN DATA - FIRST  READ CONSISTS OF SOIL PARAMETERS
C                SECOND READ CONSISTS OF LOAD PARAMETERS
C                THIRD  READ CONSISTS OF COMPUTATIONAL PARAMETERS
C                FOURTH READ CONSISTS OF LOAD CURVE
        READ (5,100) RHO,PO,E,C,PHI
        READ (5,101) TD,FPL,PKP,WOT,IB,IEN
        READ (5,102) H,DT,M,N
        READ (5,140)  (PCU(I),I=1,21)
        N1=N-1
        M1=M-1
C CALCULATE OTHER SOIL PARAMETERS AND PRINT THEM OUT FOR REFERENCE
        G=144.*E/(1.+PO)/2.
        C2=SQRT(G*32.2/RHO)
        C1=C2*(2.*(1.-PO)/(1.-2.*PO))**0.5
        AL=2.*PO*G/(1.-2.*PO)
        WRITE (6,103)
        WRITE (6,104) RHO,PO,E,G,C2,C1
        WRITE (6,105) C,PHI
        PHI=PHI*3.1415927/180.
        CC=(3.-SIN(PHI))*3.**0.5
        AP=2.*SIN(PHI)/CC
        AAP=AP*AP
        YS=6.*C*COS(PHI)/CC
        WRITE (6,106) AP,YS
        WRITE (6,111)
        WRITE (6,113) TD,FPL,PKP,IB,IEN
        WRITE (6,107)
        WRITE (6,108) H,DT,M,N,WOT
        WRITE (6,109)
        WRITE (6,110) FPL,TD,YS
C NON-DIMENSIONALIZING ALL PARAMETERS AND CALCULATE SOME CONSTANTS THAT
C WILL BE USED IN THE LATER LOOPS
        AL=AL/YS
        G=G/YS
        GG=2.*G
        H=H/FPL
        SQR2=SQRT(2.)
        HH=H*SQR2
        FPL=FPL/12.
        DTT=DT/TD
        CO1=YS*TD*TD*32.2/(RHO*FPL*FPL)
        CO3= AP*(1.+PO)/(1.-2.*PO)
        P=GG/(0.5+3.*CO3*AP)
        DTG=DTT*GG
```

148

```
       DTP=DTT*P
C MODIFY BASIC LOAD CURVE FOR THE SPECIFIED PEAK LOAD, CALCULATE LOAD
C INCREMENTS AND NON-DIMENSIONALIZING BOTH, CALCULATE THE NUMBER OF
C LOAD INCREMENTS IN A LINE SEGMENT.  PRINT OUT ALL FOR REFERENCE
       WRITE (6,115)
       NIN=0.025/DTT+0.001
       FNIN=NIN
       NTO=40*NIN
       TTO=0.
       NG=0
       FP=PKP/10000.
       PC=PCU(1)
       DO 163 J=1,20
       TTO=TTO+0.025
       NG=NG+NIN
       JJ=J+1
       PI=(PCU(JJ)-PC)*FP/FNIN
       PC=PCU(JJ)
       PCM=PC*FP
       PIN(J)=PI/YS
       PCU(JJ)=PCM/YS
   163 WRITE (6,116)   J,TTO,PC,PCM,PI,PCU(JJ),PIN(J),NG
C READ IN THE VALUE OF THE COHESION OF THE TAPE DATA WHICH IS USED FOR
C  CONVERSION.
       READ (5,140) CT
C READ IN TAPE NUMBERS OF THE TAPE SETUP ON UNIT 9 AND 10,RESPECTIVELY
       READ (5,141) NIT,NOT
C READ IN STARTING LOAD INCREMENT NUMBER AND ENDING LOAD INCREMENT
C NUMBER, AND OTHER CONTROL INDICES.  CALCULATE THE PRINT CONTROL
C INDICES, THE TIME OF THE PULSE, AND THE INITIAL APPLIED PRESSURE  SI,
C AND PRINT OUT FOR REFERENCE.
       READ (5,141) LB,LEN,ILI,IEI,JLI,NT1,NT2,NT3,LPP,ITI,ITO,ICV
       ILP=LB+ILI-1
       IF=LB+IEI-1
       JLL=LB+JLI-1
       BL=LB-1
       TM=BL*DT
       TB=TM/TO/0.025+1.0
       KT=TB+0.001
       IF (KT.LT.41)  GO TO 170
       SIK=0.
       SI=0.
       GO TO 171
   170 TK=KT
       KN=KT
       LS=KT*NIN
       KU=1
       IF (KT.LE.20)  GO TO 165
       KT=42-KT
       KU=-1
       KL=KT-1
   165 SIK=FLOAT(KU)*PIN(KN)
       KTU=KT+KU
       SI=(TB-TK)*(PCU(KTU)-PCU(KT))+PCU(KT)+SIK
```

149

```
      171 WRITE (6,117)
          WRITE (6,118)  L3,LEN,SI,SIK,TM
          WRITE (6,135) LB,LEN,ILI,IEI,JLI,NT1,IT2,NT3,LPP,ITI,NTO,ICV
C IF CONVERSION IS NEEDED, CALCULATE THE CONVERSION FACTOR FOR THE
C  STRESSES.
          IF (ICV.EQ.0) GO TO 159
          CCNV=ST/C
      159 CONTINUE
          IF (LB.NE.1) GO TO 164
C IF THIS IS THE VERY FIRST RUN, ALL STRESSES AND DISPLACEMENTS ARE
C FIRST SET EQUAL TO ZERO, AND THE YIELD INDICATING MATRIX IS SET TO BE
C ELASTIC
          DO 7 J=1,N
          DO 7 I=1,M
             U(I,J)=0.
             V(I,J)=0.
             UD(I,J)=0.
             VD(I,J)=0.
             UT(I,J)=0.
             VT(I,J)=0.
             UDT(I,J)=0.
             VDT(I,J)=0.
             UDDT(I,J)=0.
             VDDT(I,J)=0.
             UI(I,J)=0.
             VI(I,J)=0.
             SX(I,J)=0.
             SY(I,J)=0.
             SXY(I,J)=0.
             SXT(I,J)=0.
             SYT(I,J)=0.
             SXYT(I,J)=0.
             SZ(I,J)=0.
      7   YIT(I,J)=-1.
          RETURN
C REARRANGE DESIGNATION OF UNIT OF TAPES DEPENDING ON NTI  AND  NTO
      164 IF (NTI.EQ.9) GO TO 173
          ILL=NIT
          NIT=NOT
          NOT=ILL
      173 WRITE (6,138) NIT
C IF THIS IS A CONTINUATION RUN, THE STRESSES, DISPLACEMENTS, AND
C     YIELD INDICATING TABLE OF THE PRECEDING RUN ARE READ IN FROM INPUT
C     TAPE. DATA READ IN, IF NO REDUNDANCY OCCURRED, ARE SAVED IN DISK
C     UNIT 8 FOR TRANSFER TO OUTPUT TAPE.
          DO 162 I=1,NT1
          READ (NTI) UT,UDT,UDDT,UI,VT,VDT,VDDT,VI,SXT,SYT,SXYT,YIT,SZ,W
          ILL=SYT(1,1)
          WRITE (6,139)  ILL
          IF (I.NE.IT2)  GO TO 162
          WRITE (8)  UT,UDT,UDDT,UI,VT,VDT,VDDT,VI,SXT,SYT,SXYT,YIT,SZ,W
      162 CONTINUE
C READ FROM DISK UNIT 8 THE DESIRE STARTING STRESSES AND DISPLACEMENTS
C FOR THE CONTINUATION RUN.
```

```
      IF (NT2.EQ.0)  GO TO 175
      REWIND 8
  174 READ (8)    UT,UDT,UDDT,UI,VT,VDT,VDDT,VI,SXT,SYT,SXYT,YIT,S7,W
      ILL=SYT(1,1)
      REWIND NT1
  175 IF (ILL.NE.(LR-1))  GO TO 99
      NT1=0
C EQUATE THE CURRENT DISPLACEMENTS AND STRESSES WITH THE PREVIOUSLY
C  SAVED DISPLACEMENTS AND STRESSES. MAKE STRESS CONVERSION IF THE TAPE
C  DATA IS NORMALIZED DIFFERENTLY.
      DO 8 J=1,N
      DO 8 I=1,M
       U(I,J)= UT(I,J)
      V(I,J)=VT(I,J)
      UD(I,J)=UDT(I,J)
      VD(I,J)=VDT(I,J)
      IF (ICV.EQ.0) GO TO 176
       SXYT(I,J)=SXYT(I,J)*CONV
       SYT(I,J)= SYT(I,J)*CONV
       SXT(I,J)= SXT(I,J)*CONV
  176   SX(I,J)= SXT(I,J)
       SY(I,J)= SYT(I,J)
       SXY(I,J)=SXYT(I,J)
    8 CONTINUE
      RETURN
   99 RETURN
  100 FORMAT(F6.1,F6.2,3F8.1)
  101 FORMAT (2F10.3,F10.2,E10.2,2I5)
  102 FORMAT (F8.3,F12.6,2I5)
  103 FORMAT(1H1,19X,15HSOIL PROPERTIES)
  104 FORMAT(23X,7HDENSITY,17X,5HRHO =,F10.1,10H LBS/CU-FT/
     1        23X,14HPOISSONS RATIO,11X,4HPO =,F10.2/
     2        23X,14HYOUNGS MODULUS,12X,3HE =,F10.1,4H PSI/
     3        23X,13HSHEAR MODULUS,13X,3HG =,F10.1,10H LBS/SQ-FT/
     4        23X,29HSHEAR WAVE VELOCITY        C2 =,F10.1,7H FT/SEC/
     5        23X,29HDILATATIONAL WAVE VEL.     C1 =,F10.1,7H FT/SEC//)
  105 FORMAT(23X,8HCOHESION,18X,3HC =,F10.1,1CH LBS/SQ-FT/23X,14HFRICTIO
     1N ANGLE,10X,5HPHI =,F10.1,4H DEG//)
  106 FORMAT(23X,29HFOR YIELD CRITERIA     ALPHA =,E16.8/49X,3HK =,E16.6,
     110H LBS/SQ-FT//)
  107 FORMAT(1H0,19X,24HCOMPUTATIONAL PARAMETERS)
  108 FORMAT(23X,10HSPACE MESH,
     116X,3HH =,F10.4,3H IN/23X,29HBASIC TIME INCREMENT      DT =,
     2F10.7,4H SEC//23X,11HNUMBER OF I,15X,3HM =,I4/23X,11HNUMBER OF J,
     315X,3HM =,I4/23X,29HUNLOADING TOLERANCE      WOT =,1PE10.2//)
  109 FORMAT(1H0,19X,50HCHARACTERISTIC PARAMETERS FOR NON-DIMENSIONALIZI
     1NG)
  110 FORMAT(23X,14HLENGTH = FPL =,F10.2,3H IN/23X,14HTIME    = TO  =,F10
     1.2,4H SEC/23X,14HSTRESS = K    =,F10.2,10H LBS/SQ-FT///)
  111 FORMAT (1H0,19X,15HLOAD PARAMETERS)
  112 FORMAT (1H////)
  113 FORMAT (23X,29HTIME DURATION OF PULSE    TO =,F10.3,4H SEC/
     1          23X,29HTIRE FOOTPRINT LENGTH    FPL =,F10.3,3H IN/
     2          23X,29HPEAK PRESSURE OF PULSE   PKP =,F10.1,10H LBS/SC-FT/
```

```
  3           23X,29HLOAD BORDER INDEX-BEGIN  IB =,I10/
  4           23X,29HLOAD BORDER INDEX-END    IEN =,I10//)
115 FORMAT (6X,99H AT DIMENSIONLESS     BASIC LOAD     DIMENSIONED
   1DIMENSIONED     DIMENSIONLESS     DIMENSIONLESS/105H    J       TIME
   2 T/TO        CURVE      LOAD CURVE     LOAD INCREMENT       LOAD
   3 CURVE    LOAD INCREMENT//)
116 FORMAT (1X,I3,F14.3,F18.1,F16.3,F16.5,1PE19.7,E18.7,I8)
117 FORMAT (1H1,18X,34HPARAMETERS FOR THIS PARTICULAR RUN)
118 FORMAT (23X,37HSTARTING LOAD INCREMENT NUMBER    LB =,I6/23X,37HEND
   1ING   LOAD INCREMENT NUMBER   LEN =,I6/23X,37HSTARTING SURFACE PRES
   2SURE         SI =,1PF17.7,16H (DIMENSIONLESS)/23X,37HPRESSURE (OR L
   3OAD) INCREMENT    SIK =,1PF17.7,16H (DIMENSIONLESS)/23X,13HSTARTIN
   4G TIME,20X,4HTM =,0PF12.7,4H SEC//)
129 FORMAT (4A6)
135 FORMAT (1H0,18X,32HLAST DATA CARD OF THIS RUN IS---//
   225X,57HLB  LEN   ILI   ICI   JLI   NT1   NT2   NT3   LPP   NTI   NTO   ICV//
   322X,12I5)
138 FORMAT (1H0,18X,11HTAPE NUMBER,I6,54H  CONTAINS THE RESULTS OF LOA
   1D INCREMENT NUMBER   ILL =//)
139 FORMAT (23X,I5)
140 FORMAT (5F11.2)
141 FORMAT (1X,14I5)
144 FORMAT (1H1/////1H0,47X,44HMULTI-WHEEL VERTICAL LOAD SINKAGE PREDIC
   1TION//59X,4A6)
    END




$ORIGIN          SEG1
$IBFTC MVLCAL    M94,XR7
C  THIS SUBROUTINE DOES THE MAIN CALCULATIONS OF THE ITERATIONS, PRINTS
C  OUT NEEDED RESULTS, AND SAVES RESULTS ON TAPES.
    SUBROUTINE SCALC
    COMMON/DUMMY/  VO(38,28),  UO(38,28),   V(38,28),   U(38,28),
   1               SX(38,28), SY(38,28), SXY(38,28),
   2               UT(38,28),UDT(38,28),UDDT(38,28), UI(38,28),
   3               VT(38,28),VDT(38,28),VDDT(38,28), VI(38,28),
   4               SXT(38,28),SYT(38,28),SXYT(38,28),YIT(38,28),
   5               SZ(38,28),  W(38,28),PCU(21),PIN(20),NLO(30)
    COMMON/SDAT/ WR,WRM,TM,DT,V,M,N1,M1,IB,IEN,SI,SIK,COL,HH,DTT,AL,
   1             GG,PO,CU3,P,AP,AAP,LPP,SQR2,LS,NTO,NIN,KT,KU,KN,WOT
    COMMON/CONTR/LB,LEN,ILI,ILP,IEI,IF,JLI,JLL,NT1,NT2,NT3,NTO,NTI,
   1             NIT,NUT
C THE FOLLOWING DATA STATEMENTS SUPPLY THE VARIABLE FORMATS.
    LOGICAL FRNT,LAST
    DIMENSION  FMS(3),FMW(3),FMY(3)
    DATA FMS(1)/18H(1X,I2,12   F10.6)/,
   1      FMW(1)/18H(1X,I2,12   F10.6)/,
   2      FMY(1)/18H(1X,I2,13   F10.6)/,
   3      FX5,FX4,FX3,FX2/6HF10.5),6HF10.4),6HF10.3),6HF10.2)/
   4      ,FX6/5HF10.6)/
    SJF(V1,V2,V3,V4)=SQRT(((V1-V2)**2+(V2-V3)**2+(V3-V1)**2)/6.+V4*V4)
```

152

```
C STARTING POINT OF MOST OUTER LOOP, FOR CALCULATION OF EACH LOAD
C   INCREMENTS.
      UPL=-1.
  169 DO 250 ILL=LB,LEN
      LPT=0
      TM=TM+DT
C STARTING POINT OF THE ITERATION LOOP.
      JA=1
      IT=0
    6 IT=IT+1
      LAST=JA.EQ.2
      DFU=0.
      DFV=0.
C STARTING POINT FOR THE LOOP INCREMENTING EACH ROW GOING DOWNWARD
      DO 80 J=1,N1
      JP=J+1
      DO 80 I=1,M1
      IP=I+1
C CALCULATE, AT EACH MASS POINT, THE ACCELERATIONS FROM THE DYNAMIC
C EQUATIONS OF MOTION. THE PARTICULAR EQUATION TO USE DEPENDS ON THE
C LOCATION OF THE MASS POINT.
      IF (J.GT.1) GO TO 9
      IF (I.GE.IB.AND.I.LE.IEN)  GO TO 4
      SIX=0.
      SIY=0.
      GO TO 5
    4 IF ((I.NE.IB.OR.IB.EQ.1).AND.I.NE.IEN)  GO TO 11
      SIX=SI/2.
      SIY=SI/2.
      GO TO 5
   11 SIX=SI
      SIY=SI
    5 UDD=2.*C01*(SX(IP,JP)+SXY(I,JP)-SIX)/HH
      VDD=2.*C01*(SY(I,JP)+SXY(IP,JP)-SIY)/HH
      GO TO 10
    9 UDD=C01*(SX(IP,JP)-SX(I,J)+SXY(I,JP)-SXY(IP,J))/HH
      VDD=C01*(SY(I,JP)-SY(IP,J)+SXY(IP,JP)-SXY(I,J))/HH
C CALCULATE THE DISPLACEMENTS AND VELOCITIES AT TIME  T   FROM THE
C QUADRATURE EQUATIONS.
   10 UB    =UT(I,J)+DTT*UDT(I,J)+DTT*DTT*(UDDT(I,J)*2.+UDD)/6.
      VB    =VT(I,J)+DTT*VDT(I,J)+DTT*DTT*(VDDT(I,J)*2.+VDD)/6.
      UDB   =UDT(I,J)+DTT*(UDDT(I,J)+UDD)/2.
      VDB   =VDT(I,J)+DTT*(VDDT(I,J)+VDD)/2.
      IF (IT.NE.1) GO TO 12
       U(I,J)= UB
       V(I,J)= VB
      UD(I,J)=UDB
      VD(I,J)=VDB
      GO TO 14
C AVERAGE WITH THE DISPLACEMENTS FROM THE PRECEDING ITERATION
   12 U(I,J)=(UB+U(I,J))/2.
      V(I,J)=(VB+V(I,J))/2.
      UD(I,J)=(UDB+UD(I,J))/2.
      VD(I,J)=(VDB+VD(I,J))/2.
```

153

```
C   CALCULATE THE DISPLACEMENT INCREMENTS
    14 UI(I,J)=U(I,J)-UT(I,J)
       VI(I,J)=V(I,J)-VT(I,J)
       IF (JS.LE.2) GO TO 17
       UDOT(I,J)=UDS
       VDOT(I,J)=VDS
    17 IF (IT.LE.2) GO TO 20
C CALCULATE THE PERCENT CONVERGENCE OF THE VERTICAL DISPLACEMENT
C BETWEEN THIS AND THE PRECEDING ITERATION.  LOCATE THE LARGEST PERCENT
C AND SAVE IT FOR LATER REFERENCE.
       DU=ABS(UD/U(I,J)-1.)
       DV=ABS(VD/V(I,J)-1.)
       IF (DU.LE.DFU) GO TO 18
       DFU=DU
       ILU=ILL
       ITU=IT
       IU=I
       JU=J
    18 IF (DV.LE.DFV) GO TO 20
       DFV=DV
       ILV=ILL
       ITV=IT
       IV=I
       JV=J
C CALCULATE THE STRESSES OF THE TWO STRESS POINTS BELOW THE MASS POINT.
C   INDEX IC INDICATES WHICH STRESS POINT IS BEING CONSIDERED.
C       IC=1   IS THE ONE ON THE RIGHT
C       IC=2   IS THE ONE ON THE LEFT
    20 IC=1
       K=IP
       L=JP
    22 KM=K-1
       LM=L-1
       FRIT=IC.EQ.1.AND.K.NE.M
C SAVE THE STRESSES OF THE PRECEDING ITERATION.
       SXS= SX(K,L)
       SYS= SY(K,L)
       SXYS=SXY(K,L)
       YITS=YIT(K,L)
C CALCULATE THE STRAIN INCREMENTS.
       EX=(UI(K,L)-UI(KM,LM))/HH
       EY=(VI(KM,L)-VI(K,LM))/HH
       EXY=(UI(KM,L)-UI(K,LM)+VI(K,L)-VI(KM,LM))/HH/2.
       EE=AL*(EX+EY)
C CHECK THE YIELD INDICATING TABLE TO DETERMINE WHICH STRES-STRAIN
C   RELATION TO USE.
       IF (YITS.GE.0..AND.YITS.LT.40000.) GO TO 35
C STRESS POINT IS ELASTIC.
       SX(K,L)= SXT(K,L)+GG*EX+EE
       SY(K,L)= SYT(K,L)+GG*EY+EE
       SXY(K,L)=SXYT(K,L)+GG*EXY
       GO TO 50
C   35 STRESS POINT IS PLASTIC.
    35 UPL=-1.
```

154

```
      WC=SXS*EX+SYS*EY+SXYS*EXY
      SZS=PC*(SXS+SYS)
      SS=SXS+SYS+SZS
      SJ=SJF(SXS,SYS,SZS,SXYS)
      BE=(0.3-SS/SJ/6.
      SJ2=SJ*2.
      WE=(WC/SJ2+BE*EE/AL)*P
       SX(K,L) = SXT(K,L)+GG*EX+EE-(SXS/SJ2+BE)*WE
       SY(K,L) = SYT(K,L)+GG*EY+EE-(SYS/SJ2+BE)*WE
      SXY(K,L)=SXYT(K,L)+GG*EXY-SXYS*WE/SJ2
C  50 CHECK IF THE STRESS POINT HAS YIELDED.  THIS IS DONE ONLY FOR THE
C     FINAL ITERATION.  JA INDEX CONTROLS THE ENTRY.
   50 IF (.NOT.LAST)  GO TO 64
C CALCULATE THE YIELD FUNCTION
      SS=SX(K,L)+SY(K,L)
      SZZ=PC*SS
      SS=SS+SZZ
      SJ=SJF(SX(K,L),SY(K,L),SZZ,SXY(K,L))
      FC=AP*SS+SJ-1.
C CHECK IF THE YIELD FUNCTION IS GREATER THAN THE TOLERANCE ABOVE ZERO,
C AND MAKE THE APPROPRIATE CHANGE IN THE YIELD INDICATING TABLE
      IF (FC.GT.0.015) GO TO 55
      IF (YITS.LT.0.)  GO TO 53
      IF (FC.GT.-0.015) GO TO 55
   53 IF (FR.R)  GO TO 66
      YI=FC
      IF (FC.GT.0.) YI=-10.-FC
      GO TO 64
C 55 STRESS POINT HAS YIELDED. CHANGE CONTROL INDEX TO SAVE DATA OF THIS
C    LOAD INCREMENT ON TAPE.  CHANGE THE FORMAT OF THE YIELD INDICATING
C    TABLE PRINT OUT.
   55 IF (FRIT)  GO TO 58
      IF (LPP.NE.1) GO TO 56
      LPP=2
      FMY(3)=FXS
C CHECK FOR UNLOADING
   56 WC=SX(K,L)*EX+SY(K,L)*EY+SXY(K,L)*EXY
      IF (WC.LT.-WOT) GO TO 57
      IF (WC.GT.WOT.OR.YITS.LT.40000.) GO TO 58
   57 UPL=1.
C CALCULATE THE STRESS CORRECTION FACTOR.
   58 SSP=(1.-AP*SS)**2
      SJS=SJ*SJ
      PH=(SJS-SSP)/(2.*SJS+12.*AAP*SSP)
      PZK=PH*((1.+6.*AAP)*SS/3.-2.*AP)
      RIT=1.-PH
      FCJ=AINT(10000.*FC)
      IF (FC.LT.0.) FCJ=20000.-FCJ
      YI=FCJ+RIT
      IF (UPL.GT.0.)  YI=YI+40000.
C STRESS CORRECTION IS MADE BY THE FOLLOWING STATEMENTS ONLY IF THE
C YIELD FUNCTION IS GREATER THAN A TOLERANCE.
      IF (FC.LT.0.020) GO TO 64
      YI=YI+30000.
```

```
      FMY(3)=FX3
       SX(K,L)= SX(K,L)*RAT+PAK
       SY(K,L)= SY(K,L)*RAT+PAK
      SXY(K,L)=SXY(K,L)*RAT
   64 IF (FRNT)  GO TO 66
      IF (LAST)  YIT(K,L)=YI
      IF (IC.EQ.2)  GO TO 67
   66 K=I
      IC=2
      GO TO 22
   67 IF (K.NE.2)  GO TO 80
C SET SYMMETRY CONDITIONS AT AXIS OF SYMMETRY.
      SY(1,L)=SX(2,L)
      SX(1,L)=SY(2,L)
      SXY(1,L)=SXY(2,L)
      IF (LAST)  YIT(1,L)=YI
   80 CONTINUE
      IF (IT.LE.2) GO TO 6
      WRITE (6,143)  DFU,ILU,ITU,IU,JU,DFV,ILV,ITV,IV,JV
      IF (LAST)  GO TO 85
C CHECK IF THE CONVERGENCE IS GOOD ENOUGH.  RETURN TO CALCULATE ANOTHER
C ITERATION IF NOT ACCURATE ENOUGH.
      IF ((DFU.GT.0.002.OR.DFV.GT.0.002).AND.IT.LT.7) GO TO 6
C IF ACCURATE ENOUGH, ADJUST  JA  INDEX AND CALCULATE FINAL ITERATION.
      JA=2
      GO TO 6
C THE FOLLOWING LOOP SAVES ALL THE DISPLACEMENTS AND STRESSES FOR THE
C CALCULATION OF THE NEXT TIME INCREMENT.
C WITHIN THIS LOOP, THE VERTICAL DISPLACEMENTS AND STRESSES ARE ALSO
C CALCULATED FROM THE DIAGONAL DISPLACEMENTS AND STRESSES.
   85 DO 90 J=1,N
      DO 90 I=1,M
         UT(I,J)=   U(I,J)
         VT(I,J)=   V(I,J)
        UDT(I,J)=  UD(I,J)
        VDT(I,J)=  VD(I,J)
         W(I,J)=(U(I,J)+V(I,J))*1.0E06/SQR2
      IF (J.GT.1) GO TO 89
      IF (I.GT.IEM.OR.(I.LE.IB.AND.IB.NE.1))  GO TO 87
      SZ(I,1)=SI*100.
      GO TO 90
   87 SZ(I,1)=0.
      GO TO 90
   89    SXT(I,J)=  SX(I,J)
         SYT(I,J)=  SY(I,J)
        SXYT(I,J)= SXY(I,J)
         SZ(I,J)=((SX(I,J)+SY(I,J))/2.+SXY(I,J))*100.
   90 CONTINUE
C IF THE END OF A LINEAR SEGMENT OF THE LOAD CURVE IS REACHED,  SIK  IS
C CHANGED TO THE APPLIED PRESSURE INCREMENT OF THE NEXT LINEAR SEGMENT.
      IF (ILL.LT.LS) GO TO 182
      IF (ILL.GE.NTO)  GO TO 179
      LS=LS+NIN
      KT=KT+KU
```

```
         IF (KT.NE.21)  GO TO 178
         KN=21
         KU=-1
 178  KN=KN+KU
         SIK=FLOAT(KU)*PIM(KN)
         SI=PCU(KT)
         GO TO 182
C 179 IF END OF THE LOAD CURVE OCCURS,   THE SURFACE PRESSURE IS NO
C     LONGER INCREMENTED.
 179  SI=0.
         SIK=0.
 182  CONTINUE
         IF (LPP.LT.2)  GO TO  185
C THE STRESSES AND DISPLACEMENTS OF THE LOAD INCREMENT IN WHICH THE
C FIRST PLASTIC POINT OCCURS ARE SAVED ON THE OUTPUT TAPE.
         LPP=0
         WRITE (6,125)   ILL,IT
         WRITE (6,119)
         LPT=1
         GO TO 245
 185  CONTINUE
C PRINT OUT THE VERTICAL STRESSES AND DISPLACEMENTS IN THE REGION UNDER
C THE LOADED AREA FOR MONITORING THE COMPUTER RUN.
 193  IF (ILL.LT.ILP) GO TO 240
C SELECTION OF FORMAT FOR THE PRINT OUT.
         IF (ABS(SZ(IFN,1)).LT.10.  )  GO TO 209
         IF (ABS(SZ(IFN,1)).LT.100.)  GO TO 208
         FMS(3)=FX4
         GO TO 212
 208  FMS(3)=FX5
         GO TO 212
 209  FMS(3)=FX6
 212  IF (ABS(W(IB+1,1)).LT.  100.)  GO TO 218
         IF (ABS(W(IB+1,1)).LT.10000.)  GO TO 216
         FMW(3)=FX2
         GO TO 238
 216  FMW(3)=FX4
         GO TO 238
 218  FMW(3)=FX6
 238  CONTINUE
         JB=1
         JF=12
         ILP=ILP+ILI
 239  WRITE (6,125)   ILL,IT,TM,(J,J=JB,JE)
         WRITE (6,FMS)   (J,( SZ(I,J),I=JB,JE),J=1,N)
         WRITE (6,126)   ILL,IT,TM,(J,J=JB,JE)
         WRITE (6,FMW)   (J,(  W(I,J),I=JB,JE),J=1,N)
         WRITE (6,136)   ILL,IT,TM,(J,J=JB,JE)
         WRITE (6,FMY)   (J,(YIT(I,J),I=JB,JE),J=1,N)
         IF (ILL.NE.IF ) GO TO 240
         JB=13
         JE=24
         IS=IE+ICI
         GO TO 239
```

157

```
C THE INDEX  JLL   CONTROLS THE SAVING OF THE RESULTS OF A PARTICULAR
C      LOAD INCREMENT ON THE OUTPUT TAPE FOR LATER REFERENCE.   THE
C      INTERVAL IS GIVEN BY   JLI.   THE RESULTS OF THE LAST LOAD INCREMENT
C      IS ALSO SAVED FOR THE CONTINUATION RUN.
  240 IF (ILL.NE.JLL.AND.ITIME(NT).GT.10)  GO TO 250
  245 NT1=NT1+1
      NLO(NT1)=ILL
      SXT(1,1)=TM
      SYT(1,1)=ILL
      JTM=ITIME(NT)
      WRITE (NTO) UT,UDT,UDDT,UI,VT,VDT,VDDT,VI,SXT,SYT,SXYT,YIT,SZ,W
      IF (LPT.EQ.1)  GO TO 185
      IF (JTM.LT.10)  GO TO 99
      JLL=JLL+JLI
  250 SI=SI+SIK
      NT2=NT1
      WRITE (6,138) NOT
      DO 205 I=1,NT1
  205 WRITE (6,139) NLO(I)
C THE RESULTS FROM THE INPUT TAPE SAVED IN UNIT 8 IS TRANSFERRED TO THE
C OUTPUT TAPE BEHIND THE OUPUT OF THIS RUN.
      IF (NT3.EQ.0)  GO TO 199
      DO 210 I=1,NT3
      READ (NTI)  UT,UDT,UDDT,UI,VT,VDT,VDDT,VI,SXT,SYT,SXYT,YIT,SZ,W
      NT1=NT1+1
      ILL=SYT(1,1)
      WRITE (NTO) UT,UDT,UDDT,UI,VT,VDT,VDDT,VI,SXT,SYT,SXYT,YIT,SZ,W
      WRITE (6,139)  ILL
      IF (ITIME(NT).LT.3)  GO TO 199
  210 CONTINUE
  199 NT3=NT1
      LEN=LEN+1
      ICV=0
      WRITE (6,137) LEN,ILI,IEI,JLI,NT1,NT2,NT3,LPP,NTO,NTI,ICV
   99 RETURN
  119 FORMAT (3X,23HSTRESS POINT IS PLASTIC//)
  125 FORMAT (49H1VERTICAL STRESS DISTRIBUTION (SZ*100.)  AT ILL =,I5,
     16H, IT =,I3,8H, TIME =,F10.6,5H  SEC//1X,I9,11I10//)
  126 FORMAT (58H1VERTICAL DISPLACEMENT DISTRIBUTION (W*10.0E 06)  AT IL
     1L =,I5,6H, IT =,I3,8H, TIME =,F10.6,5H  SEC//1X,I9,11I10//)
  136 FORMAT (40H1YIELD INDICATING TABLE (YIT)  AT ILL =,I5,6H, IT =,
     1I3,8H, TIME =,F10.6,5H  SEC//1X,I9,11I10//)
  137 FORMAT (1H0,3X,71HFOR CONTINUING RUN, ONLY NEED TO CHANGE THE LAST
     1 DATA CARD AS FOLLOWS--//
     211X,57HLB  LEN  ILI  IEI  JLI  NT1  NT2  NT3  LPP  NTI  NTO  ICV//
     38X,I5,5X,10I5)
  138 FORMAT (1H0,18X,11HTAPE NUMBER,I6,54H  CONTAINS THE RESULTS OF LOA
     1D INCREMENT NUMBER  ILL =//)
  139 FORMAT (23X,I5)
  142 FORMAT (F8.1,F12.8)
  143 FORMAT (2X,2(F20.8,4I8))
      END
```

THE FOLLOWING IS A SAMPLE SET OF INPUT DATA FOR THE PROGRAM.

$DATA
SPACING FACTOR, N=4.65
   130.0 0.45 8950.0 2000.0   15.0
     0.05   12.0   24600.0   5.00E-05   11   15
     3.00   6.25E-05   36   28
        0.0   -20.0   -110.0   -270.0   -580.0
    -1050.0   -1730.0   -2630.0   -3750.0   -4890.0
    -5890.0   -6770.0   -7540.0   -8190.0   -8730.0
    -9170.0   -9500.0   -9740.0   -9900.0   -9980.0
   -10000.0
      400.00   500.00
    930 2445
      1   50   5   10   50   0   0   0   1   9   10   0
$EOF

LIST OF SYMBOLS

AL	Lame constant (λ) in psf; later becomes dimensionless (λ/k)
AP	Soil parameter (σ')
BE	A variable in the plastic relation related to the stress invariants (B)
C	Cohesion (c) in psf
CT	The value of the cohesion of the saved data on tape; used in conversion
C1	Dilatational wave velocity in fps
C2	Shear wave velocity in fps
DFU, DFV	The value of the maximum percent convergence of U and V displacements between successive iterations among all the mass points
DT	Time increment (Δt) in seconds
DTT	Dimensionless time increment ($\frac{\Delta t}{t_d}$)
DU, DV	Percent convergence of the U and V displacements between successive iterations
EX, EY, EXY	Strain increments ($\Delta\epsilon_\eta$, $\Delta\epsilon_\zeta$, and $\Delta\gamma_{\eta\zeta}$) at time t
FC	Yield function
FP	Load curve adjustment factor
FPL	Width of loaded area (a) in inches; later becomes in feet
G	Shear modulus (G) in psf; later becomes dimensionless (G/k)
H	Grid size, the distance between mass points (h) in inches; later becomes dimensionless (h/a)
I	Index in the horizontal direction (i)
IB	I-index of the mass point at the beginning of the loaded area
IC	Index for controlling the particular surrounding stress point to be calculated
IEI	The number of load increments skipped in the printout for the whole region
IEN	I-index of the mass point at the end of the loaded area

160

ILI	The number of load increments skipped in the printout for a limited region
ILP	Index for controlling which load increment is to be printed out
IT	Iteration index
J	Index in the downward direction (j)
JA	Index for controlling, during the final iteration, the entry to program for checking if the stress point has yielded
KT	Index for indicating the particular linear segment of the load curve that is being considered
LB	Starting load increment number for the particular computer run
LEN	Ending load increment number for the particular computer run
M	The number of grid points in the horizontal direction
N	The number of grid points in the downward direction
NIN	The number of load increments in a linear segment of the load curve
P	A constant in the plastic relation (Q)
PCU	Magnitude of the applied pressure after each linear segment of the load curve
PH	Stress correction factor (η_c)
PHI	Frictional angle (ϕ) in degrees; later becomes in radians
PIN	Applied pressure increment within each linear segment
PKP	Peak load of load pulse in psf
PO	Poisson's ratio (ν)
RAT	Stress correction factor ($1 - r_c$)
RHO	Weight density (ρ) in lb/ft^3
SI	The current applied surface pressure that is prescribed at the fictitious stress points
SIK	The particular applied pressure increment being considered
SJ	Second stress invariant of the stress tensor (J)
SS	First stress invariant of the stress tensor (I)
SX, SY, SXY	Normal and shear stresses in the (η, ζ) directions (σ_η, σ_ζ, $\tau_{\eta\zeta}$) at time t

SXS, SYS, SXYS	The stresses of the previous iteration at the surrounding stress point being considered
SXT, SYT, SXYT	Normal and shear stresses in the (η, ζ) directions $(\sigma_\eta, \sigma_\zeta, \tau_{\eta\zeta})$ at time $t-\Delta t$
SZ	Vertical normal stress $(\sigma_z) \times 10^2$; use for printout purpose
SZZ	Normal stress in the direction normal to (η, ζ)
TD	Time duration of the load pulse (t_d) in seconds
TM	Time in seconds (t)
TTD	Dimensionless time (t/t_d) at the end of each linear segment of the load curve
U, UD, UDD	Displacement, velocity, and acceleration in the η-direction $(u, \dot{u}, \ddot{u})$ at time t
UI	Displacement increment (Δu) in the η-direction at time t
UPL	A variable for indicating unloading; UPL = -1.0 is not loading and UPL = 1.0 is unloading
UT, UDT, UDDT	Displacement, velocity, and acceleration in the η-direction $(u, \dot{u}, \ddot{u})$ at time $t-\Delta t$
V, VD, VDD	Displacement, velocity, and acceleration in the ζ-direction $(v, \dot{v}, \ddot{v})$ at time t
VI	Displacement increment (Δv) in the ζ-direction at time t
VT, VDT, VDDT	Displacement, velocity, and acceleration $(v, \dot{v}, \ddot{v})$ at time $t-\Delta t$
W	Vertical displacement $(w) \times 10^6$, use for printout purpose
WO	Incremental plastic work done (ΔW)
WR	A reference plastic work done
YI	Yield indicating table at time t
YIT	Yield indicating table at time $t-\Delta t$
YS	Yield stress in shear (d) in psf

APPENDIX IV

MULTIPLE WHEEL VERIFICATION TESTS

Soil Tests and Preparation

Classification

Both of the soils selected for the test program have been used extensively by WES in previous mobility studies and the classification properties have been reported previously. For comparison purposes, the grain size distribution and limits properties are given for the buckshot clay in Figure 59, and the grain size distribution for the mortar sand is shown in Figure 60.

California Bearing Ratio

The CBR is a plate bearing test using a three-square inch piston which is penetrated continuously into the soil to a depth of one-half inch while continuously recording the load resistance with depth. Annular surcharge weights are placed around the piston prior to its penetration. The ratio of the load at 0.1 inch penetration to that load supported by a standard well graded crushed gravel multiplied by 100 is defined as the CBR of the soil.

Cone Penetrometer Resistance

The mobility cone penetrometer is a rod device having a thirty degree cone tip and has a cross section base area of 0.5 square inch. The shaft is narrowed above the cone to minimize the friction between the side of the shaft and the hole. The cone penetrometer, which is pushed into the soil at a standard rate, measures the resistance to penetration (Cone Index) in pounds per square inch. The Cone Index is a measure of soil shear strength and its variation with depth. The CI value is usually given as the average resistance over the first 6" of depth.

Table 29 gives the cone index values taken in the tire ruts after one pass of the test carriage. For tandem-tracking tests, the rut was was formed by both tires and the strength value given represents the after test soil strength caused by two passes of a tire. For the twin
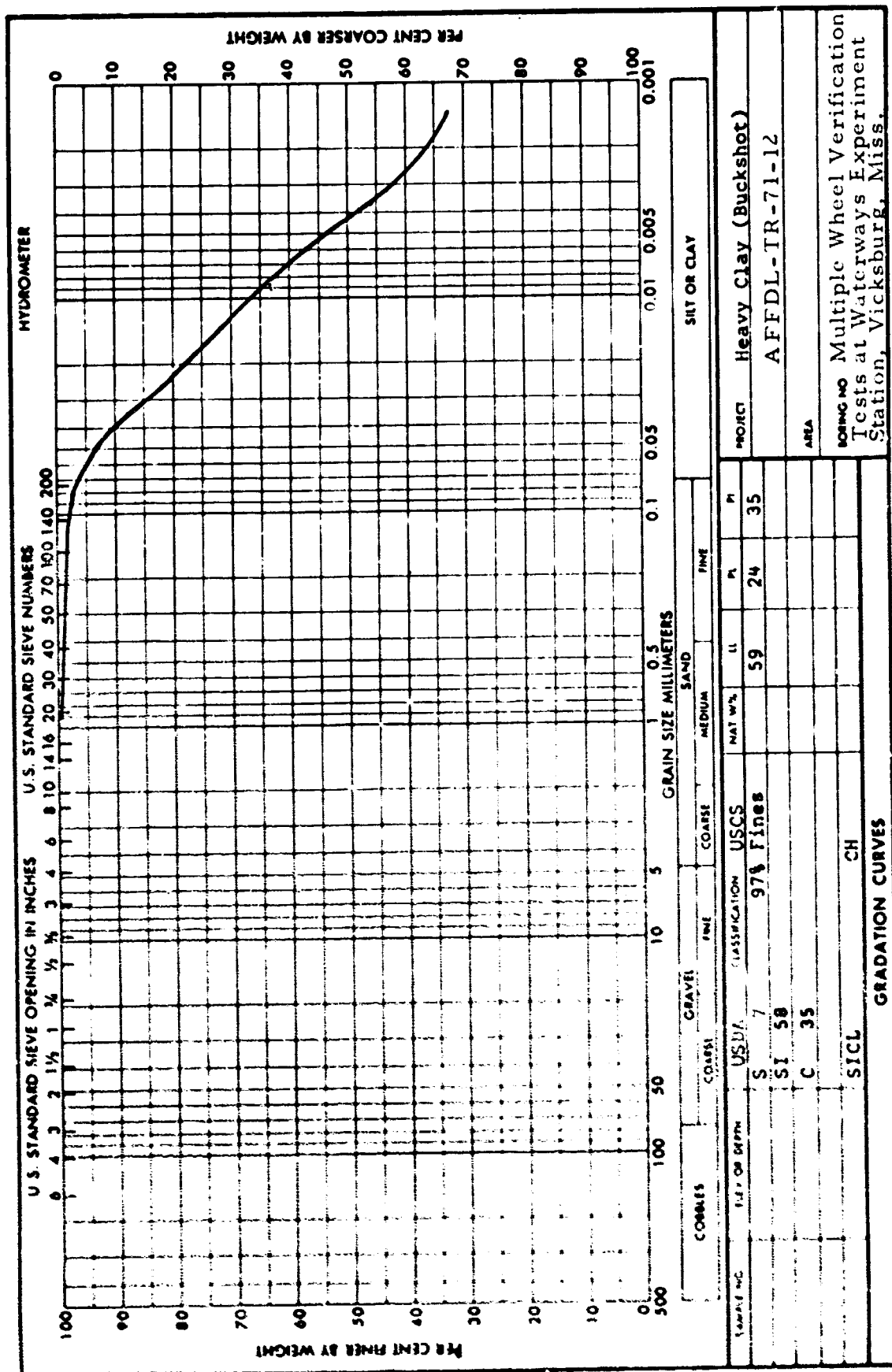
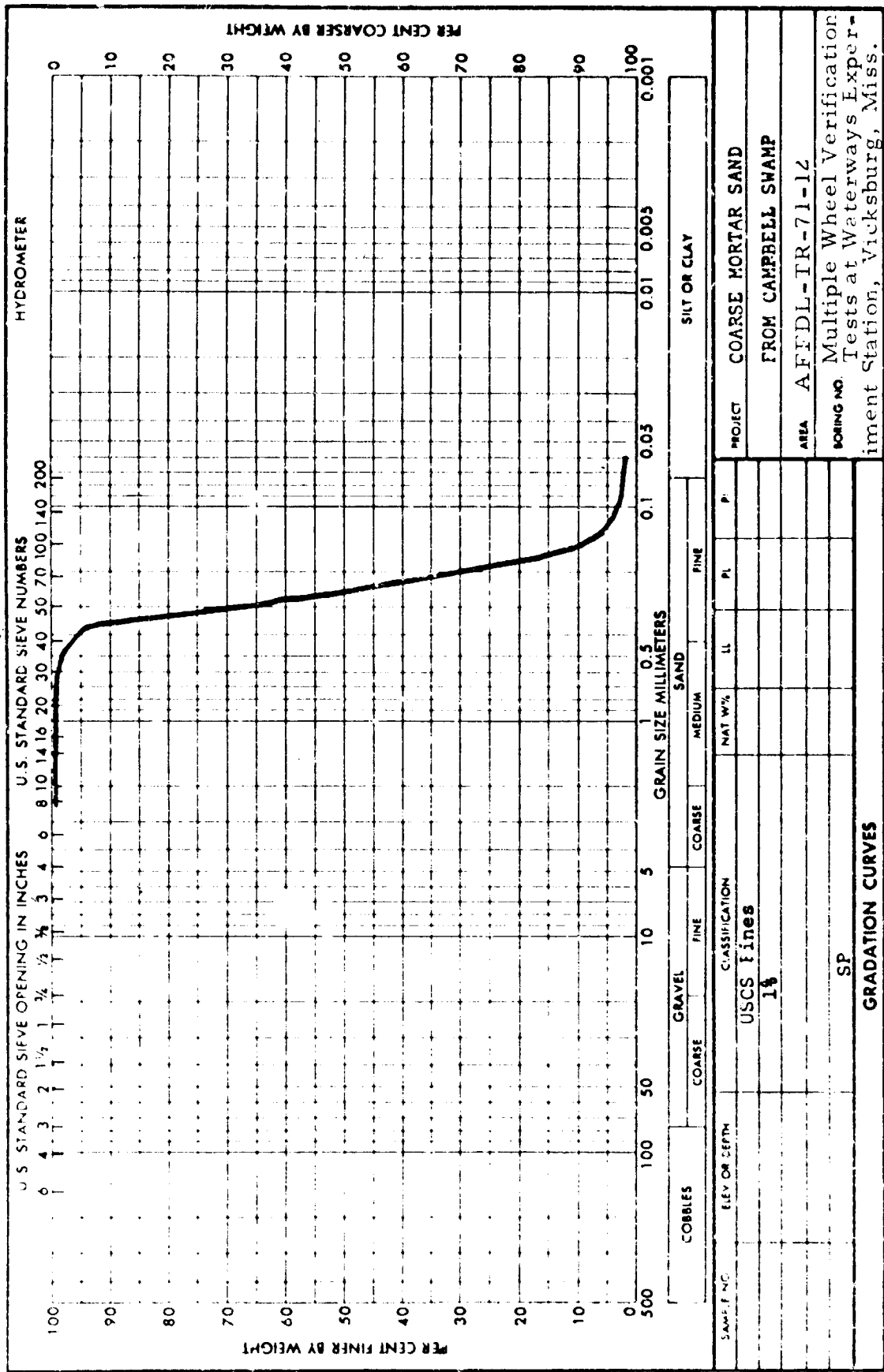Figure 59. Grain Size Distribution, Buckshot Clay

Figure 60. Grain Size Distribution, Mortar Sand

TABLE 29

Soil Strength Consistency and After Test Strength

Test No.	Mortar Sand				Buckshot Clay			
	Before Test CI avg	Before Test High CI	Before Test Low CI	After Test CI avg	Before Test CI avg	Before Test High CI	Before Test Low CI	After Test CI avg
1	42.2	42.6	41.6	28.8	24.2	25.2	23.3	21.4
2	42.4	44.3	40.5	27.5	19.7	20.9	19.0	19.0
3	48.1	49.7	46.3	31.9	21.7	23.1	21.0	19.6
4	37.5	37.9	36.9	25.4	22.4	24.1	21.2	21.5
5	39.9	40.4	39.2	26.0	22.6	24.4	21.0	21.6
6	42.0	43.5	40.9	26.3	23.4	25.5	21.5	22.8
7	40.6	42.5	39.3	26.7	22.5	24.0	20.9	20.4
8	37.8	39.5	35.8	26.1	21.0	22.9	19.8	19.8
9	44.5	45.9	43.8	31.4	22.8	24.3	21.9	22.8
10	40.9	42.4	39.4	26.4	23.1	24.5	21.8	22.6
11	42.3	43.8	40.1	26.2	21.2	22.2	19.8	21.9
12	39.6	41.1	38.5	25.9	23.6	25.1	21.9	23.0
13	40.3	41.9	38.7	25.4	23.0	25.2	20.8	21.2
14	39.3	40.6	37.2	24.0	20.8	23.1	18.6	20.6
15	40.7	42.5	38.6	23.5	19.9	21.6	18.8	20.0
16	42.2	45.2	39.8	26.8	20.7	22.1	19.0	20.9
17	38.0	38.8	37.6	22.6	19.9	21.2	19.1	19.2
18	39.2	40.4	38.4	26.7	22.9	24.9	20.8	21.8
19	38.3	39.1	38.0	25.4	22.1	24.2	19.4	22.0
20	40.0	40.9	38.7	26.5	21.5	22.9	19.8	21.6
21	40.6	41.2	39.8	27.6	21.9	23.6	20.7	22.4
22	40.6	41.5	39.7	27.7	22.6	24.9	21.1	22.3
23	39.1	41.0	38.2	26.8	23.5	25.9	21.3	24.2
24	28.7	29.2	28.2	22.2	23.8	26.0	21.0	23.1
25					22.6	24.2	20.8	21.8
26	42.8	43.5	42.3	23.4	21.1	21.8	20.3	22.3
27	39.0	39.7	38.6	23.7	24.6	25.8	23.5	24.5
28	38.5	39.8	37.9	23.7	25.9	27.4	24.4	25.7
29	42.8	44.0	41.0	26.6				

167

and tandem-nontracking tests, the value given represents only one pass soil strength alteration. Also included in this table is the before traffic CI values and the high and low value of all the tests to indicate the soil bed uniformity. As noted previously, the CI_{avg} indicates that the values given are an average of at least five separate tests.

Triaxial Tests

Undrained, unconfined triaxial tests were run on undisturbed clay specimens taken from the test soil carts for the soil conditions of $CI \approx 20$. The triaxial specimens with zero confining pressure were approximately 1.75 inches in diameter by 4.5 inches high. Each test specimen was extruded from a piston type soil sample similar to shelby tube samples. Only the specimen ends needed trimming before testing. The results of the unconfined tests are plotted in Figure 61.

Triaxial tests were also conducted on air dried samples of the mortar sand. The specimen size was 2.8 inches in diameter by 6.0 inches high and the samples were prepared to a unit weight of 98.0 pcf ± 1.0 pcf which was the average soil unit weight in the soil carts for the CI=40 test condition. The results of the triaxial tests on the sand are shown in Figure 62.

Soil Preparation

The buckshot clay was processed, placed, and compacted at predetermined moistures and densities corresponding to the desired soil strength. The soil is first passed through a roller crusher and then placed in a pug mill where the soil-water mixing takes place at a selected moisture content. The soil is then placed in the soil carts in 6 inch layers with each layer compacted by pneumatic tired rollers. Previously developed empirical relationships between buckshot clay moisture content and compactive effort permitted the soil to be placed near the design soil conditions.
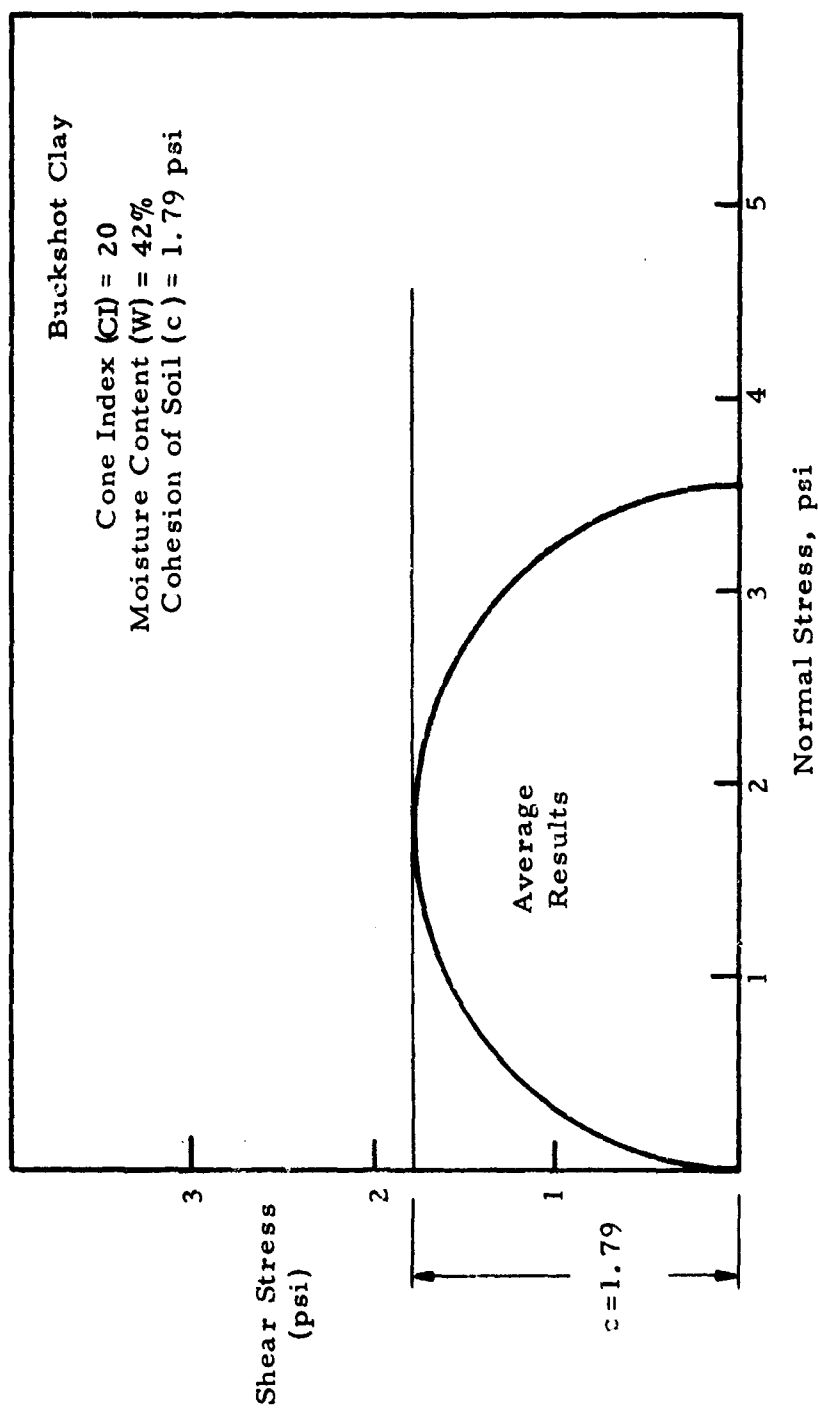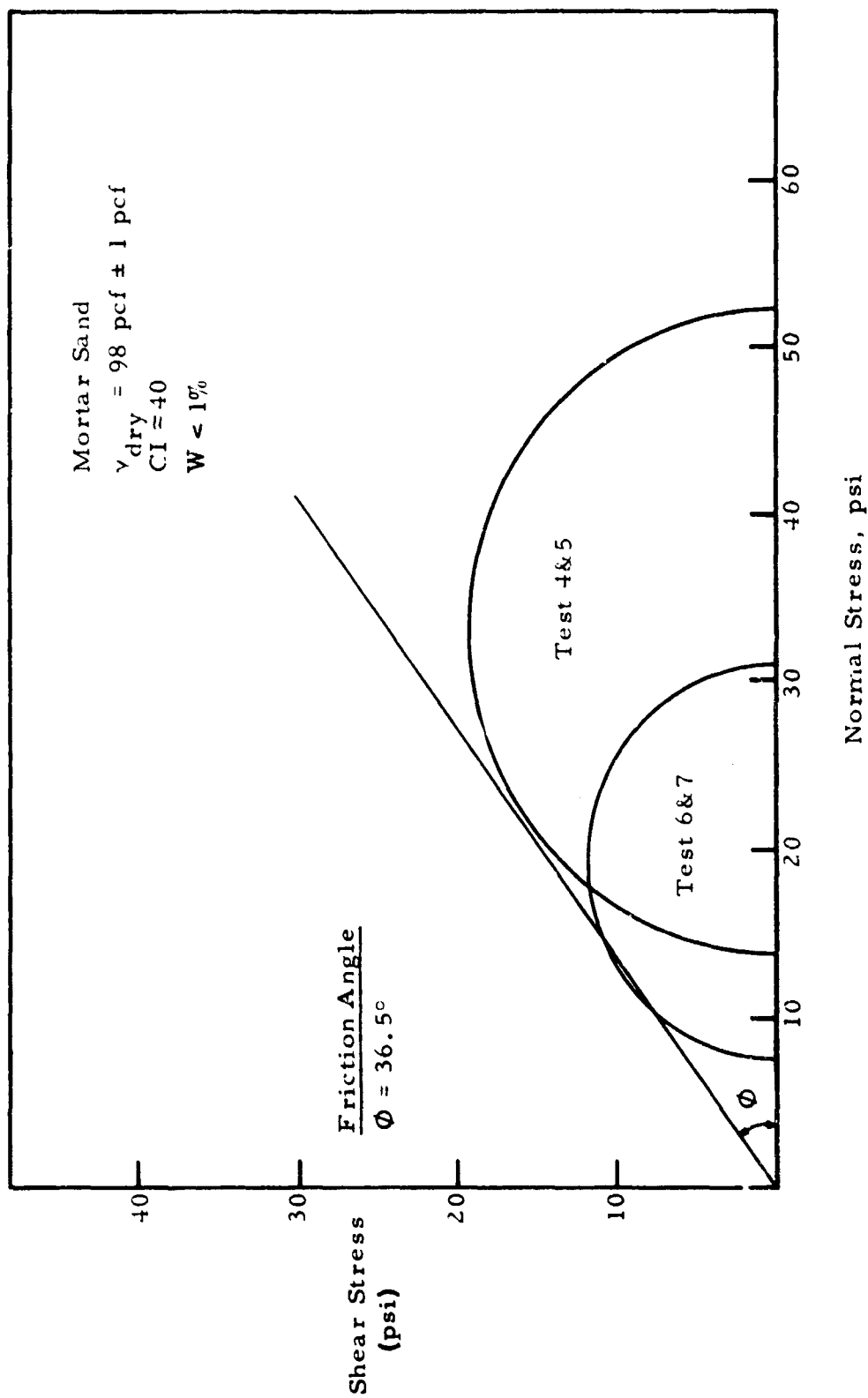
Figure 61. Triaxial Results, Buckshot Clay

169

Figure 62. Triaxial Results, Mortar Sand

170

The mortar sand was prepared in an air dried condition. Different soil strengths were achieved by varying the density of placement of the soil. The sand was placed in uniform layers which were screened and vibrated on the surface as the filling progressed. Empirical relationships between the thickness of layer, vibratory effect, and soil density permitted the sand to be placed near the design soil conditions.

Test Procedures

The test procedures for running a single test in sand are:

(1) Loosen sand section by plowing

(2) Check weakened state by Cone Index tests

(3) Vibrate sand to desired soil strength

(4) Check strength by Cone Index tests

(5) Take final soil strength and surface elevation profile

(6) Calibration checks between recording station and computer

(7) Make a test run without load on test tires (in-air run)

(8) Load tire and check inflation pressure and deflection

(9) Run test

(10) Take post test soil strength and rut depth profile.

The test procedure for running a test in clay differs from the sand only in soil preparation techniques. The clay test bed has to be prepared at least ten days in advance of a test so that the water content of the clay will stabilize as described above. The only preparation needed to run a test after the soil bed has been constructed involves smoothing the soil surface and measuring the soil strength and surface profiles. Steps (7) through (10) are then completed as in sand. Preparation for succeeding tests in the same clay soil bed can involve re-rolling and smoothing the soil surface. In both the sand and clay test procedure, a test is not run unless the desired soil strength and uniformity is attained during the preparation stages.

171

Sinkage Measurement

The sinkage measurement determined for each clay test is the result of the use of deflection pins which were developed in previous testing programs such as the C-5A program. The devices consist of a flat circular plate (2" diameter) and a short 1/4" diameter rod, pointed on one end. Before each test, a rod is penetrated into the soil and then the flat plate is placed on top of the pin flush to the soil surface in the tire path. After the test, the differential movement of the pin and plate is the value of the elastic sinkage (rebound). Normally, the pin does not rebound with the soil, but the flat plate normally does.

172

APPENDIX V

WES BRAKING TEST DATA

SAND AND CLAY

173

TABLE 30

WES Braking Tests, Buckshot Clay

Tire	Tire Deflection (%)	Vertical Load P(lbs)	Soil Strength CI_{avg}, psi	Sinkage Z(in.)	Percent Slip, %	Measured R_B, lbs	R_R, lbs	Calculated	
								R_T, lbs	$\dfrac{R_T}{CI \cdot D^2(Z/D)^2} \times 10^2$
9.00-14	25	766	20	1.93	7.4	240	201	39	0.93
	25	750	20	2.20	15.4	368	225	143	3.20
	25	750	20	2.76	32.7	548	282	266	5.32
	25	752	20	3.07	49.0	689	314	375	7.11
	25	760	20	3.31	83.4	751	342	409	7.47
	25	790	30	0.51	6.6	188	55	133	4.12
	25	794	30	0.41	26.1	328	44	284	9.82
	25	790	30	0.43	37.6	390	46	344	11.62
	25	804	30	0.41	42.8	408	45	363	12.55
	25	768	30	0.39	50.7	444	42	402	14.25
4.00-7	25	181	17	1.14	3.4	61	55	6	0.52
	25	177	17	1.24	12.8	112	60	52	5.19
	25	195	17	1.34	28.0	158	71	87	8.35
	25	182	17	1.20	37.1	157	60	97	9.84
	25	184	17	1.34	52.1	171	67	104	9.98
	25	186	17	1.57	67.2	184	80	104	9.22
	25	181	17	1.49	78.3	174	74	100	9.10
	25	183	17	1.56	88.9	176	78	98	8.72
	25	197	29	0.24	5.8	29	13	16	2.13
	25	200	29	0.27	15.3	76	15	61	7.65
	25	191	29	0.31	32.4	94	16	78	9.12
	25	190	29	0.52	50.3	113	27	86	7.77
	25	203	29	0.31	66.0	105	17	88	10.29
	25	194	29	0.22	79.1	103	12	91	12.64
	25	198	29	0.31	93.3	110	17	93	10.88
	25	373	33	1.06	5.2	106	98	8	0.44
	25	378	33	1.09	13.9	158	102	56	3.07
	25	368	33	1.08	35.6	219	100	119	6.53
	25	385	33	1.60	78.4	355	158	197	8.93
	25	363	33	1.42	81.8	336	131	205	9.81

R_B = Braked Tire Drag Force

R_R = Horizontal Soil Resistance to Forward Motion Exclusive of Soil Shear Resistence During Braking

R_T = Horizontal Component of Net Shear Force Resistence

TABLE 31

WES BRAKING TESTS, SAND

Tire	Tire Deflection (%)	Soil Strength CI_{avg}, psi	Slip (%) S	Vertical Load P(lbs)	Sinkage Z(in.)	R_B (lbs)	R_R (lbs)	R_T (lbs)	$\dfrac{R_T}{(\frac{\alpha}{CI_{avg}} \rightarrow D^a)}$
9.00-14	25	37.8	90-95	718	3.2	747	259	488	1.49
9.00-14	25	34.5	90-95	729	3.7	787	300	487	1.27
9.00-14	25	54.0	90-95	1475	4.0	1550*	680	870	1.81
9.00-14	25	57.0	90-95	760	2.1	661	193	468	2.02
4.00-7	25	19.8	90-95	70	1.6	84	25	59	0.76
4.00-7	25	49.5	90-95	80	0.8	75	17	58	1.83
4.00-7	25	43.5	90-95	166	1.9	176	70	106	1.40
4.00-7	25	61.8	90-95	88	0.8	71	18	53	2.05
4.00-7	25	62.7	90-95	180	1.8	175	72	103	1.85

* Estimated

R_B = Braked Tire Drag Force

R_R = Horizontal Soil Resistence to Forward Motion Exclusive of Soil Shear Resistence During Braking

R_T = Horizontal Component of Net Shear Force Resistence

APPENDIX VI

UNIVERSITY OF DAYTON TIRE/SOIL INTERACTION
RESEARCH REPORTS AND
COMPUTER PROGRAMS

176

A summary listing is given on the following pages of each report and each computer program developed by the University of Dayton under Air Force sponsorship (Air Force Flight Dynamics Laboratory, Vehicle Equipment Division) in the research program, "Landing Gear/Soils Interaction and Flotation Criteria."

The computer programs are available for use by other organizations with Air Force permission. Additional information may be secured by contacting:

Dr. David C. Kraft
Dept. of Civil Engineering and Research Institute
University of Dayton
Dayton, Ohio 45409

Mr. George J. Sperry
Project Engineer, Vehicle Equipment Division (AFFDL/FEM)
Air Force Flight Dynamics Laboratory
Wright-Patterson Air Force Base

LANDING GEAR/SOILS INTERACTION AND FLOTATION CRITERIA PUBLICATIONS AND REPORTS

Kraft, David C., Analytical Landing Gear-Soils Interaction, Phase I, AFFDL-TR-68-88, Air Force Flight Dynamics Laboratory, Wright-Patterson Air Force Base, Ohio, August 1968.

Kraft, David C., Preliminary Single Wheel Relative Merti Index, UDRI-TR-69-16, University of Dayton, Dayton, Ohio, May 1969.

Kraft, David C., Flotation Performance of Aircraft Tires on Soil Runways, Journal of Terramechanics, Vol. 6, No. 1, 1969.

Kraft, D. C.; Luming, H.; Hoppenjans, J. R., Aircraft Landing Gear-Soils Interaction and Flotation Criteria, Phase II, AFFDL-TR-69-76, Air Force Flight Dynamics Laboratory, Wright-Patterson AFB, Ohio, November 1969.

Luming, Henry, Finite Element Approach to Axisymmetric Dynamic Soil Deformations, Symposium on Application of Finite Element Methods in Civil Engineering, Vanderbilt University, Nashville, Tennessee, November, 1969.

Kraft, David C., Liguori, Albert E., Hoppenjans, J. Richard, Twin-Vertical Plate Verification Tests, Test Report, UDRI-TR-70-27, University of Dayton Research Institute, Dayton, Ohio, May, 1970.

Luming, Henry, Multiwheel Vertical Pulse Load Analytical Sinkage Prediction Technique and Computer Program, UDRI-TR-70-22, University of Dayton Research Institute, Dayton, Ohio, May, 1970.

Luming, Henry, Analytical Aircraft Landing Gear-Soil Interaction - Phase III, Rolling Single Wheel Analytical Sinkage Prediction Technique and Computer Program, AFFDL-TR-70-142, Air Force Flight Dynamics Laboratory, Wright-Patterson Air Force Base, Ohio, September, 1970.

Kraft, David C., and Luming, Henry, Multiple Rolling Tire Sinkage and Drag Interaction Effects, accepted for presentation at Joint ISTVS-SAE Meeting, Detroit, Michigan, January, 1971.

LANDING GEAR/SOILS INTERACTION AND FLOTATION CRITERIA COMPUTER PROGRAMS

Title of Computer Program: Transient Loading-Sinkage Analysis, Computer Program - 1

Brief Description: The computer program calculates the instantaneous (time-dependent) sinkage into a soil medium of a rolling aircraft tire. The rolling aircraft tire loading is simulated as a dynamic pulse loading applied in a vertical direction through a mass at the interface. The duration of the pulse is varied to simulate different forward velocities of the tire. The soil medium is assumed to be elastic and the load is applied as a uniform pressure over a circularly loaded area. The input parameters are the magnitude of the mass, shape of load pulse, duration of pulse, radius of loaded area, intensity of pressure, soil density, and soil shear modulus.

Computer Language: Fortran IV - (IBM)

Equipment: The computer program was originally written for use on the IBM 7094 at Wright-Patterson AFB, Dayton, Ohio.

178

Reference: Kraft, David C., "Analytical Landing Gear-Soils Interaction -
Phase I," AFFDL-TR-68-88, Air Force Flight Dynamics Labora-
tory, Wright-Patterson AFB, Ohio, August 1968.

Title of Computer Program: Flotation Index-Operations Index, Computer
Program -2

Brief Description: The computer program calculates the flotation capacity
of single and multiple wheel landing gear configurations for operation
on unprepared (soil) runways. The flotation capacity is expressed
by the Flotation Index (FI) and Operations Index (OI) which are
calculated based on sinkage and drag. The FI is the drag ratio of
a given aircraft based on specified operating conditions. The OI is
the ratio of sinkage to load at the same operating conditions.
Current program results include flotation ratings of all currently
used aircraft tires on cargo, bomber, and fighter type aircraft.
These results permit aircraft designers to select tires and landing
gear configurations for optimum flotation (minimum drag). Program
was revised 6-70.

Computer Language: Fortran IV - (IBM)

Equipment: The computer program was originally written for use on the
IBM 7094 at Wright-Patterson AFB, Dayton, Ohio.

Reference: Kraft, David C., Luming, Henry, and Hoppenjans, J. R.,
"Aircraft Landing Gear-Soils Interaction and Flotation Criteria -
Phase II," AFFDL-TR-69-76, Air Force Flight Dynamics
Laboratory, Wright-Patterson AFB, Ohio, November 1969.

Title of Computer Program: Sinkge Wheel Stationary Pulse Load-Sinkage
Prediction, Computer Program - 3

Brief Description: This computer program calculates the instantaneous
sinkage into a soil medium caused by a rolling aircraft tire. The

179

interface contact of the rolling tire is simulated by a stationary circular surface contact pressure which is uniform over the contact area and varies with time in the form of a pulse. The magnitude of the pressure changes in the same manner as the pressure experienced by a soil particle near the surface of the soil as the tire rolls over it. The soil is assumed to be an elastic-plastic material with elastic deformation governed by Hooke's law, the plastic deformations governed by an incremental stress-strain relation which is based on the normality flow rule, and the plastic yielding governed by the Drucker-Prager yield criterion with no strain-hardening. The input soil parameters are the density, the Young's modulus, the cohesion, and the friction angle. The numerical method used in solving the boundary value problem is the lumped parameter iteration method. This method uses an axisymmetric lumped parameter model to approximate the continuous medium and an iterative procedure to calculate the displacements and the stresses at the discrete points of the model.

Computer Language: Fortran IV - (IBM)

Equipment: This computer program was originally written for use on the IBM 7094-DCS at Wright-Patterson AFB, Dayton, Ohio. It has a 32K-word core capacity.

Reference: Kraft, David C., Luming, Henry, and Hoppenjans, J. R., "Aircraft Landing Gear-Soils Interaction and Flotation Criteria - Phase II", AFFDL-TR-69-76, Air Force Flight Dynamics Laboratory, Wright-Patterson AFB, Ohio, November 1969.

Title of Computer Program: Rolling Single Wheel Sinkage Prediction, Computer Program - 4

Brief Description: This computer program calculates the instantaneous sinkage into a soil medium caused by a rolling aircraft tire. The

180

interface contact of the rolling tire is simulated by a surface contact pressure which is applied uniformly over an area equivalent to the tire footprint area and is moved across the surface at the aircraft horizontal ground velocity. The magnitude of the uniform pressure increases over a finite rise time from zero to a pressure equal to the vertical tire load divided by the contact area. The soil medium is assumed to be an elastic-plastic material with elastic deformations governed by Hooke's law, the plastic deformations governed by an incremental stress-strain relation which is based on the normality flow rule, and the plastic yielding governed by the Drucker-Prager yield criterion with no strain-hardening. The input soil parameters are the density, the Young's modulus, the cohesion, and the friction angle. The numerical method used in solving the boundary value problem is the lumped parameter iteration method. This method uses a three-dimensional lumped parameter model to approximate the continuous medium and an iterative procedure to calculate the displacements and stresses at the discrete points of the model. An input-output scheme is also used for utilizing the limited core capacity for the three dimensional problem.

Computer Language: Fortran IV-(IBM)

Equipment: This computer program was originally written for use on the IBM 7094-DCS at Wright-Patterson AFB, Dayton, Ohio. It has a 32K-word core capacity.

Reference: Luming, H., "Analytical Landing Gear-Soil Interaction - Phase III, Rolling Single Wheel Analytical Sinkage Prediction Technique and Computer Program," AFFDL-TR-70-142, Air Force Flight Dynamics Laboratory, Wright-Patterson AFB, Ohio, September 1970.

Title of Computer Program: Multiwheel Stationary Pulse Load Sinkage Prediction, Computer Program - 5

Brief Description: This computer program calculates the instantaneous
sinkage into a soil medium caused by a pair of rolling twin aircraft
tires. If the sinkages for various twin-wheel spacings were cal-
culated and compared with the corresponding single-wheel sinkage,
twin wheel effects of aircraft landing gear configurations could be
obtained for use in flotation studies. The interface contacts of the
rolling twin tires are simulated by two stationary surface pressure
strips which are uniformly distributed and vary with time in the
form of a pulse. The magnitude of the pressure changes in the same
manner as the pressure experienced by a soil particle near the
surface of the soil as the tire rolls over it. The soil is assumed
to be an elastic-plastic material with elastic deformations governed
by Hooke's law, the plastic deformations governed by an incremental
stress-strain relation which is based on the normality flow rule,
and the plastic yielding governed by the Drucker-Prager yield
criterion with no strain-hardening. The input soil parameters are
the density, the Young's modulus, the cohesion, and the friction angle.
The numerical method used in solving the boundary value problem is
the lumped parameter iteration method. This method uses a plane-
strain two dimensional lumped parameter model to approximate the
continuous medium and an iterative procedure to calculate the dis-
placements and stresses at the discrete points of the model.

Computer Language: Fortran I\ -(IBM)

Equipment: This computer program was originally written for use on the
IBM 7094-DCS at Wright-Patterson AFB, Dayton, Ohio. It has a
32K-word core capacity.

Reference: Luming, Henry, "Multiwheel Landing Gear-Soil Interaction -
Phase III, Multiwheel Vertical Pulse Load Analytical Sinkage Pre-
diction Technique and Computer Program," R&D Computer Program
Report, Report No. UDRI-TR-70-22, University of Dayton Research
Institute, Dayton, Ohio, May 1970.